**THE UNIVERSITY OF NAIROBI**

**COLLEGE OF ARCHITECTURE AND ENGINEERING**

**EFFECT OF TRANSITION ELEMENTS ON MICROSTRUCTURE AND MECHANICAL PROPERTIES OF SECONDARY Al-7Si-Mg CAST ALUMINIUM ALLOY**

By

NGERU TIMOTHY NGIGI

F56/75498/2014

A dissertation submitted in partial fulfillment for the Degree of Master of Science in Mechanical Engineering in the Department of Mechanical and Manufacturing Engineering of the University of Nairobi.

**JUNE 2017**

# DECLARATION

"This thesis is my original work and has not been presented for a degree in this or any other university."

Signed: ........................................ 29/09/2017

Timothy N. Ngeru

Date

"This thesis has been submitted for examination with our approval as university supervisors."

Signed: ........................................ 22 - 09 - 2017

Dr. Thomas O. Mbuya

Date

Signed: ........................................ 13 - 11 - 2017

Dr. Bruno R. Mose.

Date

Signed: ........................................ 13 - 11 - 2017

Prof. Michael J. Witcomb.

Date

i

# ANTI-PLAGIARISM STATEMENT

This thesis has been written by me and in my own words, except for quotations from published and unpublished sources which have clearly been indicated and acknowledged. I am aware that the incorporation of material from other works or paraphrase of such material without acknowledgement will be treated as plagiarism, subject to the custom and usage of the subject, according to the university regulation on conduct of examinations.

Name
Timothy Ngigi Ngeru

Signature

Date
25/07/2018

# DEDICATION

This thesis is dedicated to my wife Magdalene Ngigi, my parents Peter and Eunice Ngeru, and siblings Loise and Esther Ngeru for their moral support and for their believe in me.

# ACKNOWLEDGEMENTS

# ABSTRACT

A majority of aluminium scrap have differences in chemical composition. Consequently, this makes the quality of recycled cast aluminium alloys to be questionable due to difficulty in chemistry control. This subsquently affects the microstructure and the general mechanical properties of these resulting products. Therefore, during aluminium recycling, it is vital to look for means of maximising the chemistry control of the alloy so as to improve the process efficiency.

The aim of this project was to contribute towards efficient aluminium recycling through the development of a model recycle friendly alloy for cylinder applications utilising direct recycling of automotive aluminium wheels. Four alloys were developed as a result of four ingots (obtained from recycled automotive wheels) being alloyed with strontium, titanium, zirconium, vanadium and copper in different proportions. The effect of these elements individually and in various combinations on the formation of intermetallic compounds was evaluated using microstructure analysis (optical, and SEM) and mechanical tests (tensile test, and fatigue tests).

The tensile tests at room temperature showed that alloy additions increased the ultimate tensile strength by as much as 31 % (from 218 MPa in alloy 356 to 285 Mpa in alloy 356+3.5Cu+X) while the fatigue strength increased by 37 % (from 71.35 MPa in alloy 356 to 98.05 MPa in alloy 356+0.5Cu+X). The alloying elements added formed compounds like $(AlSi)_xTiVZr$, with rod/blocky morphology which precipitated into very fine precipitates after heat treatment that impended the movements of dislocations thereby increasing the strength of the alloys.

With increasing the testing temperature from 25 °C to 237 °C, tensile strength drastically decreased by up to 30 % from 218 MPa in alloy 356 at room temperature to 152 MPa realised when the same alloy was tested at 237 °C. However, all is not lost since the addition of Cu, Ti, V, Zr and Cr

improved the high temperature strength of the base alloy (alloy 356) from 152 MPa to 198 MPa in alloy 356+3.5Cu+X.

Fractographic analysis after fatigue and tensile testing was done to investigate the crack initiation and propagation mechanisms. The fractographic studies revealed that the fracture characteristics were similar for all alloys. Some intermetallics and eutectic silicon particles were deboned from the matrix which was accompanied by secondary cracks between dendrites, and tear ridges. This suggests that there was a strong interaction between the dislocations and the eutectic silicon particles especially at grain boundaries leading to a contribution to inter-granular cracking.

# TABLE OF CONTENTS

# LIST OF FIGURES

# LIST OF TABLES

# NOMENCLATURE

2-D        Two-Dimensional

3-D        Three Dimensional

AA         Aluminium Association.

AD         Anderson-Darling.

AMSEN      Africa Materials Science and Engineering Network.

ASTM       American Society for Testing and Materials.

Avg.       Average

BS         British Standard.

$CO_2$     Carbon Dioxide Gas

CNC        Computer Numerically Controlled

DIN        Deutsches Institut für Normung (German Institute for Standardization).

EDS        Energy Dispersive Spectroscopy.

FEGSEM     Field Emmission Gun Scanning Electron Microscope.

HT         High Temperatures.

KWh/Kg     Kilowatt hour per kilogram.

NMC        Numerical Machining Complex.

NMISA      National Metrology Institute of South Africa.

MPa        Megapascals.

PPM        Parts Per Million.

RT         Room Temperatures.

SDAS       Secendary Dendritic Arm Spacing

SEM        Scanning Electron Microscope.

TEM        Transition Electron Microscope.

UNS        Unified Numbering System.

UTS        Ultimate Tensile Strength.

YS         Yield Strength.

wt.%       percentage Weight.

% El       Percentage elongation.

# CHAPTER 1: INTRODUCTION

## 1.1. Background

Aluminium makes up 8% of the total mass of the earth's crust. It is also the most abundant metal that is also the most used after iron [1]. It has desirable properties such as being light, having superior corrosion resistance properties, excellent castability and formability [2]. Furthermore, some aluminium alloys can be heat treated to produce a fairly strong material suitable for load bearing applications like aircraft structural members.

Aluminium alloys are available in wrought or cast form. wrought alloys are mostly used for structural applications while cast aluminium alloys are utilised to make various components with complex shapes with minimal defects. Among these cast aluminium alloys, aluminium-silicon alloys are the most popular due to their excellent fluidity, castability, good abrasion resistance and low coefficient of thermal expansion [3].

Aluminium alloys have increasingly substituted ferrous alloys in automotive components [4, 5]. This is attributable to the ever increasing necessity for weight reduction prompted by the inescapable weight increase in vehicles resulting from increased customer demand for comfort and safety (e.g. air conditioning and air bags), environmental regulatory requirements (e.g. use of catalytic converters) and other enhancements like noise reduction [5]. The use of aluminium in the automotive industry is, therefore, likely to increase due to its low weight advantage. Increased efficiency of aluminium recycling is therefore necessary because of its obvious economic and

ecological benefits as well as to ensure its continued availability at a reasonable cost. Some of the benefits of using recycled aluminium as opposed to primary aluminium include [4, 6].

1. Massive energy savings — It is estimated that aluminium recycling reduces the energy use by about 95% from the energy necessary for the production of primary aluminium (i.e. from about 45kWh/kg of primary aluminium to about 2.8 kWh/kg of secondary aluminium).

2. Reduced disposal of waste — Production of primary aluminium creates lots of solid waste. For example, mine wastes, the spent pot liner from the electrolytic cells and the red mud residue created during alumina purification. The quantity of solid and hazardous wastes from aluminium recycling are reduced by about 90%.

3. Reduced emissions — Primary aluminium production generates both hazardous (fluorides, sulphur dioxide) and nonhazardous (carbon dioxide) emissions. Aluminium production via recycling reduces emissions by over 90% per tonne.

4. Reduced capital cost — A mining operation and an aluminium extraction plant are not required.

5. Moreover, for some countries like Kenya, aluminium scrap is the most readily available source of aluminium for use by local industries and therefore significantly economical.

Based on these benefits, it has been suggested that the aluminium industry needs to look at opportunities for maximizing the advantages of aluminium recycling [6]. One of the challenges recognized as a key pillar in maximizing aluminium recycling efficiency is the broadening of the

quantity of alloys made from recycled metal to be used in the production of high quality products [6]. This aspect has generally received little attention in aluminium recycling and yet the potential economic and environmental benefits, especially as it pertains to the Kenyan industry, warrants its consideration. For example, cast aluminium alloys for automotive applications which are recycle-friendly have largely been limited to the 380 and 319 type alloys [4]. Although these alloys are broadly utilised in makining automotive components, there are numerous automotive components, such as pistons, for which they cannot be applied. Alternative recycle-friendly alloys therefore need to be developed that can be used in some of these high-value automotive applications. It is this aspect that this project aims to address. The current project is limited to developing recycle friendly cast aluminium alloys for automotive applications.

## 1.2  Problem Statement and Justification

The need for lightweight components in automobiles, aerospace, and engineering structures has led to an increased need for improved aluminium recycling efficiencies. To achieve this, one of the key areas that researchers and industry players need to focus on is the development of a wide range of recycle-friendly alloys that can still be used in high-value engineering components. Little effort has so far been expended towards meeting this goal.

Automotive wheels were traditionally made from steel, but are now mostly made from aluminium alloys [1]. This is because they can be made easily by casting. Furthermore, they are light in weight, which leads to fuel economy (compare the density of Al of 2.8 $g/cm^3$ to that of steel of 7.8

g/cm$^3$ [7]). Moreover, they also have superior corrosion and aesthetic properties over their steel counterparts and, as a consequence, they tend to last longer.

End-of-life automotive wheels are a good candidate raw material for alloys suitable for manufacturing several automotive components such as cylinder heads. This is because they have an almost similar composition with some of the alloys that are used for making these components (i.e., A356 type alloys). They also make up a big percentae of aluminium scarp, they can be dismantled easily and are manufactured from homogenous alloys [8]. For all the potential applications of recycled aluminium from automotive wheels, there is limited information available in the published literature that documents effective methods of doing this and the process-microstructure-property relationships of the resulting alloys.

Cast A356 alloy are extensively used to manufacture cylinder heads owing to their outstanding charecteristics, namely good specific strength, corrosion resistance, and excellent castability. Nevertheless, the alloy's strength reduces rapidly with time at working temperatures higher than 120°C since the strengthening precipitates coarsen at these high temperatures [9]. It has however been reported that addition of transition metals such as Sc, Ti, Zr, Cr, V, Mn, and Co can improve the elevated temperature strength [9–12]. The effect of these alloying elements on the castability, mechanical performance and microstructure is however not well understood especially with regard to the secondary cast aluminium alloys that generally have higher impurity metal content.

Control of the chemical composition can be a significant challenge during aluminium recycling. As such, it is common to find a significantly higher level of minor and impurity elements in

secondary alloys, which cannot be easily removed. These trace elements may influence castability parameters such as fluidity, feedability, and porosity formation and consequently not only affect microstructural features but also properties such as resistance to corrosion and mechanical performance. As a result, special attention needs to be focused on the effect of these trace elements during Al recycling and their possible influence on both physical and mechanical properties.

## 1.3. Aim and Objectives

### 1.3.1 Broad Aim

The overall aim of this research is to develop a recycle-friendly Al-7Si-Mg (Cu) alloy suitable for automotive and other load bearing applications.

### 1.3.2 Specific Objectives

1. To develop a recycle friendly secondary cast Al-Si alloy that can be obtained via recycling of automotive wheels for applications in cyclinder heads and other load bearing components.

2. To evaluate the effect of Sr and selected transition elements (Cu, Cr, V, Ti and Zr) on the microstructure and mechanical properties of the secondary alloy.

# CHAPTER 2: LITERATURE REVIEW

## 2.1 Introduction

Cylinder heads have historically been made of cast iron. However, they are now being made of aluminium due to its low weight, corrosion resistance, and excellent castability. This is also encouraged through strict emission regulations. Thus, there is much effort in developing superior alloys that can operate at elevated temperatures and pressures to achieve increased engine efficiency.

Cylinder heads are subjected to severe thermal fatigue in the combustion chamber due to thermal cycling between ambient temperatures to about 300°C resulting in repeated constrained thermal expansion and contraction [14]. The material suitable for such application must therefore have a low thermal expansion coefficient, high tensile and compression strength as well as a high creep resistance at elevated temperatures. Furthermore, the alloy should have a high thermal conductivity, corrosion resistance and must remain dimensionally stable during service [15].

A lot of resources and effort have been dedicated to research and development of alloys for high temperature applications. Literature data indicates that for automotive powertrain components operating at higher temperatures, such as gasoline and diesel engine cylinder heads, the following alloys have been used or are being considered for future applications:

(i)    Al-Si-Mg (A356, A357) characterized by good ductility, but lack sufficient strength above 200°C.

(ii)     Al-Si-Mg-Cu alloys (319, A356 + 0.5 wt.% Cu) characterized by good ductility and strength between 200 and 250 °C [16],

(iii)    Al-Si-Mg-Cu alloys modified with Ti, Cr, V, Zr, Mn and Zr (e.g., A319 + 0.25 wt.% V + 0.15 wt.% Mn + 0.15 wt.% Zr) characterized by higher yield stress, lower ductility and improved creep at 250°C [17].

However, the effects of the various alloying elements both individually or in combination are not fully known and need further investigation. For example, due to the deteroriation of the mechanical strength of Al-Si based alloys as a result of precipitates coarsening at temperatures above 150°C [11], the high temperature mechanical properties are improved by modification of the base alloy chemistry by the addition of transitional metallic elements [10]. Recent discoveries [12, 17], have revealed that high-temperature properties can be improved by the addition of elements such as Ti, V, or Zr which develop precipitates that are stable and which don't coarsen at high temperatures such as at 300°C.

## 2.2 Cast Aluminium Alloys

As a results of their excellent castability, corrosion resistance and specific mechanical strength, cast aluminium alloys are extensively utilised in many economical sectors especially in transportation such as in automotive, rail, marine, and aerospace. Currently, it is undisputed that the automotive sector is the most significant end user of aluminium alloy castings. The net utilisation of cast aluminium alloys in automobile applications increases gradually each year [19]. This is particularly true in the last two to three decades during which the production of vehicles

with many aluminium parts increased tremendously. Components like pistons, engine blocks, cylinder heads, pistons, transmission cases, oil pans, and frames are now usually cast from aluminium.

Cast aluminium alloys are manufactured with varying compositisions with each having different capabilities. Compositions numbering 100 and beyond, are in the Aluminium Association's register, and approximately, three hundred alloys are in use internationally [20]. There are various designation systems including the BS (British Standard) system, DIN (Deutsches Institut für Normung) system, UNS (Unified Numbering System) designation system, the AA (Aluminium Association) designation system. The AA designation system, which is the one mostly used has seven basic families as shown in Table 2.1.

Table 2.1. Aluminium alloy classification system [15].

| Series | Alloy Type |
|--------|-----------|
| 1xx | 99.0% minimum aluminium |
| 2xx | Al-Cu |
| 3xx | Al + (Si-Mg), (Si-Cu) or (Si-Mg-Cu) |
| 4xx | Al-Si |
| 5xx | Al-Mg |
| 7xx | Al-Zn |
| 8xx | Al-Sn |

Currently, almost all shape castings are produced from aluminium-silicon based alloys (i.e. 3xx and 4xx series). It is due to the excellent castability that is required for shaped castings that Al-Si casting alloys have been leading other casting alloy compositions in terms of usage. This is irrespective of their average general properties [15, 20, 21] as it can be seen from Table 2.2. Undeniably, Al-Zn-Mg-Cu, and Al-Cu alloys have significantly higher strength at room temperatures than Al-Si. On the other hand, Al-Cu-Mn alloys have superior creep resistance while Al-Zn-Mg and Al-Mg alloys have better corrosion resistance [16].

Table 2.2 Qualitative comparison of the key aluminium alloy properties [21].

| System | Strength | Thermal Stability | Casting Properties | Corrosion Resistance | Formability | Weldability |
|---|---|---|---|---|---|---|
| Al-Si | 1* | 1 | 3 | 2 | 2 | 3 |
| Al-Si-Mg | 2 | 1 | 3 | 2 | 1-2 | 3 |
| Al-Si-Cu | 2 | 2 | 2-3 | 1 | 1-2 | 3 |
| Al-Si-Cu-Mg | 2-3 | 2 | 2-3 | 1 | 1 | 3 |
| Al-Cu | 3 | 3 | 1 | 1 | 3 | 1-2 |
| Al-Mg | 1-2 | 1 | 1-2 | 3 | 3 | 3 |
| Al-Mg-Zn | 2-3 | 1 | 1 | 3 | 2 | 2 |
| Al-Zn-Mg-Cu | 3 | 1 | 1 | 1 | 2 | 1 |

*1: Low level, 2: average level, and 3: high level.

Al-Si alloys therefore continue to be the favourite casting alloys. Silicon ensures good castability due to the rather thin range of solidificattiion and the development of a significant quantity of eutectics inside the microstructure [23]. In Aluminium-Copper and Aluminium-Magnesium alloys, a high eutectic volume fraction can be realised, but a high concentrations of copper and/or magnesium will be required which will lead to loss of strength and fracture toughness [22].

Aluminium and silicon form a simple binary eutectic with the reaction occuring at 11.7 wt.% Si and 577°C. The aluminium rich constituent, under conditions of equilibrium comprises of 1.60 wt.% Si, and the constituent which are rich in silicon contains 0.5 wt.% aluminium at this temperature [16]. Binary Al-Si alloys have outstanding castability, fluidity, and corrosion resistance. They also exhibit small specific gravity values in addition to low coefficients of thermal expansion. Additionally, Aluminium-Silicon alloys that have substituted cast irons in many automotive components posses exceptional tribological qualities [24] with superior thermal conductivities which cast irons do not have [14].

However, binary Aluminium-Silicon alloys are practically limited for use in automotive and structural requirements where certain properties, in particular strength, are desired. Therefore, commercial Aluminium-Silicon alloys, therefore, are alloyed with different amounts of elements, so that their microstructure can be transformed for the projected uses.

### 2.2.1 Common Commercial Cast Aluminium Alloys

This sub-section gives a summarised overview of the microstructural characteristics of some common cast aluminium Al-Si alloys as influenced by various factors such as alloy additions. Table 2.3 lists the chemical composition specifications for various cast aluminium alloys while Table 2.4 tabulates typical mechanical properties of some of the alloys after selected temper treatments.

Table 2.3 Compositions of common commercial aluminium alloys [2].

| Alloy* | Composition (wt.%) | | | | | | | |
|--------|------|------|--------|-----------|----------|------|---------|-----------|
|        | Si   | Fe   | Cu     | Mn        | Mg       | Ni   | Zn      | Ti        |
| 319.0  | 5.5-6.5 | 1.0 | 3.0-4.0 | 0.5 | 0.1 | 0.35 | 1.0 | 0.25 |
| C355.0 | 4.5-5.5 | 0.20 | 1.0-1.5 | 0.1 | 0.4-0.6 | - | 0.1 | 0.20 |
| 356.0  | 6.5-7.5 | 0.6 | 0.25 | 0.35 | 0.20-0.45 | - | 0.1 | 0.20 |
| A356.0 | 6.5-7.5 | 0.2 | 0.20 | 0.10 | 0.25-0.45 | - | 0.1 | 0.20 |
| A357.0 | 6.5-7.5 | 0.20 | 0.20 | 0.10 | 0.4-0.7 | - | 0.1 | 0.04-0.20 |
| A380.0 | 7.5-9.5 | 1.3 | 3.0-4.0 | 0.5 | 0.10 | 0.5 | 3.0 | 0.35 |
| B390.0 | 16.0-18.0 | 1.3 | 4.0-5.0 | 0.5 | 0.45-0.65 | 0.10 | 1.5 | 0.20 |
| A413.0 | 11.0-13.0 | 1.3 | 1.0 | 0.35 | 0.10 | 0.50 | 0.50 | - |
| 535.0  | 0.15 | 0.15 | 0.05 | 0.10-0.25 | 6.2-7.5 | - | - | 0.1-0.25 |
| 712.0  | 0.30 | 0.7-1.4 | 0.35- | 0.05 | 0.25-0.45 | - | 6.0-7.0 | 0.20 |

*Single values are maximum limits of particular element composition. The balance is aluminium and other trace elements such as Cr, Pb, and Sn.

Table 2.4 Mechanical properties of certain aluminium alloys [19].

| Alloy | Temper | Yield Srrength | Ultimate Tensile | Shearing Strength | Brinell Hardness |
|---|---|---|---|---|---|
| 319.0 | F | 124 | 186 | 152 | 70 |
| 355.0 | T6 | 172 | 241 | 193 | 80 |
| 356.0 | T6 | 165 | 228 | 179 | 70 |
| A356.0 | T6 | 207 | 276 | 213 | 75 |
| A357.0 | T6 | 248 | 317 | 276 | 85 |
| 535.0 | F | 138 | 276 | 186 | 70 |
| 713.0 | F or T5 | 159 | 234 | 1827 | 75 |

## 2.2.2 Properties Desired in a Cylinder Head

Among the most vital components of an internal combustion engine, the cylinder head is one of them. It delivers fuel and air mixture to the chamber where combustion takes place and covers the cylinders. The chief role of the cylinder head is to aid the cylider head gasket in sealing the cylinders appropriately so that sufficient compression can be developed for the operation of the engine [25]. In many engines especially the four-stroke ones, the cylinder head supports the complete valve gear assembly and makes available the rudimentary structure for supporting the spark plugs, injectors as well as gas-exchange valves. Furthermore, various cooling system parts are mounted on it [26].

12

Cylinder heads need to have high fatigue resistance so as to avoid initiation and propagation of cracks due to both thermal fatigue and high-cycle mechanical fatigue (HCF). Firstly, they are subjected to high thermal fatigue due to fluctuations in temperatures between ambient and about 300°C causing repeated thermal expansion particularly in the valve bridge sections than have thin walls [26, 27]. Secondly, these heads experience HCF that arises from the rotation of the crankshaft during combustion cycles, critical high-cycle fatigue areas are on the water jacket areas. Furthermore, the cylinder head should have adequate strength and rigidity particularly at high temperatures so as to be able to share uniformly the forces generated by the gases throughout the engine block. Moreover, the alloys for manufacturing cylinder heads should be castable, machinable, have high thermal conductivity, and high creep resistance. These mechanical properties depend on the microstructure of the alloy and so impurities in the alloy must be avoided. Also, the alloying elements and the process of manufacturing the alloy and the cylinder head must be selected critically and with sound judgement.

### 2.2.3   Common Cylinder Head Alloys

*Alloy 319.0*

This alloy has excellent castability, pressure tightness, moderate strength and its microstructure and mechanical performance are not significantly influenced by a fluctuation in the level of contamination [29]. This alloys have very good weldability and corrosion resistance properties. Mechanical characteristics are superior in both the as-cast conditions and the heat-treated states [30]. 319-type alloys are continuing to gain considerable attention in the automobile sector lately

13

and are, for instance, substituting cast iron in engine blocks and cylinder heads [28–30]. They are also used to make engine crankcases, gas and oil pans and structural castings for engine parts.

*Alloy C355.0*

This Al-Si-Cu-Mg alloy with reduced iron levels is similar to alloy 355.0 except for its high purity, and superior strength. It exhibits exceptional hardness and strength albeit sacrificing the corrosion resistance and ductility. Casting properties are fair although lower than those demonstrated by Al-Si alloys with no copper [22].Though the as-cast condition characteristics could be made suitable for some uses, heat treatment is usually carried out on them for optimum properties [32]. This alloy is commonly used to make engine cooling fans, cylinder heads, crankcases, air compressor pistons, among other aerospace, automotive, structural and household components [20].

*356-Type Alloys*

The A356.0 and 356.0 alloys contain 6 wt.% silicon, 0.5 wt.% magnesium with maximum impurity limits of 0.10 wt.% Zn and 0.20 wt.% Fe. The alloys have excellent castability and machinability and are normally used after being heat treated [33]. The A356 alloy is the most commonly used cast aluminium for automotive components especially wheels and diesel engine cylinder heads due to its excellent pressure tightness, castability, lightweight, and excellent mechanical properties [34]. The alloy has been reported [14] to possess adequate mechanical characteristics up to 250°C, but these properties deteriorate at higher temperatures.

The microstructure of A356 basically comprises of 3 things, whose proportions are determined by the solidification parameters and the composition purity of the alloys. The two key items are the Aluminium-Silicon eutectic and the aluminium dendritic phase. Thirdly, there are the intermetallic compounds that arise from separation of excess elements from the primary dendritc solid solutions or as a result of positional ordering of the atoms of the components in solid solutions [22]. These intermetallics adopt various morphologies and can considerably influence the alloy's mechanical performance [21]. For example, $\beta$-$Al_5FeSi$ is a brittle phase that deteriorates the fracture resistance of the material in service. Figure 2.1 is a typical micrograph of a hypo-eutectic alloy Al-Si showing Aluminium-Silicon eutectic sorrounding the primary Al dendrites .
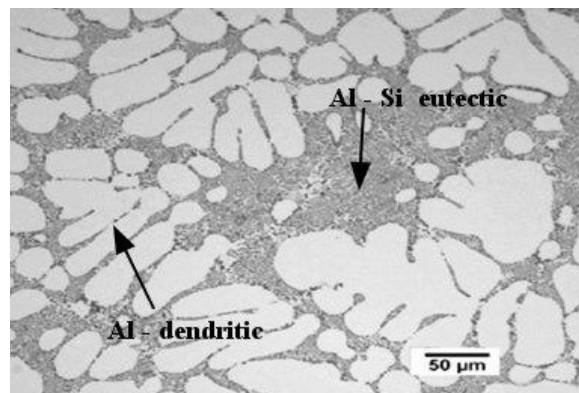


Figure 2.1. General microstructure of a hypo-eutectic Al-7Si-Mg (A356) alloy [9].


The new A356+0.5 wt.% Cu alloy is reported to have good yield strength without loss of elongation in the 200-250°C temperature range while the ductility is the same as A356 [14], [35] and it is therefore widely used in industry today for cylinder head application. However, the gain in mechanical performance from Cu addition is reported to disappear completely at 300°C [35].

15

## 2.3 Overview of Al-Si-Mg-Cu Cast Alloys

The non-heated microstructure contains dendrites of alpha aluminium comprising of magnesium and silicon. This is enclosed by a eutectic Aluminium-Silicon phase arising from the eutectic reaction as depicted in the phase diagram presented in Figure 2.2 [36]. The shape and size of the eutectic silicon depend on the melting conditions and the presence of modifiers such as strontium, sodium or antimony. Without change, the eutectic silicon is formed as thick platelets shown in Figures 2.3 (a) and (d) whereas a fine 'fibrous' structure occurs in modified alloys as shown in Figures 2.3 (c) and (f) [37].
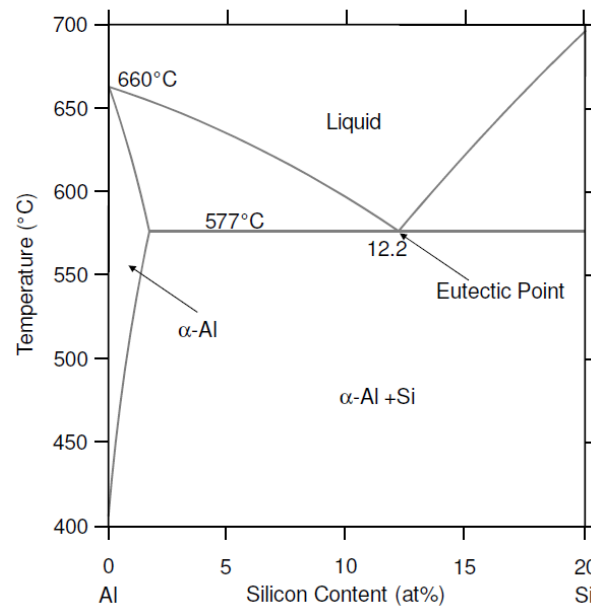


Figure 2.2. Equilibrium binary phase diagram of Al-Si system [35].

16
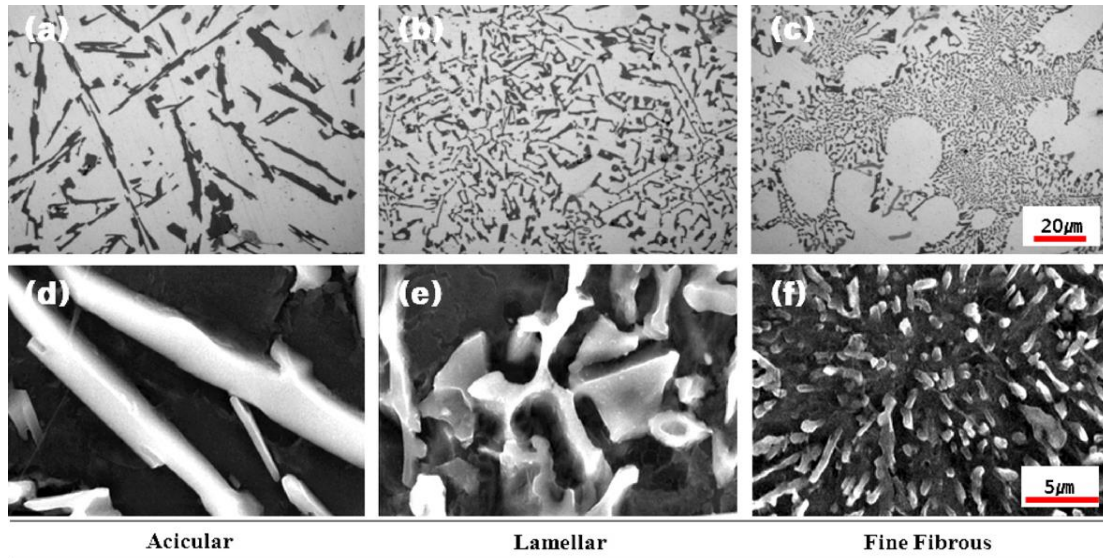
Figure 2.3. Optical and SEM micrographs showing the size and distribution of the eutectic Si in the Al–10.5Si–2.0Cu alloys with different Sr contents. (a and d) 0.0% Sr, (b and e) 0.02% Sr, (c and f) 0.03% [36].

Magnesium reacts with silicon to form particles of Mg2Si that have a Chinese script morphology. It is obtained in solid solution and precipitated during thermal treatment [38]. On the other hand, copper forms an intermetallic phase with Al which precipitates during solidification as $CuAl_2$ in blocks or as finely dispersed eutectic $CuAl_2$ particles containing alternate sheets of $\alpha$-Al + $CuAl_2$. The $CuAl_2$ phase particles in the block are difficult to dissolve during the heat treatment in solid solution, unlike the fine particles of $CuAl_2$ which can be dissolved within two hours of thermal treatment in solid solution [39]. The $Al_5Cu_2Mg_8Si_6$ phase also occurs when Mg is present even in smaller quantities than the $Al_2Cu$ phase [38].

17

Depending on the composition, other phases can be found in the microstructure. For example, $\pi$-$Al_8Mg_3FeSi_6$, $\alpha$-$Al_{15}$ (Fe, Mn) $_3Si_2$, $\beta$-$Al_5FeSi$, $Al_4FeSi_2$, $Al_9Fe_2Si_3$ and $Al_8SiFe_2$ are some of the phases arising from the presence of impurities such as iron and manganese [40]. B-$Al5FeSi$ is the iron phase most commonly observed in Al-Si-Mg-Cu alloys with iron greater than 0.1%. It is always a primary phase, seen as 3-D platelets and as 2-D needles, as shown in Figure 2.4
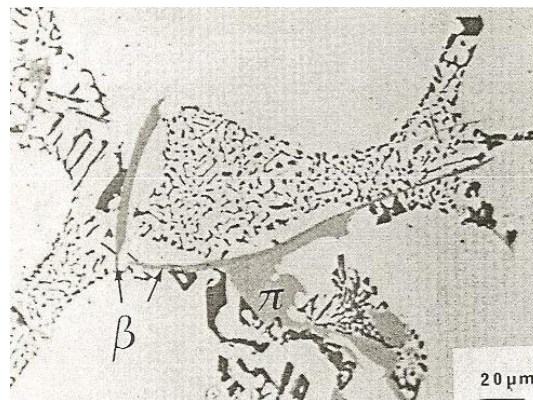


Figure 2.4. $\beta$-$Al_5FeSi$ and $\pi$-$Al_8Mg_3FeSi_6$ phases in an A356 alloy with 0.52 wt. % Fe [38].

Copper and magnesium have a significant hardening effect due to the formation of secondary precipitates such as $Al_2Cu$, $Mg_2Si$ and/or $Al_2CuMg$, which are fairly stable and provide high temperature resistance for propulsion applications. However, these precipitates are usually vulgarized and decomposed at a higher temperature (greater than 200 °C).

## 2.4 Microstructure and Mechanical Properties of Al-Si-Mg-Cu alloys

The mechanical properties of aluminous alloys Al-Si depend not only on their chemical composition, but above all on microstructural characteristics such as α-Al morphology and other dendritic intermetallics present in the microstructure. The morphology and size of the eutectic and the hardening steps of the precipitation during the heat treatment exert an important influence on the mechanical properties. Consequently, the following sections will discuss the effects of alloy elements and heat treatment on the mechanical properties of Al-Si alloys.

### 2.4.1   Effect of Selected Elements in Cast Al-Si Alloys

*Influence of Copper.*

Copper significantly increases the hardness and strength of the non-heat treated and heat treated alloys. Alloys having 4.0 to 5.5 wt. % copper are more responsive to heat treatment and have relatively better castability. However, Cu usually decreases the total resistance of corrosion and in certain compositions and material conditions the susceptibility to stress. In addition, copper reduces rupture strength and increases inter-dendritic shrinkage potential.

The investigation of the microstructures and tensile properties of Al-Si-Cu-Mg alloys with different contents of copper and copper to magnesium ratios by Zheng et al. [42] revealed that the $Mg_2Si$, Q-$Al_2Cu$ and Q phases were produced in the Al-Si-Mg-Cu subject to the copper/magnesium ratio and the copper content. The $Mg_2Si$ phase is formed in the fairly low Mg/Cu alloy ratio, while the high Mg/Cu ratio causes the formation of Q-phase and θ-phase. At

the same Mg/Cu ratio, the high levels of magnesium and copper increases the θ-phase and Q-phase formation simultaneously. Observation of the microstructure of alloys tempered in the T6 condition has indicated that the content of copper and the Mg/Cu ratio governor the primary intermetallic phases dissolution rate and the creation of intermetallics, thus influencing the ductility and strength.

Jahn, *et al.* [43] have widely studied the hardening of aluminum precipitates in 319 aluminium castings. They discovered that age hardening in 319 alloys is mainly due to precipitation of θ' ($Al_2Cu$) in plate form, but also precipitates containing magnesium were detected in specimens aged between 150 to 305°C.

Shabestari *et al.* [44] investigated the copper effect and the solidification state on the mechanical performance and the microstructure of Al-Si-Mg alloys. They used Cu ranging from 0.2 to 2.5% by weight in aluminum alloy A356 and at different casting conditions (graphite, sand, cast iron, and copper moulds). They discovered that the alloy's ultimate tensile strength increases with cooling rate of the mould, heat treatment (T6), and level of copper up to 1.5%. They credited the increase in UTS to the precipitation of copper phases in the interdendritic space caused by the increase in copper content. They also found that the best mechanical performance were realised in the Al-Si-Mg alloy with copper of about 1.5% cast in graphite moulds.

Murayama *et al.* [45] found that hardness at peak aging and tensile strength increased with decreased elongation when the copper content was increased in an Al-1.23 at.% Si - 0.64 at.% Mg alloy. The study by transmission electron microscopy (TEM) on the behaviour of dispersoids

precipitated in the course of ageing indicates that addition of copper increases the amount of $\beta''$ precipitates and encourages precipitation of Q-phase precursors at the peak aging condition. With high copper content, the phase , $\theta'$-$Al_2Cu$ also precipitated when artificial aging was carried out.

*Influence of Magnesium.*

Magnesium is the basis for the development of hardness and strength in thermally treated Al-Si alloys containing Cu, Ni and other elements. The hardening phase $Mg_2Si$ has a very low solubility limit of approximately 0.70% Mg by weight, above which there is no additional reinforcement or there is a softening of the matrix. Common compositions of high strength aluminum-silicon alloys specify magnesium in the range of 0.4 to 0.70% by weight.

Yang *et al*. [46] observed that the addition of magnesium in the Al-9Si-3.5Cu-0.5Mn-0.1Fe alloy effectively strengthened the alloy in the as-cast condition as well as when heat treated. They also found that the magnesium free Al-Si-Cu alloy owed its strength from the precipitation of $\theta'$–$Al_2Cu$ phase was during aging. Moreover, upon addition of magnesium and aging, the Q'-AlCuMgSi phase was precipitated on top of the $\theta'$–$Al_2Cu$ phase, which led to the joint reinforcement by precipitates to the alloy. They finally recommended that the levels of magnesium be controlled at so as not to exceed 0.73% by weight, in both heat treated and non heat-treated states which will increase strength with acceptable ductility.

Caceres *et al.* [47] studied Al-7Si-xMg, (x = 0.4 and 0.7% Mg) alloy by using different solidification rates and modifying with strontium. They observed that eutectic Si particles were large in both the modified alloys with high magnesium levels and in unmodified alloys. In addition, large $\pi$-Al$_9$FeMg$_3$Si$_5$ particles which are rich in iron were formed in 0.7 wt.% Mg alloys in addition with some minor $\beta$-phase plates (Al$_5$FeSi). On the contrary, only the $\beta$ plates were detected in the alloys with 0.4 wt. % magnesium addition. They further noted that YS values goes up with increase of magnesium content, except for 0.7% Mg, probably due to the loss of Mg to the intermetallics of $\pi$ morphology . In addition, the ductility was lower in alloys with high magnesium content than the lower magnesium containing alloys, probably due to the occurrence of larger $\pi$-based intermetallics and silicon particles.

### *Influence of Manganese.*

Manganese is usually an unwanted contamination in many cast alloys, in many gravity casting compositions, it is usually maintained and regularised to low amounts. However, low levels of Mn (usually at Mn/Fe greater or equal to 0.5) plays a pivotal function in mixing with Fe to form the $\alpha$-Fe phases that are less harmful in the place of $\beta$-Fe phases which are brittle and which acts as stress concentrators when in use and undesirably reduces the machinability and mechanical performance.

According to Hwang et al. [48], when the manganese content in an Al-7Si-3.8Cu-0.5Fe (all in wt.%) 319 alloy was increased up to 0.65% (ratio of magnesium to iron was 1.2), the UTS and elongation were increased. As of late, it was discovered that as the manganese content increments more than 0.5% in aluminum compounds, both YS and UTS rose considerably without diminishing

reducing elongation. Addition of Mn to aluminium alloys improves the UTS and also considerably enhancing low-cycle fatigue strength.

Lee et al. [49] found that the expansion of manganese to commercial 6000, 7000 and 8000 arrangement aluminum compounds altogether increments both YS and UTS without loss of elongation. They attributed this to the formation of manganese dispersoids ($Al_6Mn$) that have an incoherent relationship with the matrix and which consequently retard the movement of dislocations resulting in strength increase. They further observed that addition of manganese in the range of 0.7-1.2 wt. % not only enhanced the tensile strength but also improved the low-cycle fatigue and corrosion resistance.

Cho *et al*. [50] investigated addition of Mn, Cr, and Ti to the cast automotive piston alloy Al-12Si(CuNiMg) and found Mn to be an extremely successful alloying component which they credited to increment of the volume fraction of the intermetallic phases. They additionally noticed that option of 0.5 wt. % Mn addition together with adding the amounts of Cu and Ni, brought about the improvement of high temperature strength.

### *Influence of Iron.*

Fe is the most well-known contaminating influence in aluminum and its variants. It isn't effectively expelled and it can make unwanted impacts to castability and ductility, especially in the prominent Al-Si castings. The decision of whether to utilize alloys in view of primary aluminum (which has low iron levels but greater costs) or secondary aluminum (less expensive due to moderate to high iron contents) for a cast item is frequently a business choice. Be that as it may, a trade off might

23

be vital between the want for decreased metal cost and the need to expand the efficiency of the casting process by formation of less defects and to limit the pernicious impact of iron on mechanical properties.

Iron's reactions in Al-Si alloys generate various compounds the most widely recognized of which are $FeAl_3$, α-AlFeSi and $FeMnAl_6$. These phases which are basically insoluble are the ones that improve the strength, particularly at high temperatures, although they also cause the microstructure to become embrittled. As the percentage of insoluble stages increments with the increase in the addition of iron, casting decisions such as the characteristic of the feed are antagonistically influenced. Fe additionally partakes in the formation of slime together with Mn, Cr and various other alloying elements

The impact of iron on the mechanical performance of aluminum alloys has been evaluated widely by a few researchers [14, 48, and 49]. It is reliably known that increase of iron levels decreases the ductility of Aluminium-Silicon alloys. This is generally by a reduction in toughness together with a reduction in strength. Generally, nonetheless, the YS remains to a great extent unaffected by Fe, unless elongation is decreased to such a degree, to the point that brittle fracture happens preceding yield.

The adverse impact of iron starts at very low essential Fe levels yet turns out to be considerably more genuine once a basic Fe level (subject to amalgam sythesis) is surpassed. This negative impact of Fe on malleability is mostly because of two reasons. Right off the bat, the size and

number thickness of the malicious stages increments with iron content. These phases take part straightforwardly in the mechanism of failure and in this manner, increased levels of these phases, lowers the ductility of the alloy. Besides, as the iron level expands, porosity increments. Porosity significantly affects ductility.

### *Influence of Zirconium.*

Zirconium in the Al-Si alloys plays a grain refining role and adds into the microstructure dispersoids which are thermally steady at high temperatures and which additionally enhance mechanical performance of A356 alloys. The $Al_3Zr$ particles which are precipitated are not as successful as $Mg_2Si$ dispersoids at expanding the hardness of the alloy. Be that as it may, the moderate dissemination of Zr in Al keeps them from being coarse at temperatures of around 130-150 °C, the temperature interval at which $Mg_2Si$ particles start coarsening and lossing their strength [54].

Quite recently, investigations on the effect of transition elements specifically 0.28 V, 0.18 Ti, and 0.15 Zr (all in wt. %) in the A356 aluminum alloy demonstrated an enhancement of fatigue and tensile strengths albeit causing a detriment on ductility [9, 12]. Further, Seperhband and associates [54] altered the A319 Al-Si casting alloy by micro-alloying with Zr which enhanced the UTS and tribological qualities.

Yuan et al. [55] studied a Al-Si alloy homogenized at 550°C for 24 hours, hot-rolled and cold-rolled, solution heat treated at 550°C for half an hour, aged naturally for 14 days and artificially aged at 180°C for half an hour or 11 hours. They discovered that for the addition of zirconium by

25

over 0.15% by weight, both hardness and tensile strength increased as compared to the base alloy without zirconium addition. The researchers credited this improvement in mechanical performance to the Al$_3$Zr phase. In addition to the development of intermetallics, the grains became finer as a result of Zr additions.

Mahmudi et al. [29] investigated the impacts of 0.15 wt.% Zr increases on the mechanical performance and wear characteristics of an A319 casting aluminiumm alloy. They found no confirmation of Al-Zr particles in the modified alloy as indicated by similar hardness values with the base alloy. They reasoned that no zirconium-rich intermetallics were developed during solidification. Be that as it may, a 15% distinction was found between the hardness of the two alloy variants after a 24 hour solutionising at 503°C which they credited this distinction to the development of Al3Zr particles.

Baradarani and Raiszadeh [56] investigated strength increase by precipitation hardening on a zirconium containing Al-Si cast aluminum alloy and found that the grouping of Zr in the combination (0.1– 0.3 wt.%) did not have any huge effect on the grain refinement of the as-cast structure or on the hardness of the age-solidified amalgam. Furthermore, Fasoyinu et al [57] investigated the impact of B, Sc, Ti and Zr on grain refinement and reasoned that Zr as a viable grain refiner ought to be available at levels of 0.37-0.69 wt.%.

*Influence of Vanadium.*

Vanadium can be found as an impurity in Al-Si alloys from the primary production process. Ludwig [58] and co-workers believe that this impurity will increase in the coming years due to

26

increased contamination from raw materials such as alumina, petroleum coke, coal tar pitch, and recycled anode butts which are used during electrolytic reduction to produce primary aluminium. Vanadium is also added in small amounts so as to form thermally stable precipitates for applications requiring high-temperature strength [10].

Casari et al. [33, 56] examined the impact of vanadium and nickel on the mechanical performance of A356 aluminum cast alloys and found that vanadium enhances the tensile properties and the toughness as depicted by impact testing of the alloys, which they attributed to the formation of $Al_{10}V$ and $Al_3V$ stages. Vanadium levels of 0.1-0.2 wt.% are accounted for to refine the FeMn mixes. As indicated by Mondolfo [21], vanadium has a gentle grain refinement impact, however contrasted with ordinary grain refiners, for example, Ti and $TiB_2$, vanadium is somewhat wasteful. The phase that is associated with grain refinement is $Al_3V$ that has an $Al_3Ti$-like crystal structure. In this manner vanadium could hypothetically substitute for titanium and go about as the covering layer on $TiB_2$. There is, nevertheless, significant difference in the materials science field as to what degree vanadium assumes a part as a grain refiner. Edwards et al. [23] detailed a reduction in grain size in a near-eutectic Aluminium-Silicon automotive piston alloy with a consolidated inclusion of Zr, Vand Ti. Maitland [60] discovered a mild grain refining effect with the addition of vanadium. This was most noticeable for a mix of manganese and vanadium addition in wrought AlMgSi alloys.

*Influence of Titanium*

It is normal practice to include titanium in little sums (i.e. < 0.02 wt.%) to Al-Si casting alloys due to its intense grain refining impact. It develops $TiAl_3$ which nucleates essential aluminum dendrites. More regular nucleation of dendrites implies a bigger number of littler grains [21]. Saheb *et al.* [24] found that the addition of Ti (up to 4 wt.%) to an Aluminium-Silicon alloy brought

about an increment in the hardness and the wear strength of the binary compound because of the precipitation of the moderately hard intermetallic compound $Al_3Ti$ stage.

Be that as it may, Saheb et al. [24] watched that extra titanium may cause issues in the fluid metal process and result in casting defects, as a result of coarse TiAlSi precipitation over the fluid temperature.

Zeren and Karakulak [62] characterized the microstructure of an Aluminium-Silicon alloy with 13.1 wt.% Si (near eutectic) with 0, 0.1, 1, 2, and 5 wt.% titanium. They observed that titanium containing compounds can have diverse morphologies (petals and flakes) contingent upon the titanium content, other alloying components and the warm history of the composite. The petal-like particles were found in the cast Al-Si-1Ti microstructure while the piece like particles were found in the cast Al-Si-2Ti and the Al-Si-5Ti microstructures. They additionally noticed that despite the fact that the compounds had a most extreme vanadium substance of 0.2 wt.%, the impact of vanadium was not watched, so the connection of titanium and vanadium should be examined further. The scientists likewise detailed that expanding the Ti content up to 5 wt.% Ti expanded the hardness of the compound which they ascribed to an expanded volume part of hard TiAlSi intermetallics. Also, they watched that the weight reduction of the as-cast Al-Si-Ti combination diminished with expanding Ti content up to 1 wt.% Ti.

### *Influence of Chromium.*

Chromium is commonnly added to many aluminium-magnesium-silicon alloys in small quantities, usually less than 0.35wt.% so as to improve ductility and toughness due to modification of $Al_5FeSi$

29

intermetallic inclusions from a platelet to a cubic form. In overabundance of these points of confinement, exceptionally coarse constituents are formed together with other additions or impurities such as Mn, Fe, and Ti [21].

Chromium is also used to prevent recrystallization of grains in Al-Mg-Si alloys during heat treatment or hot rolling [22]. Moreover, chromium is reputable of having the potent to modify and eliminate the $\beta$-Al$_5$FeSi intermetallic phase [67].

Abdulwahab [68] discovered that upon addition of Chromium and Manganese in different percentages, i.e. from 0.1 to 0.5% (0.1, 0.2, 0.3, 0.4, and 0.5%) to an aluminium-silicon-iron alloy with the percentages of iron and silicon kept constant, fine precipitates of (Fe)$_3$SiAl$_{12}$ and CrAl$_2$ were formed and which were responsible for the alloy's UTS and hardness enhancement. Nevertheless, the addition of Chromium weakened the impact strength of the alloy.

*Influence of Strontium.*

Strontium is known to modify eutectic Si particles in Al-Si cast alloys from large acicular form to a fine fibrous structure that is less detrimental to mechanical properties such as ductility and fracture toughness [65]. Strontium has become the most popular modifier in industry because it is semi-permanent in nature (the effect of modification with strontium retains evens after repeated re-melting processes) unlike the modification with the other modifiers like sodium which fades on re-melting.[2]. Modification treatments improve strength, ductility, and machinability. Strontium is also known to influence the formation Fe- and Cu-bearing intermetallic particles. However, an excess amount of strontium tends to lead to porosity [69].

30

## 2.4.2   Effect of Heat Treatment on Cast Al-Si Alloys

Heat-treatment improves the hardness, tensile strength, resistance to creep and fatigue in aluminum alloys by precipitation hardening a strengthening process of non-ferrous alloys. Heat treatment happens amid the cooling and heating of an Al alloy during which precipitates that restrict/hinder the motion of dislocations are developed in the Al dendritic matrix. Firstly, the alloy must be solutionised by heating lower than the eutectic temperature for a sufficient period to permit solutionising of the intrmetallics. The alloy should then be quenched to low temperatures usually room temperature before aging by heating to moderate temperatures so as to permit precipitation to take place [82].

The solutionising temperature should be selected close to the last solidified phase and should enable the complete dissolution of the available phases while incipient melting of some phases like the Q-$Al_5Cu_2 Mg_8Si_6$ phase that melt at low temperatures should be avoided because that would lead to a reduction in the alloy's mechanical performance as a result of void formation. The solutionising time also have to be optimised as a solutionising time that is too short will not be sufficient to dissolve all the alloying elements and make them present for precipitation hardening, on the other hand, solutionising for too long a period uses a lot of energy than would be required.

Studies by Lombardi *et al.* [83] revealed that solutionising at 500 °C for 8 hours lessened the volume fraction of the $Al_2Cu$ phase by up to 70% and higher solutionising period at 500°C caused a steady increase yield strength and ultimate tensile strength increase although this increment was fairly less and does not warrant the extra solutionising time. They further noted that solutionising

at 515 °C and 530 °C caused a decrease in yield strength and ultimate tensile strength, they attributed this reduction in strength to incipient melting of $Al_5Mg_8Cu_2Si_6$ and $Al_2Cu$ phases which caused harmful ultra-fine eutectic groups to form.

Wang *et al.* [84] while did a differential scanning calorimetry study on an Al-11Si-4Cu-0.3Mg (wt.%) alloy so as to optimize its solutionising time illustrated that after 10 hours of solutionising at five hundred degrees celsius , the eutectic copper phase had dissolved fully. They also concluded that lower melting point polynary phases were produced when the copper content exceeded 2 percent with an increase in its amount being witnessed as the copper content was also increased. Therefore, they suggested the constricting solutionising temperature where incipient melting of the grain boundaries should respectively be 500, 500, 500, 535, and 555°C for Al-11Si-xCu-0.3Mg alloys with 4, 3, 2, 1 and 0 wt.% Cu.

More research on dissolution of $Al_2Cu$ phase in 319 alloys by Han *et al.* [85] revealed that the undissolved $Al_2Cu$ phase volume fraction was lowest after eight hours of solution treatment at 490 °C, moreover, Sokolowski *et al.* suggested a 2-step solutionising procedure of eight hours at 495 °C + two hours at 520 °C. Therefore, the phase Q-$Cu_2Mg_8Si_6Al_5$ with that melts at 507°C would have its dissolution occuring in the first stage due to its low melting point. The second step which has a high solution treatment temperature dissolves the remainder of the copper containing phases and homogenize the alloy's microstructure further.

Artificial aging occurs when the supersaturated solid solution which are not stable thermodynamically achieved by quenching is allowed to reach equilibrium conditions by

accelerated precipitation of atoms at a relatively higher temperature (as compared to the natural aging that occurs at room temperature) for a period of time. The aim is to produce an array of finely dispersed precipitates from the saturated solid solution. Growth of the precipitates occurs where atoms from the solid solution which is supersaturated difuse out [86]. Temperature and time are the key variables of aging which influence the mechanisms of strengthening in precipitation hardening.

Shaha *et al.* [87] studied the ageing characteristics of Aluminium-Silicon-Copper-Magnesium alloys with additions of Ti, Zr, Cr, and V alloying elements. During artificial ageing at 200°C after 1 hour, a hardness value of 93 HRF was realised in the alloy while it reached peak hardness after 9 hours at 150°C. However, a drop in the maximum hardness is experienced due to an increase in the ageing period for the alloy aged at 200°C. Also, after aging for 9 hours at 100°C and 250°C, peak hardness was not realised in this alloy. They therefore concluded that this failure to reach peak hardness was caused by slow diffusion of the Ti, Cr, Zr and V atoms in aluminium dendritic matrix at these temperatures and consequently resulted in a low percentage of the precipitate's volume fraction.

Colley [91] experimented with an A356 alloy aged at 150, 180 and 200 °C and found out that it achieved a yield strength of 256 MPa after 3 hours at 180°C while for the alloy aged at 200°C, the maximum yield strength of 250 MPa was achieved after only 1 hour. The researcher also observed the over-ageing behaviour of the material at artificial ageing times longer than 3 hours at 180°C. The decrease in yield strength took place very slowly compared with the strengthening observed

33

during under-ageing. Most of the strengthening during under-ageing at 180°C was achieved within the first 30 minutes, whereas a yield strength of 210 MPa was measured after artificial ageing for 60 hours. The ductility of the alloy also appeared to recover slightly during over-ageing, as precipitated particles become larger, weaker and less able to prevent dislocation movement.

# CHAPTER 3: METHODOLOGY

## 3.1 Preparation of Secondary Cast Al-7Si-0.45Mg Ingots

70 kg of post-consumer aluminium wheels were sourced from scrap vendors in Nairobi, removed of external parts and cleaned. The aluminium wheels were then melted up to 740°C under a cover flux in an oil fired crucible furnace at J.K.U.A.T. The melt was skimmed before pouring onto a preheated ladle and then transferred into mild steel ingot moulds as shown in Figure 3.1 and allowed to solidify. Samples for chemical analysis were taken from the molten bath and rapidly solidified in a specially fabricated copper mould made to ASTM specification E716-94 [70, 71] by immediately immersing in cold water. The solidified samples were then machined and subjected to Spark Optical Emission Spectroscopy (OES) at Numerical Machining Complex (NMC) in Nairobi. The chemical composition of the scrap ingot is given in Table 3.1.



Figure 3.1. Pouring of the cast aluminium melt into (a) a preheated ladle and then (b) the ingot steel moulds.

Table 3.1. Chemical composition of base alloy (scrap Ingot).

|  | Composition (wt. %) | | | |
|---|---|---|---|---|
| Element | Trial 1 | Trial 2 | Trial 3 | Average |
| Si | 7.05 | 6.66 | 7.15 | 6.95 |
| Cu | 0.0941 | 0.0759 | 0.0960 | 0.0887 |
| Mg | 0.500 | 0.371 | 0.465 | 0.445 |
| Fe | 0.232 | 0.199 | 0.200 | 0.210 |
| Mn | 0.161 | 0.152 | 0.161 | 0.158 |
| Cr | 0.0180 | 0.0165 | 0.0177 | 0.0174 |
| Ti | 0.0547 | 0.0629 | 0.0592 | 0.0589 |
| Zr | 0.00130 | 0.00100 | 0.00980 | 0.00403 |
| V | 0.00680 | 0.00710 | 0.00780 | 0.00723 |
| Sr | 0.00090 | 0.00100 | 0.00093 | 0.00094 |
| Al | Bal. | Bal. | Bal. | Bal. |

## 3.2 Preparation of Permanent Mould Bar Castings

### 3.2.1 Mould Design and Fabrication

Cast iron blanks were used to machine permanet moulds by a computer aided milling machine. The mould consists of two parts and was designed such as to avoid turbulent surface film and bubble entrainment in the liquid. Figures 3.2, 3.3 and 3.4 show the design and drawings of the mould. The CNC milling machine used for the machining is shown in Figure 3.5 while Figure 3.6 shows one half of the mould being machined.
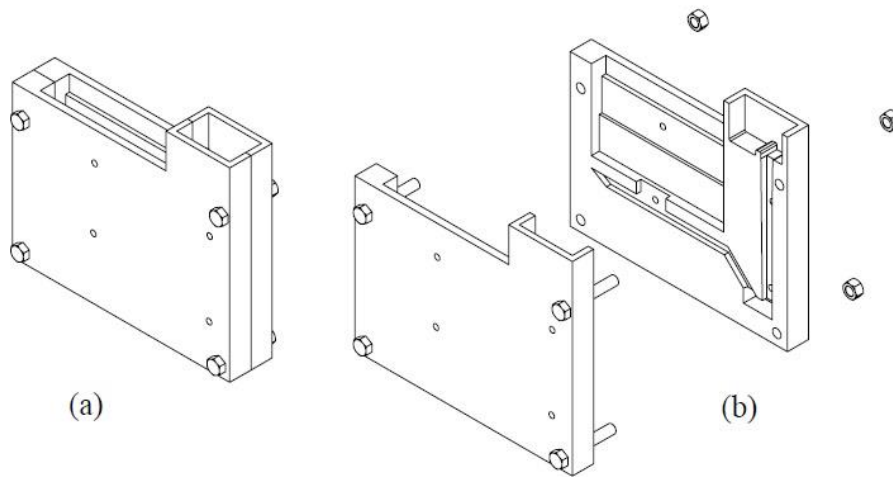
Figure 3.2. (a) A schematic diagram of the assembled permanent mould used to produce stepped bar castings. (b) an exploded view of the mould.
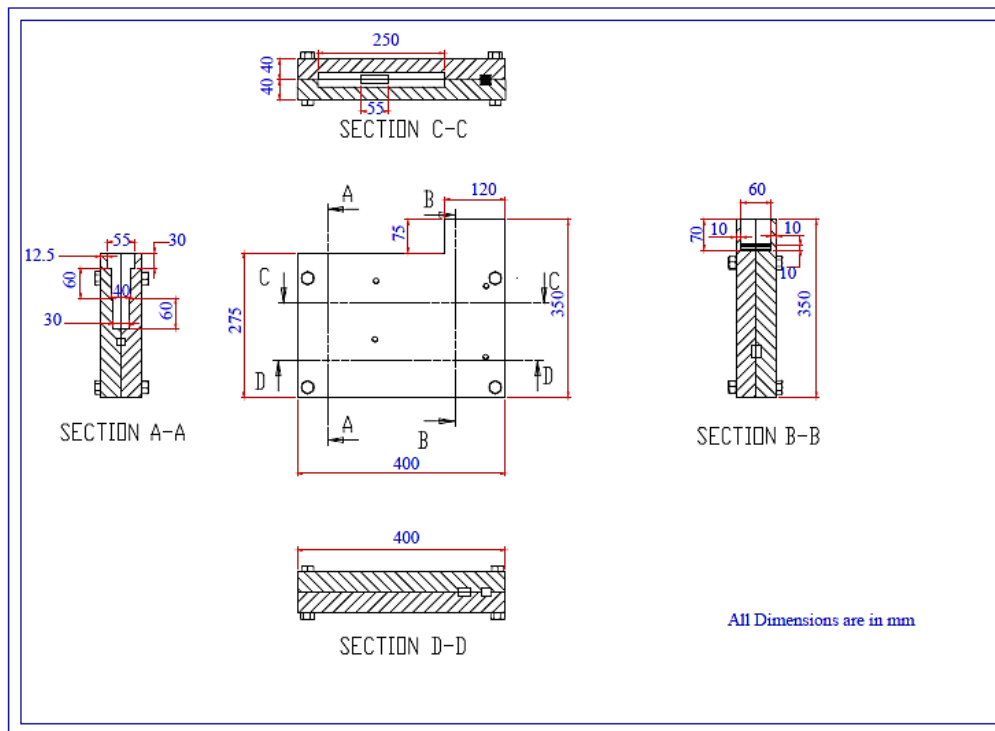


Figure 3.3 Fabrication drawing with dimensions of the permanent mould..

37
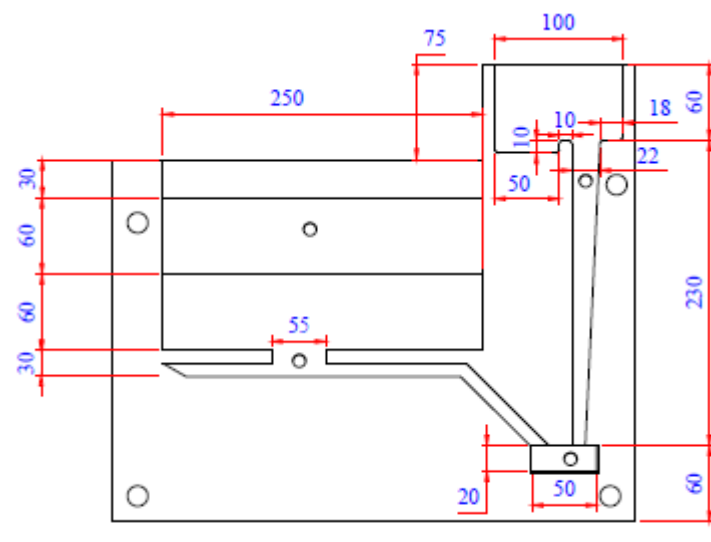
Figure 3.4. More details of the mould shown in the centre of Figure 3.2.



Figure 3.5. The computer numerically controlled (CNC) milling machine used to machine the permanent mould.

38
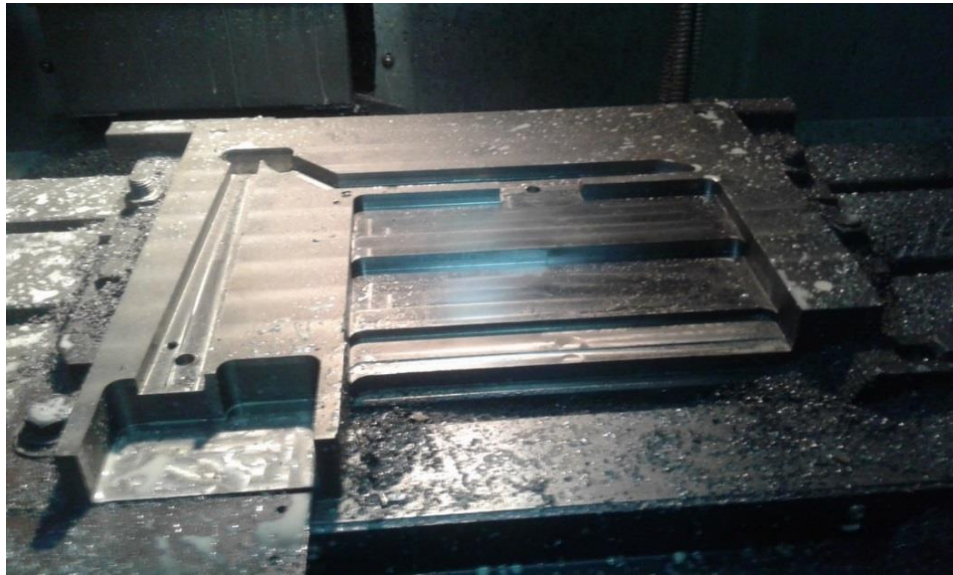
Figure 3.6. One half of the permanent mould inside the CNC milling machine.

### 3.2.2 Preparation of Bar Castings

Melting of the aluminium ingots was carried out in a 5 kg capacity graphite crucible using an electric muffle furnace at the Department of Mechanical and Manufacturing Engineering workshops at the University of Nairobi. The furnace temperature was maintained at 740°C. Master alloys of Al-50 wt. % Cu, Al-15 wt. % Ti, Al-5 wt. % V, Al-10 wt. % Zr, and Al-10 wt. % Cr were added in the form of briquettes so as to achieve the target chemistry while Al-10 wt. % Sr was added in rods so as to achieve modification of the microstructure. The melt was stirred to allow for complete dissolution and homogenization of the alloy. Nitrogen gas was used for degassing the melt by passing through a ceramic tube immersed deep into the molten metal. The degassed melt was then skimmed to remove dross and surface oxides before pouring into the permanent metal mould that had been preheated to 495°C.

A ceramic foam filter with dimensions of 50x50x20 mm and 30 pores per inch (PPI) was placed in the mould for each casting to minimize turbulence during pouring and to trap inclusions. Figure 3.7 shows the casting that was obtained after the molten aluminium solidified and was removed from the mould and the compositions of base alloy variants that were developed for testing is given in Table 3.2. The chemical composition presented in Table 3.1 for the ingot alloy shows that it is a 356 type alloy. The alloy variants in Table 3.2 that were obtained by addition of Cu, V, Ti, Zr and Sr are therefored coded based on the 356 alloy.



Figure 3.1. The bar casting obtained after the melt had solidified inside the permanent mould.

Table 3.2. Experimental alloys produced and codes assigned.

| Alloy code | Experimental alloys with the total composition of each additive element in the alloy (wt. %). |
|---|---|
| 356 | As per Table 3.1 |
| 356+TiSr[a] | 356 + 0.15% Ti + 0.015% Sr. |
| 356+0.5Cu+X[b] | 356 + 0.5% Cu + 0.15% Ti + 0.15% Zr + 0.25% V + 0.15%Cr + 0.015% Sr. |
| 356+3.5Cu+X | 356 + 3.5% Cu + 0.15% Ti + 0.15% Zr + 0.25% V + 0.15%Cr + 0.015% Sr. |

[a]*TiSr = ∼0.15%Ti+0.015%Sr;* [b] *X= ∼0.22%V+0.15%Cr+0.1%Zr+0.15%Ti+0.015%Sr*

### 3.3 Hot Isostatic Pressing

Hot Isostatic Pressing (HIPping) is a post-casting process used to remove porosity in castings and thus minimizes scatter in the mechanical properties as well as to improve its fatigue resistance, ductility, and impact toughness. The process subjects the material which is contained in a hot chamber to an inert gas under high pressure for a specific duration of time and thereby closing up porosity. All test castings in this work were shipped to Quintus Technologies in Vasteras, Sweden for HIPping. The castings were held 3 h at 500°C inside a pressurised argon atmosphere of 150 MPa.

### 3.4 Preparation of Specimens and Heat Treatment

The specimens for mechanical property testing and microstructure investigation were sectioned from the top larger section of the bar castings and subjected to a T6 heat treatment in a Nabertherm® electric muffle furnace located at the Department of Physics of the University of Nairobi. The alloys with copper in their composition were solution heat treated at 500 °C for 6 h, quenched in water at 60°C, immediately aged at 190°C for 100 h and left to cool in air. The alloys without copper in their composition were solution heat treated at 540°C for 6 h, quenched in water at 60°C, immediately aged at 190°C for 100 h and left to cool air.

### 3.5 Tensile Testing

The tensile specimens were machined according to the ASTM B557M-02a standard as shown in Figures 3.8 and 3.9. The tests was performed at both room and at 237°C using an Instron® 300DX universal testing machine (see Figure 3.10) located at the Department of Civil Engineering of

Masinde Muliro University of Science and Technology in Kakamega, Kenya. The load train includes two push rods and threaded holders in order to pull M10x1.25 threaded end specimens whose details are shown in Figures 3.8 and 3.9. A computer interfaced with the machine is used capture the load increaments together with the corresponding guage length extension as measured by an extensometer. At high temperature (237°C). The universal testing machine was coupled with an SF-16 split furnace with a 3 x 11-inch heat zone that can heat up to 1200°C. K-type thermocouples give signals to a three-zone temperature control system that controls electrical power to each zone in the furnace chamber.

The temperature on the specimen was determined by attaching a thermocoulple to the gauge section of the specimen. Model RT-214 high-temperature extensometer made by instron was used to measure strains. As a result, the high-temperature tensile properties such as yield strength, ultimate tensile strength, and elongation were determined. Actual specimens used for both the room and high-temperature tests are shown in Figures 3.9.
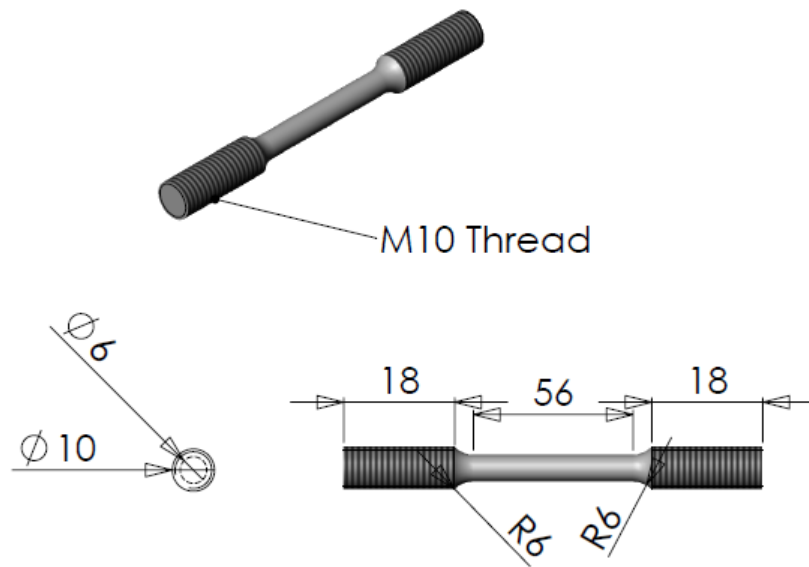
Figure 3.8. Details of the room and elevated temperature tensile test specimens.



Figure 3.2. Specimens used for the tensile test.

Figure 3.10. The Instron 300Dx universal testing machine (UTM) used for tensile testing.

## 3.6 Fatigue Testing

Specimens for the fatigue life testing were prepared according to ASTM E606 specifications using a CNC lathe machine at NMC. The dimensions of the specimens and a picture of the specimen before the test are depicted in Figures 3.11 and 3.12 respectively. An SM 1090 rotating bending fatigue machine from TecQuipument Ltd was used for the test and is shown in Figure 3.13.
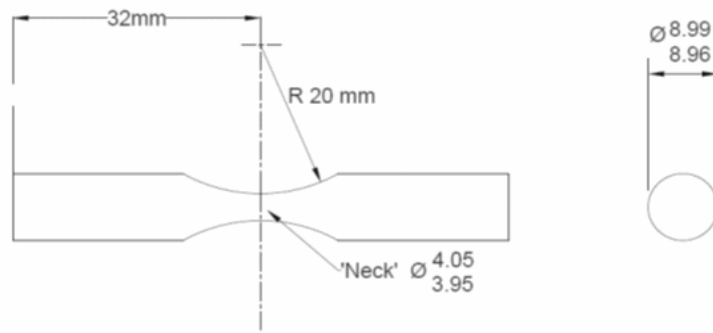
Figure 3.3. Fabrication details of the fatigue specimen.



Figure 3.4. Specimens used for the fatigue test.
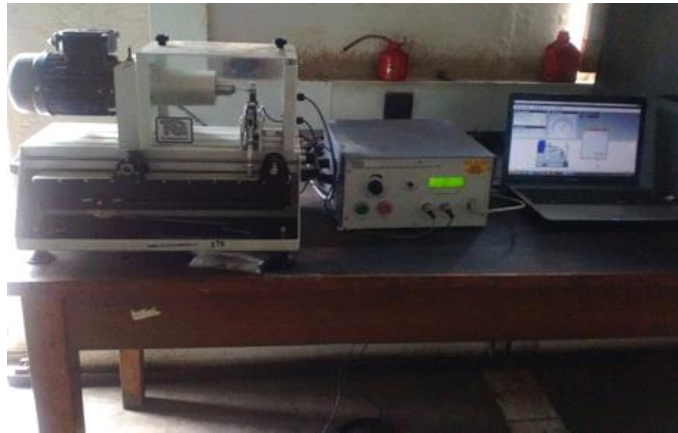
Figure 3.5. SM 1090 rotating bending fatigue machine.

All of the fatigue tests were conducted at room temperature at a frequency of 60 Hz using the staircase method. The objective of the tests was to find the fatigue strength at $10^7$ cycles. The initial stress for all the four alloys was chosen as 75.8 MPa and the test was done sequentially with a stress increment/decrement of 8.9 MPa depending on whether the previous specimen was a failure or a run-out. If the specimen failed before reaching $10^7$ cycles, the stress level for the next specimen was decreased by 8.9 MPa. Conversely, if the specimen reached the $10^7$ cycles without failing (i.e., a run-out), then the stress level for the next specimen was increased by 8.9 MPa. This process was repeated until all the 8 specimens allocated for each alloy were used up.

### 3.7 Metallography

Specimens for microscopy were sectioned and subjected to standard metallographic methods of grinding and polishing. Grinding was carried out using successively finer grades of silicon carbide paper (i.e. 800 and 1000 grit) and then polished with 6 μm, 3 μm, 1 μm, and ¼ μm diamond paste

46

impregnated in appropriate polishing cloths. The final polishing was achieved with 0.05 μm oxide particle suspension (OPS). Any left-over OPS particles were washed away with water at this final stage and the sample carefully dried using a drier and swabbed using cotton drenched in methanol.

Fractured tensile and fatigue test samples were mounted in bakelite resin and a low-speed diamond cutter was used to cut at the edge so as to split the specimen axially (perpendicular to the fracture surface) and expose one half of the specimen. The same procedure used for grinding and polishing specimens for microstructure investigation was also used for these fractographic specimens.

## 3.8 Microstructure Characterisation

Optical images were taken at various magnifications using an optical microscope (BX 41M Olympus Microscope) located at the Department of Mechanical Engineering in JKUAT. Figure 3.14 shows the microscope together with the computer. The optical images taken were used to determine the SDAS and quantitative particle analysis using ImageJ (https://imagej.nih.gov/ij/). The linear intercept method was used for SDAS measurements where a line drawn across dendrites is divided by the number of dendrites it crosses over. These SDAS values were taken randomly from the microstructures of ten micrographs taken at a magnification of X200. For quantitative particle analysis, imageJ was used to determine area, circularity and aspect ratio of 20 images per alloy specimen and the data obtained was analysed using Minitab® (http://www.minitab.com/en-us/).

Scanning electron microscopy (SEM) was carried out using a Carl Zeiss LEO 1525 Field Emission Gun Scanning Electron Microscope (shown in Figure 3.15) at the National Metrological Institute

of South Africa (NMISA) in Pretoria, South Africa. Analysis of the second phases was performed with spot analysis by an Oxford Aztec Energy dispersive spectroscopy (EDS) detector, which was also used to create elemental maps. An accelerating voltage of 20 kV and a beam current of 10 μA were chosen to minimize the penetration volume whereas a working distance of 15 mm was chosen to get sufficient X-Ray signals for elemental analysis.
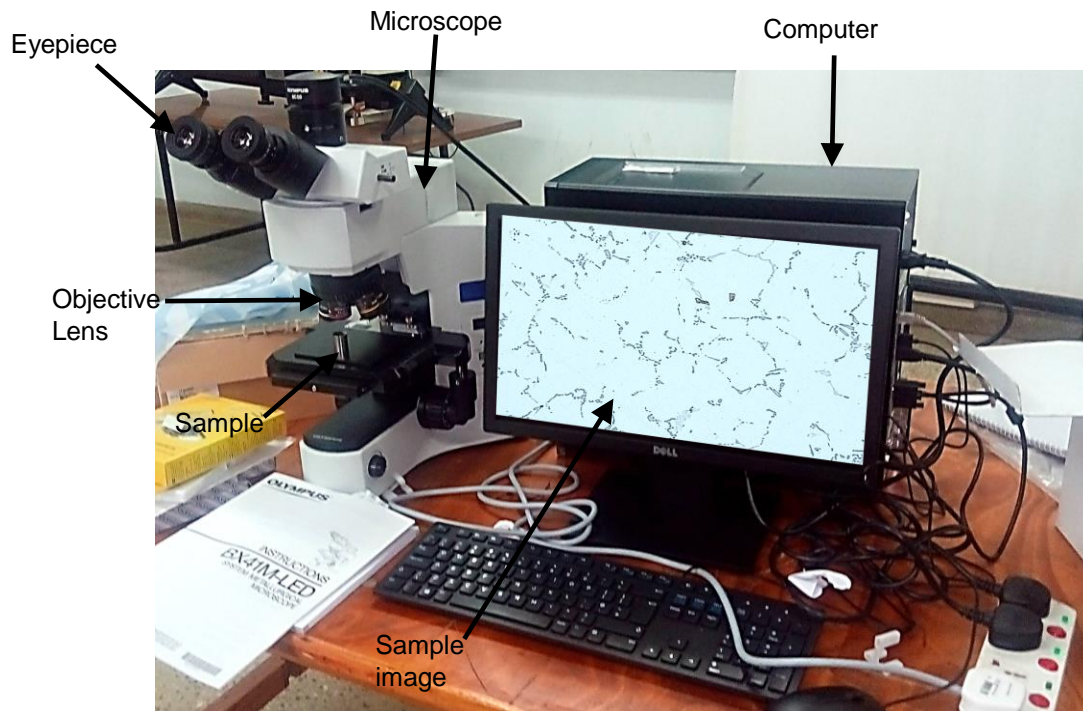


Figure 3.6. Optical microscope connected to the computer at JKUAT.

Figure 3.7. Scanning electron microscope at NMISA.

# CHAPTER 4: RESULTS

## 4.1 Qualitative Microstructural Analysis

As shown in Figure 4.1, the typical optical microstructures of these alloys exhibit $\alpha$-Al dendrites which are surrounded by an Al-Si eutectic and intermetallic phases. It can be seen that the microstructures do not have casting defects such as porosity due to HIPping.

Secondary dendrite arm spacing (SDAS) is directly related to the average cooling rate and usually ranges between 10-40 µm for permanent mould castings and 25-100 µm for sand castings [69]. Alloy 356+TiSr had an SDAS value of 28.4 µm while 356+0.5Cu+X had an SDAS of 32.6 µm. The 356 base alloy and alloy 356+3.5Cu+X had unmodified microstructures that do have exhibit well defined dendrite arms. It was therefore difficult to make meaningful SDAS measurements.

## 4.1.1 Alloy 356

The microstructure is unmodified since Sr was not added in this alloy. Therefore, coarse acicular eutectic silicon particles are present in this alloy as can be seen in Figure 4.1. The primary $\alpha$-Al matrix and intermetallic phases can also be identified. Figure 4.2a is an elemental EDS mapping of the alloy showing the phases present while Figure 4.2b is a backscattered SEM image showing some of the phases in the microstructure that were identified by EDS spot analysis. Figure 4.3 is an image of the spectra for phases identified. It can be seen that AlSiMgFeMn and AlSiCrVFeMn phases are present in the alloy.
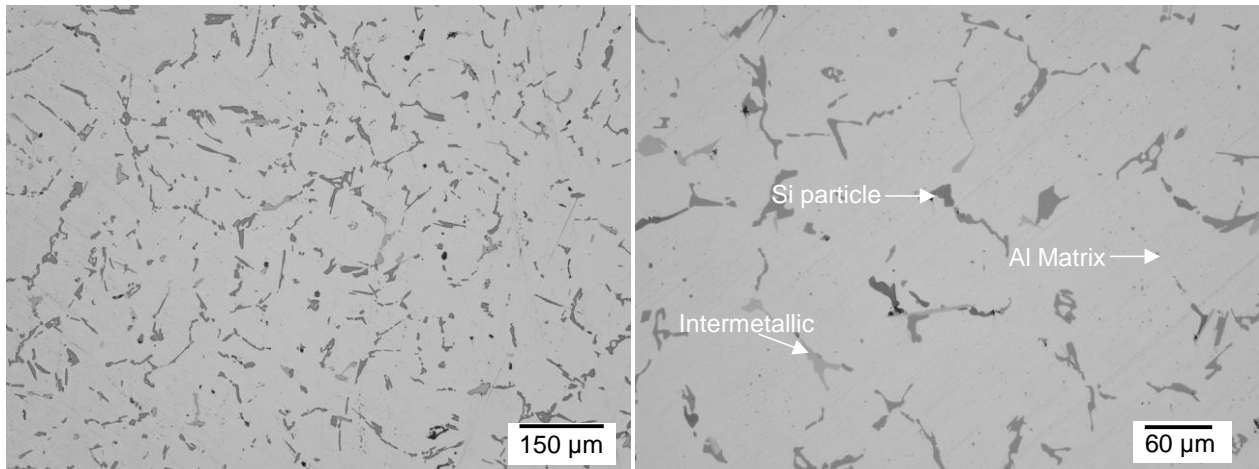
Figure 4.1. Optical Micrograph of alloy 356 showing an unmodified microstructure with an Al matrix, Si particles and intermetallics.
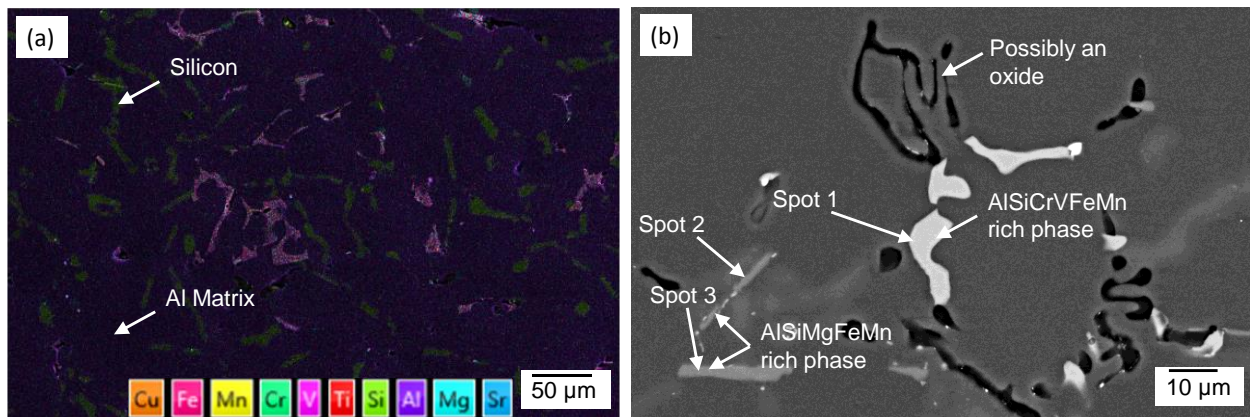


Figure 4.2. SEM Micrographs of alloy 356. (a) An elemental map of the alloy with particular colour codes indicating presence of specific elements in the alloy, (b) A backscattered electron SEM image of the alloy.
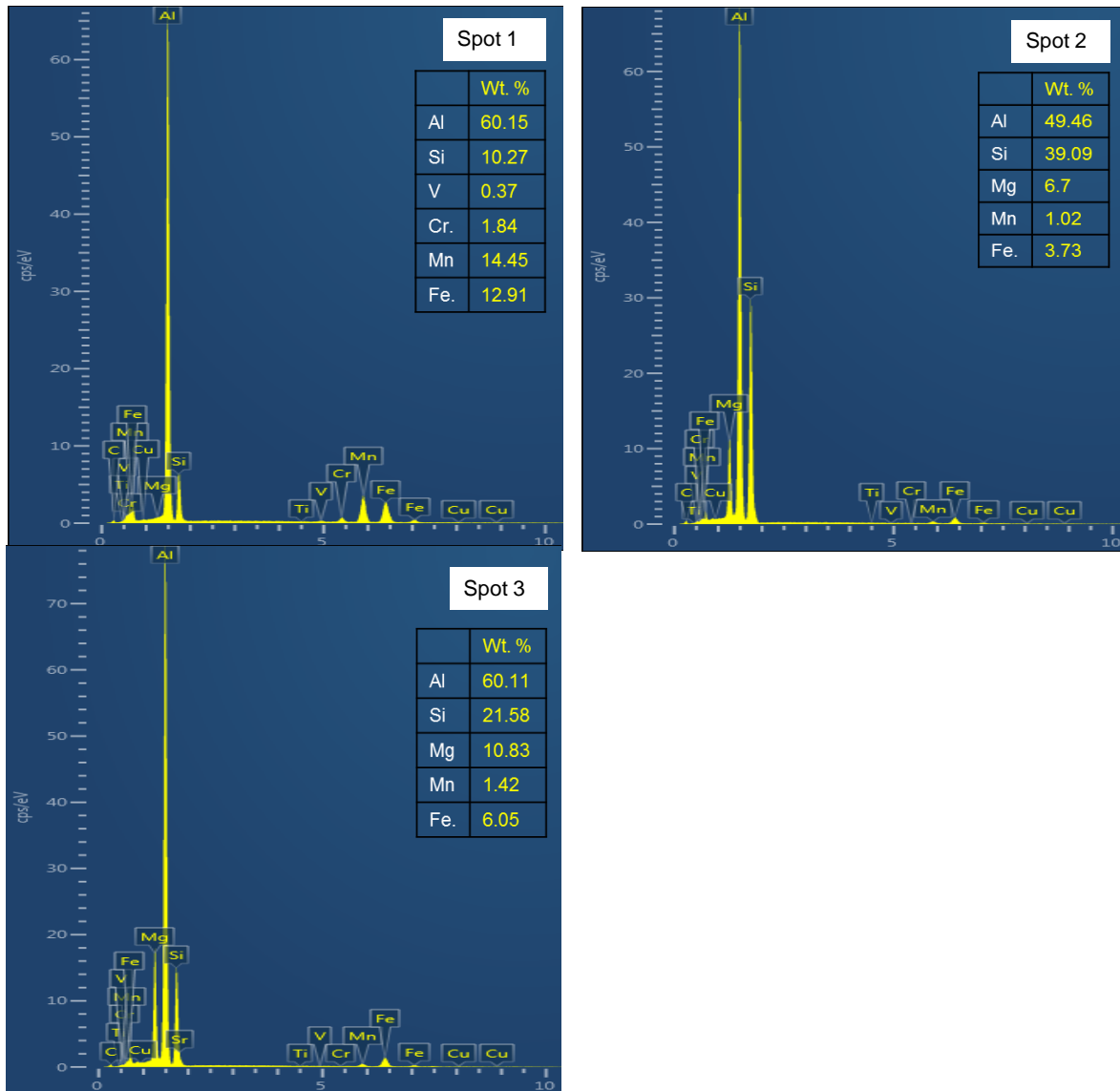
Figure 4.3. EDS Spectra of Phases in alloy 356. Peaks of the various elements i.e. Al, Si, V, Cr, Mn and Fe can be seen with a tabulation of the actual composition for each element.

## 4.1.2 Alloy 356+TiSr

Figure 4.4 shows the primary α-Al matrix, modified eutectic silicon particles and intermetallic phases present in this Sr modified alloy containing 0.15%Ti. Figure 4.5 shows elemental EDS mapping of the alloy and the phases present. Figure 4.6 shows the spectra for the phases identified in Figure 4.5. In this alloy, it is clear that the addition of Sr modified the microstructure from a coarse acircular Si particles to a fine fibrous structure as seen in the optical micrographs in Figure 4.4 compaired with the unmodified base alloy microstructure shown in Figure 4.1. It can also be seen that the AlMgSiMnFe phase present in the base alloy is also identified in this alloy.
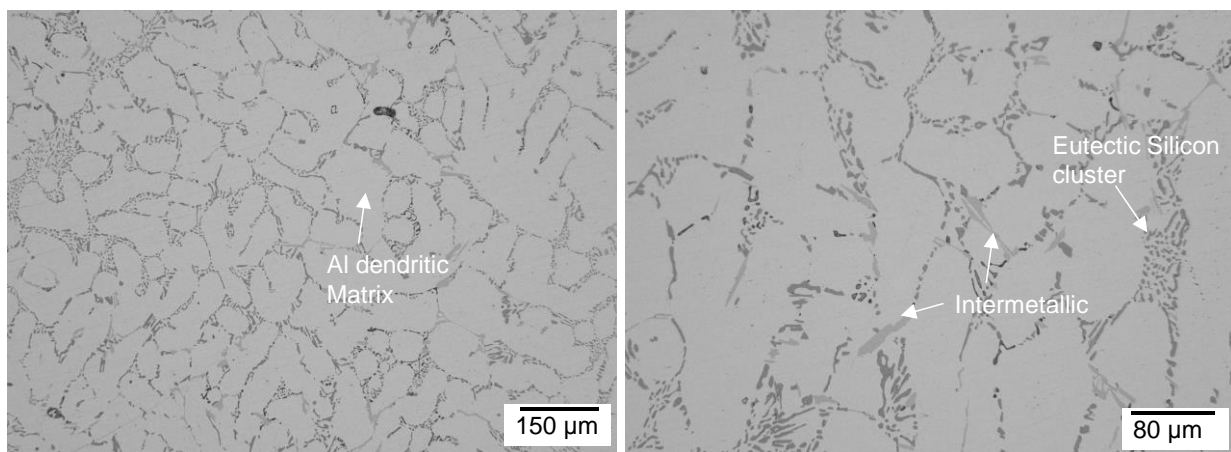


Figure 4.4. Optical Micrograph of 356+TiSr. In the micrograph, a modified microstructure with eutectic silicon particles, aluminium dendritic matrix, and intermetallics can be seen.

53
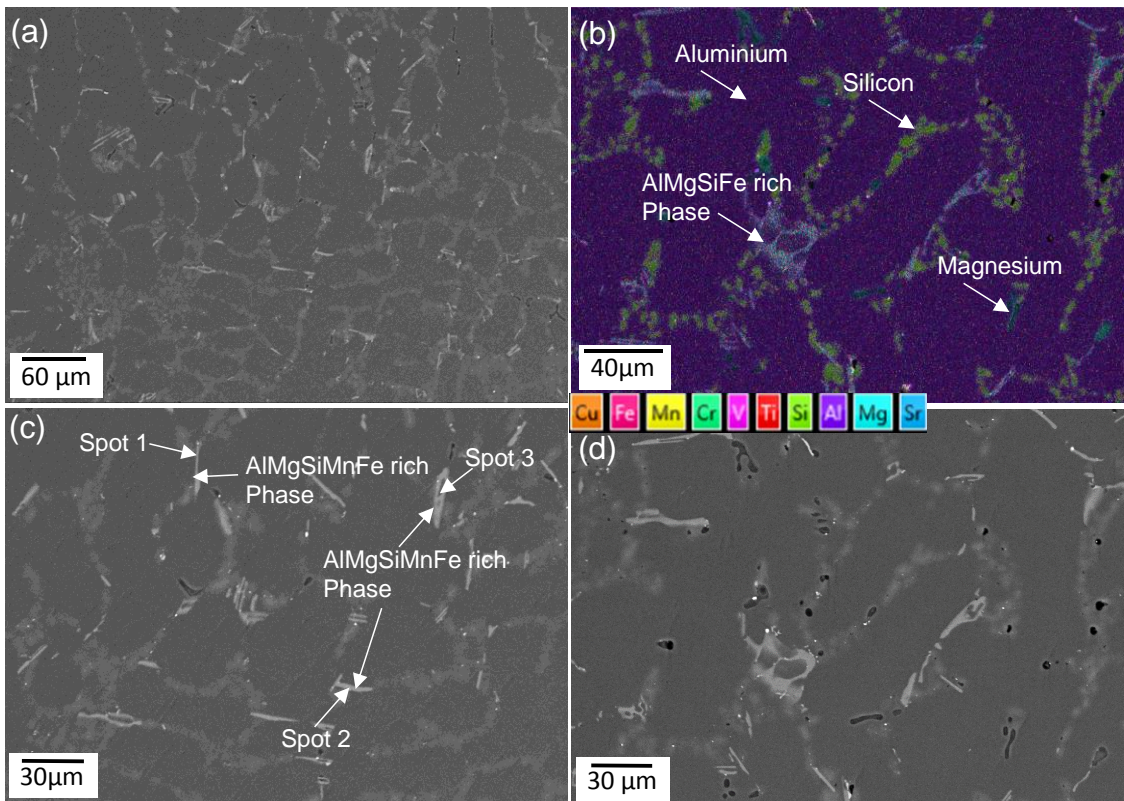
Figure 4.5. SEM Micrograph of 356+TiSr. (a), (c) and (d) are backscattered images at different magnifications. (b) is an elemental mapping of the microstructure. Phases identified by EDS (their spectra are in Figure 4.6) are labelled in (c).

| | Wt. % |
|---|---|
| Al. | 62.69 |
| Si. | 24.15 |
| Mg | 7.73 |
| Mn. | 0.67 |
| Fe. | 4.77 |

Spot 1

| | Wt. % |
|---|---|
| Al. | 63.55 |
| Si. | 19.29 |
| Mg | 9.74 |
| Mn. | 1.29 |
| Fe. | 6.14 |

Spot 2

| | Wt. % |
|---|---|
| Al. | 85.27 |
| Si. | 8.84 |
| Mg | 3.59 |
| Mn. | 0.39 |
| Fe. | 1.98 |

Spot 3
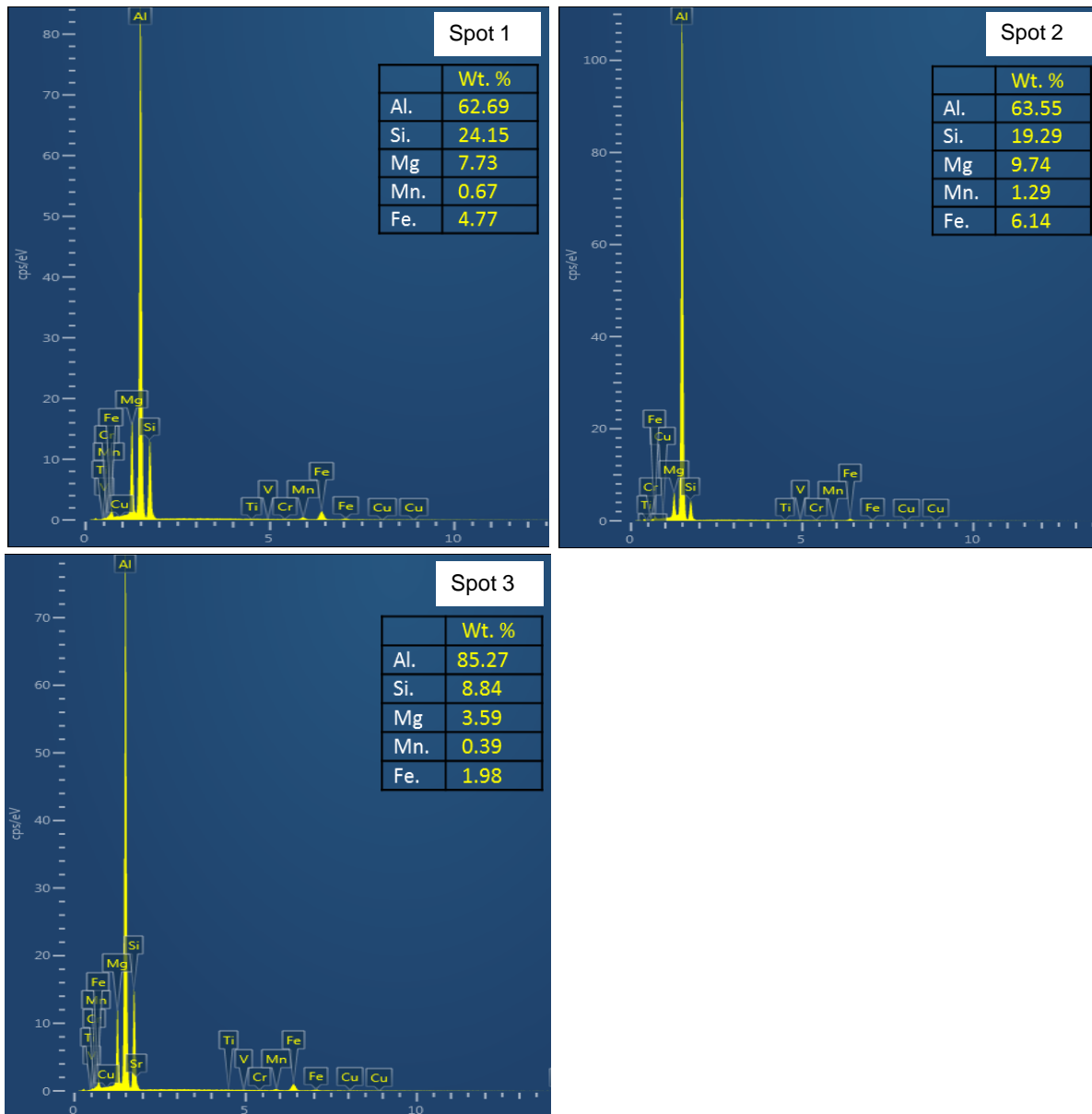
Figure 4.6. EDS Spectra of Phases in 356+TiSr as labelled in Figure 4.5(c). Peaks of the various elements i.e. Al, Si, Mg, Cr, Mn and Fe can be seen with a tabulation of the actual composition for each element.

### 4.1.3 Alloy 356+0.5Cu+X

This alloy contains a modified microstructure with fine fibrous eutectic silicon particle, as shown in shown in Figure 4.7. Figure 4.8a and b are elemental EDS mapping images of the alloy showing the phases present while c and d are backscattered SEM images of the alloy showing phases that were identified by EDS spot analysis. In Figure 4.9, the spectra of the phases identified in Figure 4.8 are shown. AlSiMgTiV and AlSiTiVZr phases can be observed in the micrographs together with other Ti and V rich phases.
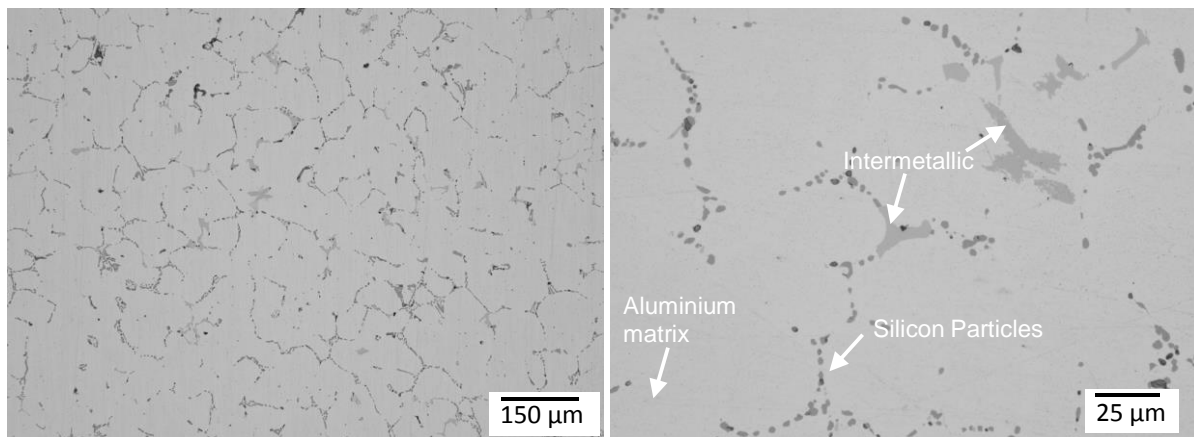


Figure 4.7. Optical micrograph of alloy 356+0.5Cu+X. It can be seen that the microstructure is modified and contains fine silicon particles, an aluminium matrix and intermetallics.
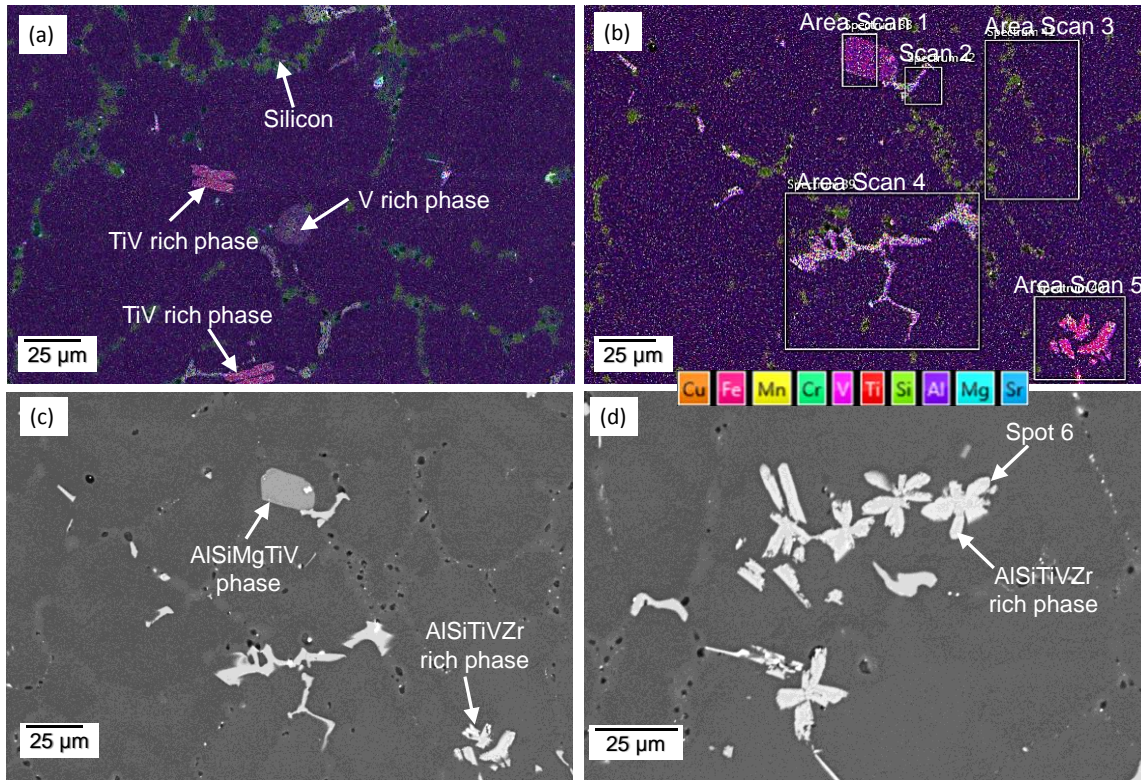
Figure 4.8. The different phases observed in 356+0.5Cu+X by SEM. (a) and (b) are elemental EDS mapping images of the alloy showing the phases present while (c) and (d) are backscattered SEM images of the alloy showing phases that were identified by EDS spot analysis.

**Spot 6**

| | Wt.% |
|---|---|
| Al. | 67.51 |
| Si. | 7.43 |
| Mg. | 0.2 |
| Ti. | 11.22 |
| V. | 6.57 |
| Cr. | 0.29 |
| Zr. | 6.76 |

**Area Scan 1**

| | Wt.% |
|---|---|
| Al. | 80.61 |
| Si. | 2.46 |
| Mg. | 4.87 |
| Ti. | 2.01 |
| V. | 7.63 |
| Cr. | 0.93 |
| Cu. | 0.49 |
| Zr. | 1 |

**Area Scan 5**

| | Wt.% |
|---|---|
| Al. | 86.15 |
| Si. | 4.97 |
| Mg. | 0.3 |
| Ti. | 3.58 |
| V. | 2.09 |
| Cr. | 0.26 |
| Cu | 0.38 |
| Zr. | 2.66 |

**Area Scan 2**

| | Wt.% |
|---|---|
| Al. | 89.58 |
| Si. | 5.39 |
| Mg. | 0.34 |
| V. | 0.58 |
| Cr. | 0.89 |
| Mn. | 0.97 |
| Fe. | 1.72 |
| Cu. | 0.53 |
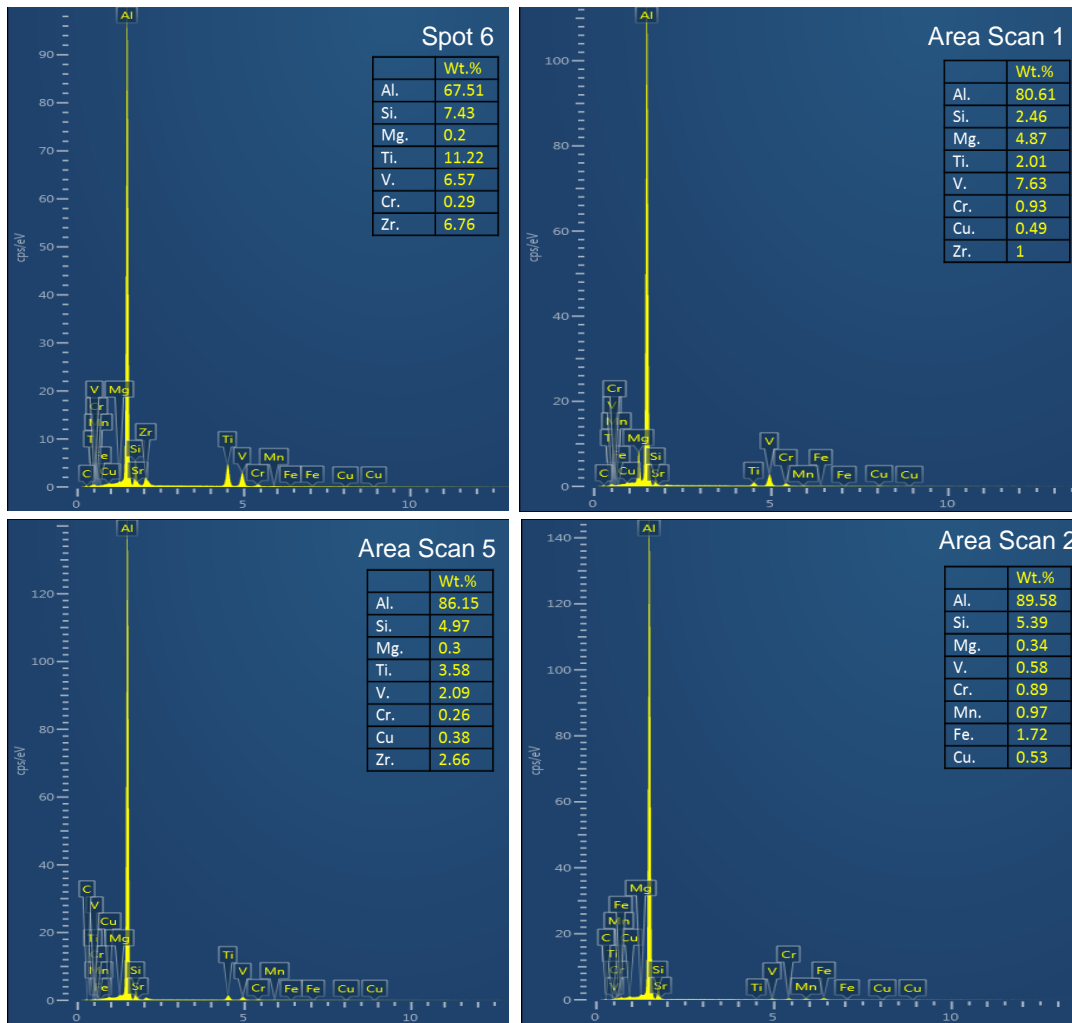
Figure 4.9. EDS elemental mapping of alloy 356+0.5Cu+X.The particular phases identified are labelled in figure 4.8 (b) and (d). Peaks of the various elements i.e. Al, Si, Mg, Ti, V, Zr, Cu, Cr, Mn and Fe can be seen with a tabulation of the actual composition for each element.

## 4.1.4 Alloy 356+3.5Cu+X

Figure 4.10 shows the microstructure of 356+3.5Cu+X that has coarse eutectic silicon particles, the primary $\alpha$-Al matrix and large script-like intermetallics. Figure 4.11(a) is an elemental EDS mapping image of the alloy showing the AlSiVCrMn phase and large unmodified silicon particles present in the alloy. Figure 4.11b, c, and d are backscattered SEM images of the alloy showing phases that were identified by EDS spot analysis such as AlSiTiZr and AlSiCrMnFeCu. Moreover, fine AlSiTiVCu precipitates were identified by an area scan of the matrix. Also, note the cracking of the blocky intermetallics in Figure 4.11c that is believed to be due to HIPping.
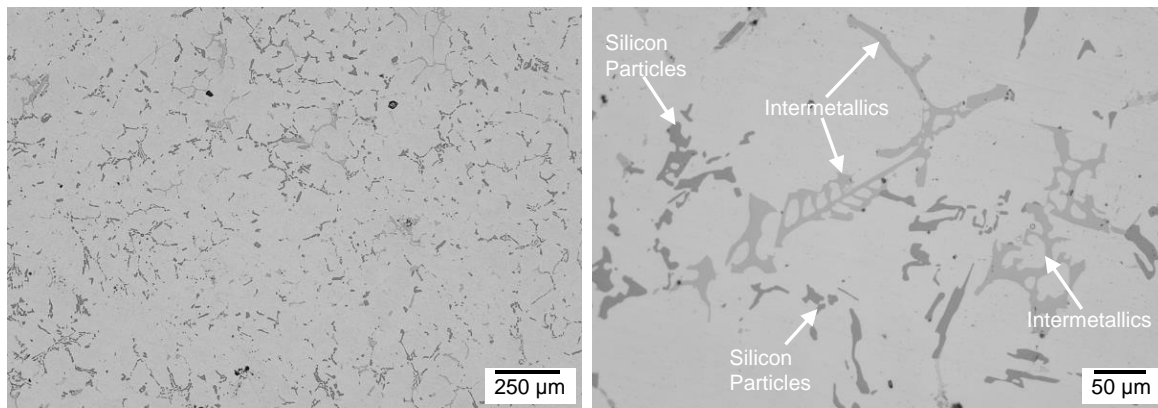


Figure 4.10. Optical micrograph of 356+3.5Cu+X. An unmodified microstructure with large intermetallics and silicon particles can be seen in (b).
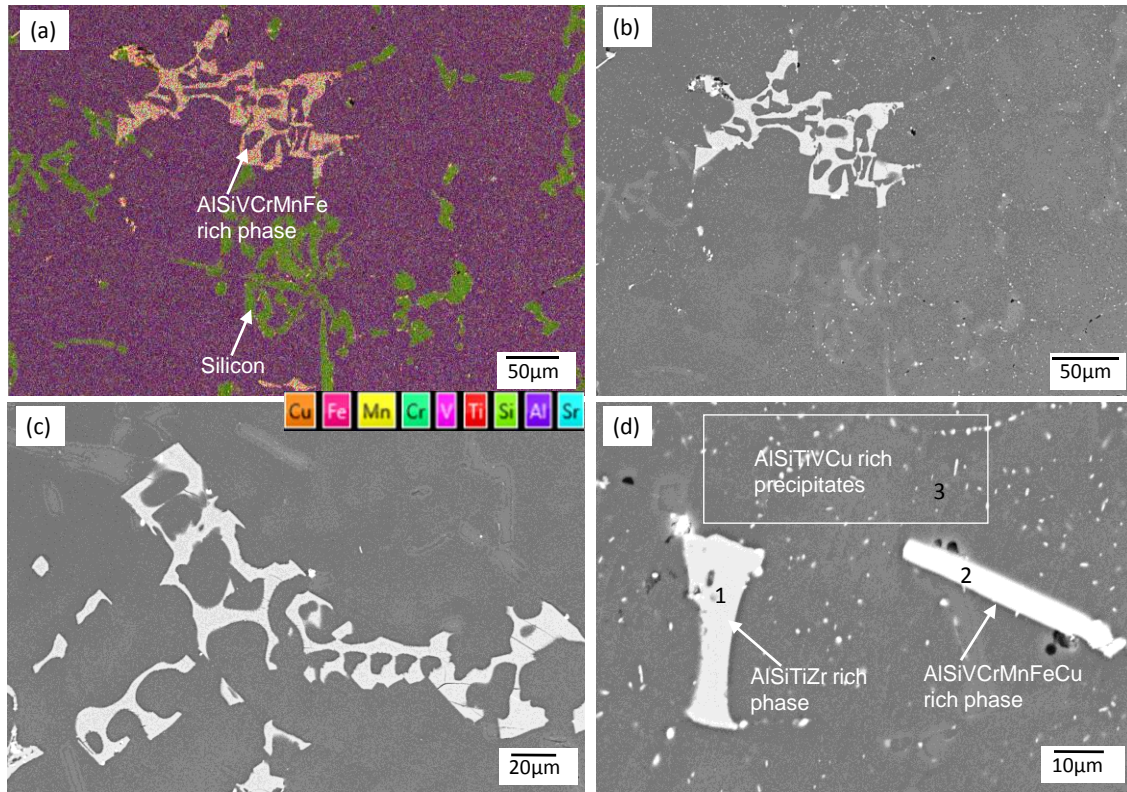
Figure 4.11. Typical SEM micrograph of 356+3.5Cu+X. (a) An elemental EDS mapping image of the alloy showing the AlSiVCrMn phase and large unmodified silicon particles (b), (c), and (d) are backscattered SEM images of the alloy showing phases that were identified by EDS spot analysis.
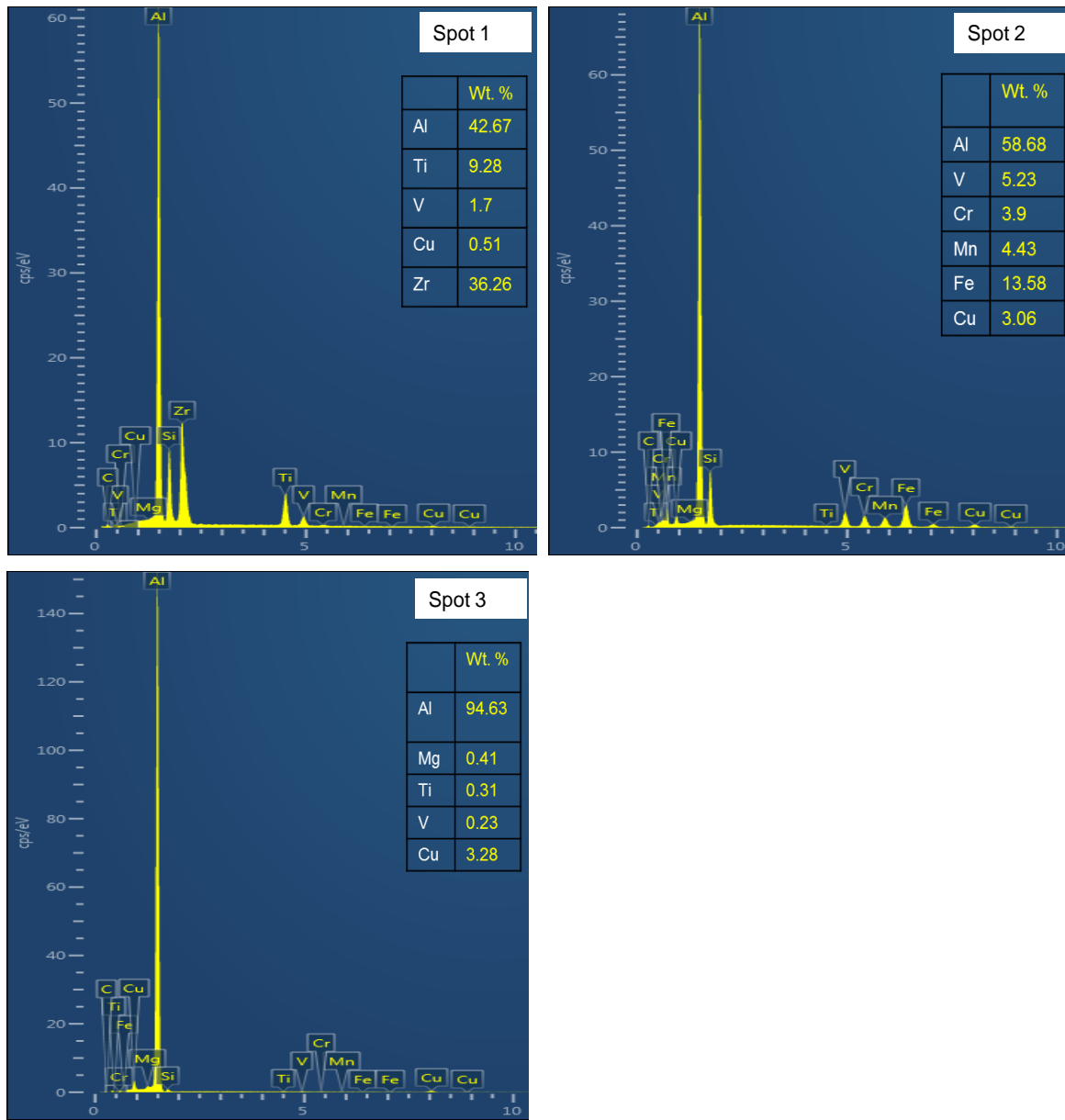
Figure 4.12. EDS elemental mapping of 356+3.5Cu+X. The particular phases identified are labelled in figure 4.11 (d). Peaks of the various elements i.e. Al, Mg,Ti, V, Zr, Cu, Cr, Mn and Fe can be seen with a tabulation of the actual composition for each element.

## 4.2 Quantitative Microstructural Analysis

Particle size data obtained from ImageJ mesearements were fitted into the 3-Parameter Weibull and 3-Parameter Lognormal distributions to establish the best fit. These are shown Figures 4.13, and 4.14 respectively.

There are various ways to know whether the data is normally distributed or not. The first is to look at the p-value, if it is less than 0.05 (5 percent threshold), we can confidently reject the null hypothesis. i.e. there is sufficient evidence to conclude that the distribution is not normally distributed. If the p-value is greater than 0.05, we fail to reject the null hypothesis (there isn't sufficient evidence that the distribution is not normally distributed). Secondly, the Anderson darling value can give an indication whether the distribution is normally distributed or not. If the Anderson-Darling is greater than 1 then the data cannot be regarded as normally distributed and vice versa [79, 80]. Lastly, looking at the line itself and the data points can give an indication whether the data is nornmally distributed or not. A straight line with all data points lying on this line is a sign of normally distributed data and the converse is true.

From figures 4.13 and 4.1, we seen that the data is not normally distribured because of presence of data that is spilling out of the guide line and large Anderson Darling values. However, of all the probability functions tried, the 3-parameter lognormal plot is the closest fit and was adopted nonetheless.

62

| | Loc | Scale | Thresh | N | AD | P |
|---|---|---|---|---|---|---|
| ● 356 | 3.709 | 1.522 | 4.752 | 833 | 2.215 | * |
| ■ 356+TiSr | 3.014 | 1.292 | 4.798 | 2472 | 2.888 | * |
| ◆ 356+0.5Cu+X | 2.555 | 1.165 | 4.376 | 2513 | 1.508 | * |
| ▲ 356+3.5Cu+X | 3.109 | 2.116 | 5.065 | 940 | 2.907 | * |
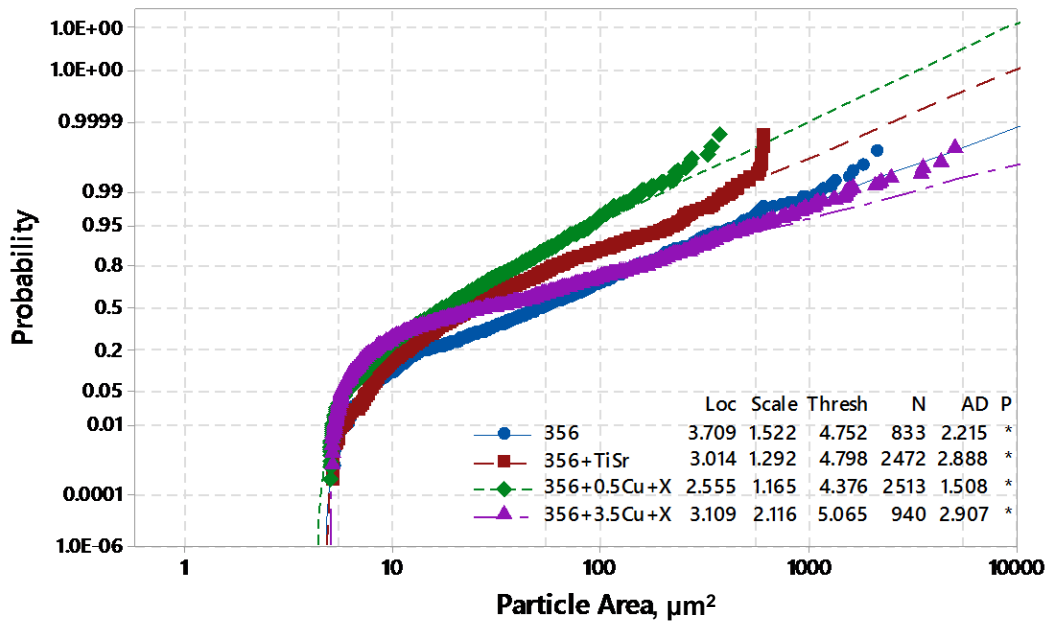
Figure 4.13. The 3-Parameter Lognormal probability plot of particle size for the four alloys.

63

| | Shape | Scale | Thresh | N | AD | P |
|---|---|---|---|---|---|---|
| 356 | 0.6956 | 83.97 | 5.221 | 833 | 2.923 | <0.005 |
| 356+TiSr | 0.7556 | 38.28 | 5.099 | 2472 | 38.716 | <0.005 |
| 356+0.5Cu+X | 0.8438 | 21.30 | 5.025 | 2513 | 8.286 | <0.005 |
| 356+3.5Cu+X | 0.5119 | 63.18 | 5.078 | 940 | 5.433 | <0.005 |
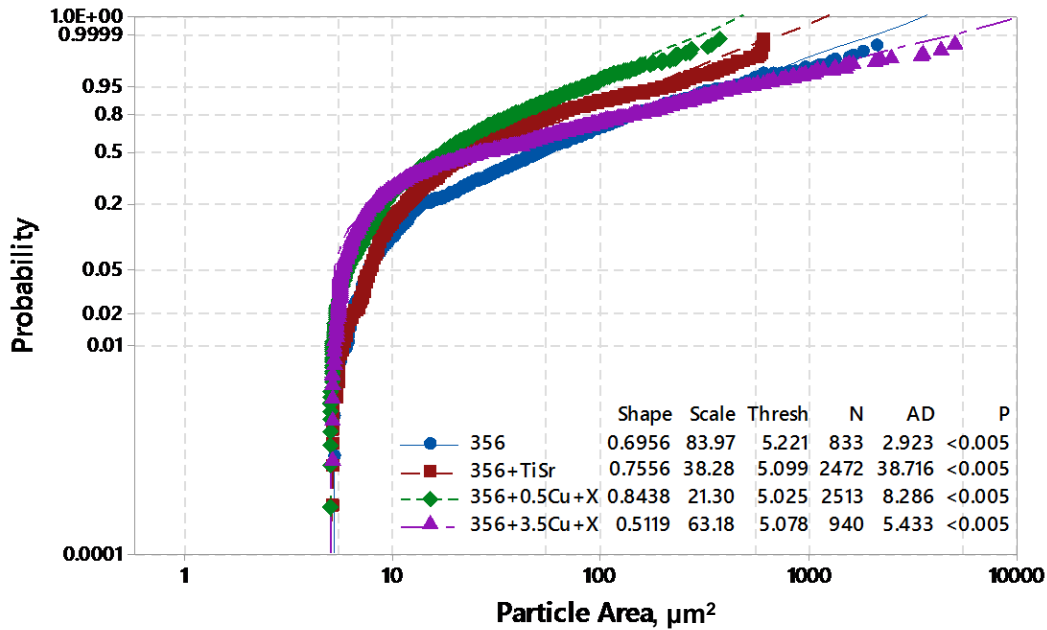
Figure 4.14. The 3-Parameter Weibull probability plot of particle size for the four alloys.

As observed by Mbuya [94], failure in cast Al-Si alloys originates from intermetallic particles which lie at the upper tail of the particle size distribution. Therefore, it was important to analyse data on this spectrum of the population and compare it to data from the whole population. The largest 0.1 percentage of the particle population was determined and fitted into various distribution plots with the 3-parameter lognormal and 3-parameter Weibull functions depicting good Anderson-Darling values for all the four alloys (Figures 4.15 and 4.16 respectively).

The Gumbel distribution function is one of the extreme value distribution functions that is used for minimum and extreme values of sample data. It is used for large particles in castings and it was expected that the upper tail of the particle size data would fit well into this function. However, for the Gumbel probability function, Anderson-Darling values are greater than 1 for all alloys except 356+0.5Cu+X and is therefore not a close fit as seen in Figure 4.17.
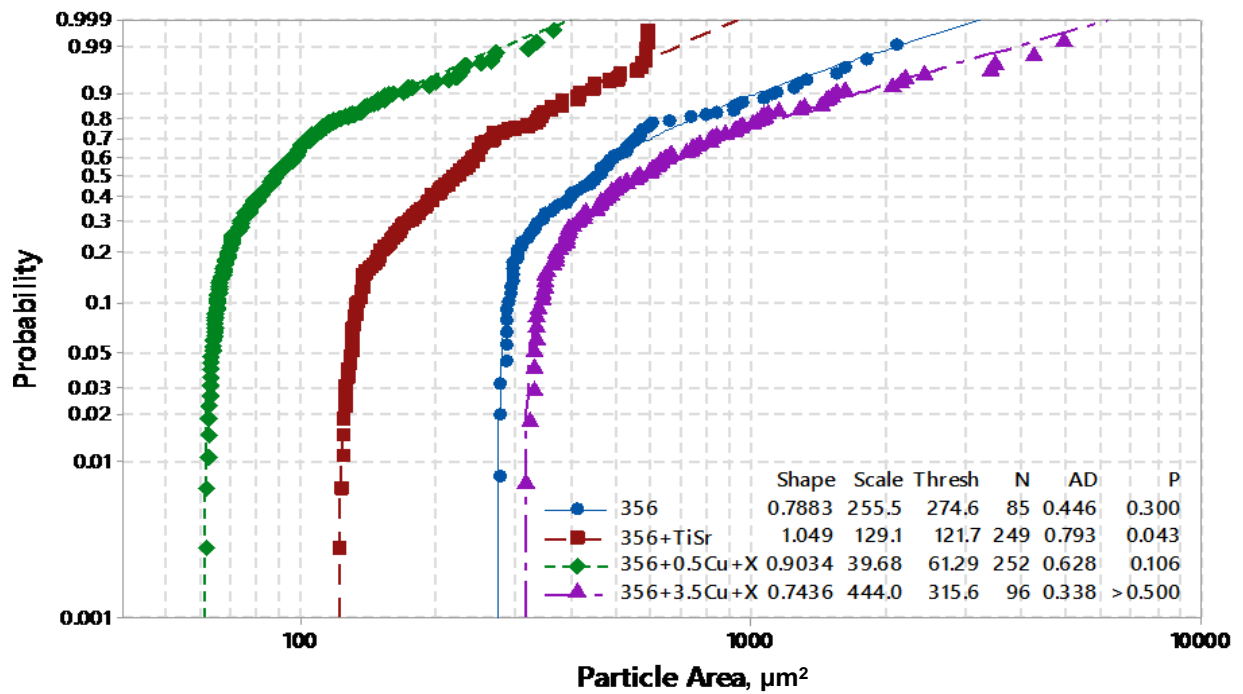


Figure 4.15. The 3-Parameter lognormal probability plots of the largest 0.1% of the particle size distribution of the alloys.

| | Shape | Scale | Thresh | N | AD | P |
|---|---|---|---|---|---|---|
| 356 | 0.7883 | 255.5 | 274.6 | 85 | 0.446 | 0.300 |
| 356+TiSr | 1.049 | 129.1 | 121.7 | 249 | 0.793 | 0.043 |
| 356+0.5Cu+X | 0.9034 | 39.68 | 61.29 | 252 | 0.628 | 0.106 |
| 356+3.5Cu+X | 0.7436 | 444.0 | 315.6 | 96 | 0.338 | >0.500 |
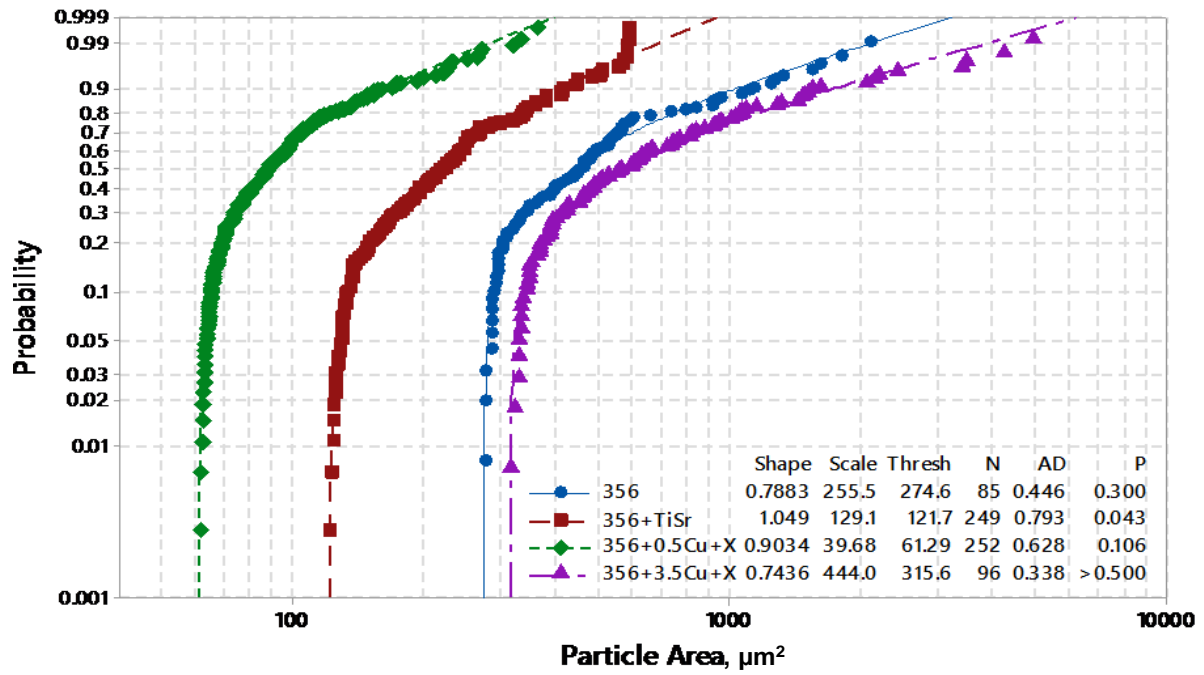
Figure 4.16. The 3-Parameter Weibull probability plots of the largest 0.1% of the particle size distribution of the alloys.
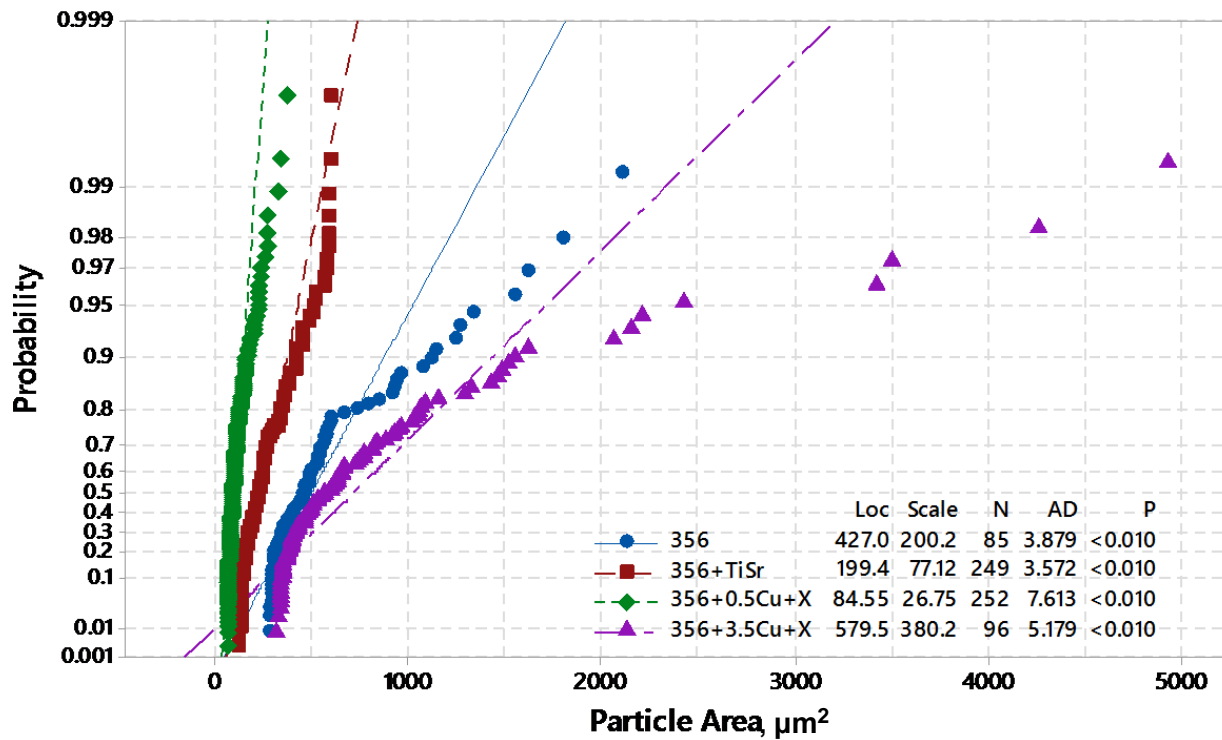
Figure 4.17. The Gumbel probability plots of the largest 0.1% of the particle distribution in the alloys.

Figure 4.18 shows a 3 parameter lognormal cumulative distribution plot of the particle area for the four alloys. It shows that the particle size distribution is heavily skewed towards smaller particles, the figure also displays the descriptive statistics (mean, median, minimum and maximum area) for each alloy. It can be seen that 356+0.5Cu+X has small particle sizes with the maximum particle size being 356.58 $\mu m^2$, while 356+3.5Cu+X has the largest at 4931.88 $\mu m^2$, alloy 356 has a maximum particle area of 2450.48 $\mu m^2$ while the largest particle of alloy 356+TiSr has a size of

67

1118.92 $\mu m^2$. This can be explained by the fact that 356 and 356+3.5Cu+X do not have modified microstructures while alloys 356+TiSr and 356+0.5Cu+X are modified. Modified silicon particles are small and near spherical shaped while on the contrary, unmodified silicon particles are large and irregular. Particle size and shape has significant effect on the damage and failure mechanisms when the material is subjected to mechanical loads. As discussed in section 4.4, the fatigue life of alloy 356+0.5Cu+X that is modified and has the smallest particle size is the greatest at 98 MPa. The 356 alloy that is unmodified and with one of the largest maximum particle size has the lowest fatigue strength at 71 MPa. However, other contributing factors like oxide films has not been considered at this point.

For the unmodified alloys, the damage is initiated by the cracking of eutectic silicon particles and intermetallic compounds. Since silicon crystals possess low fracture toughness, they do no deform but fracture easily when the load is applied. In addition, intermetallics are hard and brittle and also possess large size and aspect ratio, and so their presence in a soft Al matrix increases the crack nucleation tendency[96].

For the Sr-modified alloys, eutectic silicon particles which have small size and aspect ratio are more efficient in transfering load to the matrix and therefre less suscepticle to cracking as reported by Mbuya *et al.* [97]. Near-spherical shaped eutectic silicon particles delay crack nucleation and thus improve fatigue strength.

| | Min | Median | Mean | Max |
|---|---|---|---|---|
| 356 | 5.0 | 44.31 | 96.21 | 2450.48 |
| 356+TiSr | 5.0 | 24.23 | 44.78 | 1118.92 |
| 356+0.5Cu+X | 5.0 | 17.85 | 28.49 | 365.58 |
| 356+3.5Cu+X | 5.0 | 34.29 | 135.70 | 4931.88 |

| | Loc | Scale | Thresh | N |
|---|---|---|---|---|
| 356 | 3.509 | 1.572 | 4.530 | 2106 |
| 356+TiSr | 2.975 | 1.211 | 4.533 | 3914 |
| 356+0.5Cu+X | 2.555 | 1.165 | 4.376 | 2513 |
| 356+3.5Cu+X | 3.145 | 2.127 | 4.989 | 1263 |
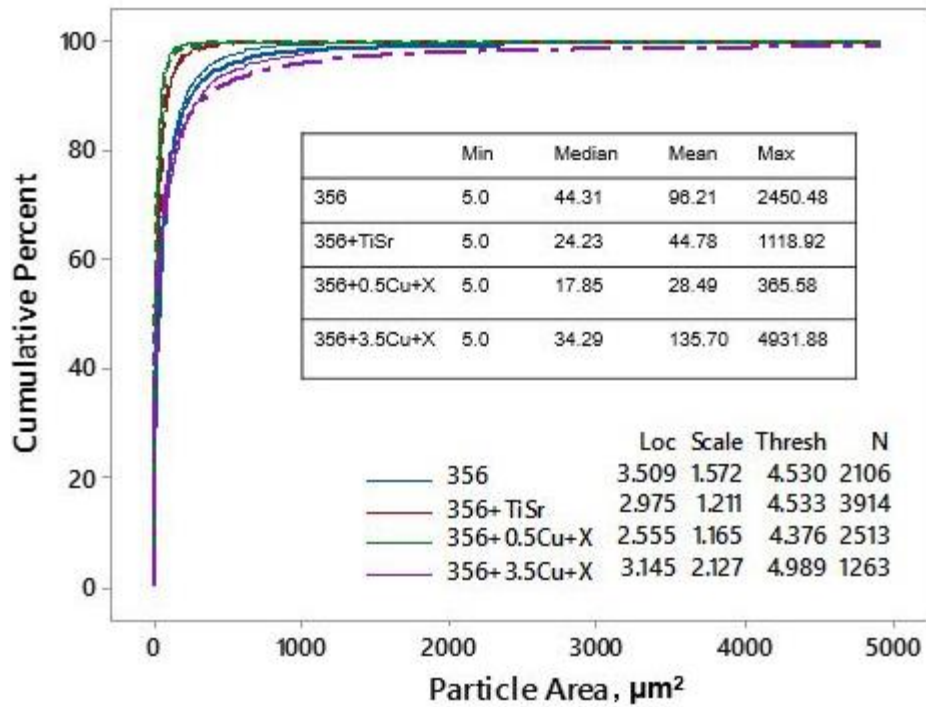
Figure 4.18. 3-parameter lognormal cumulative distribution plots of intermetallic particles for alloys 356, 356+TiSr, 356+0.5Cu+X, and 356+3.5Cu+X. Also, note the descriptive statistics.

Circularity is one of the parameters used to measure a particle's shape and it is calculated by $4\pi(A/P)^2$, A being the particle's area while P is its perimeter. If it has a shape very close to that of a circle, the circularity value will be very near to 1 and vice-versa. Figure 4.19 shows plots of circularity Vs particle area for the entire particle size distribution while Figure 4.20 shows circularity plotted against particle area for the upper tail of the distribution (0.1 % of largest particles). The statistics on the circularity of the particles indicate that most small particles have circularity in the range between ~0.1 to 1. On the other end, all large particles (those that fall within 0.1 percent of the entire population) had a maximum circularity of 0.2. This observation is in line

69

with expectation since larger particles are normally intricate, interconnected and having irregular morphology.
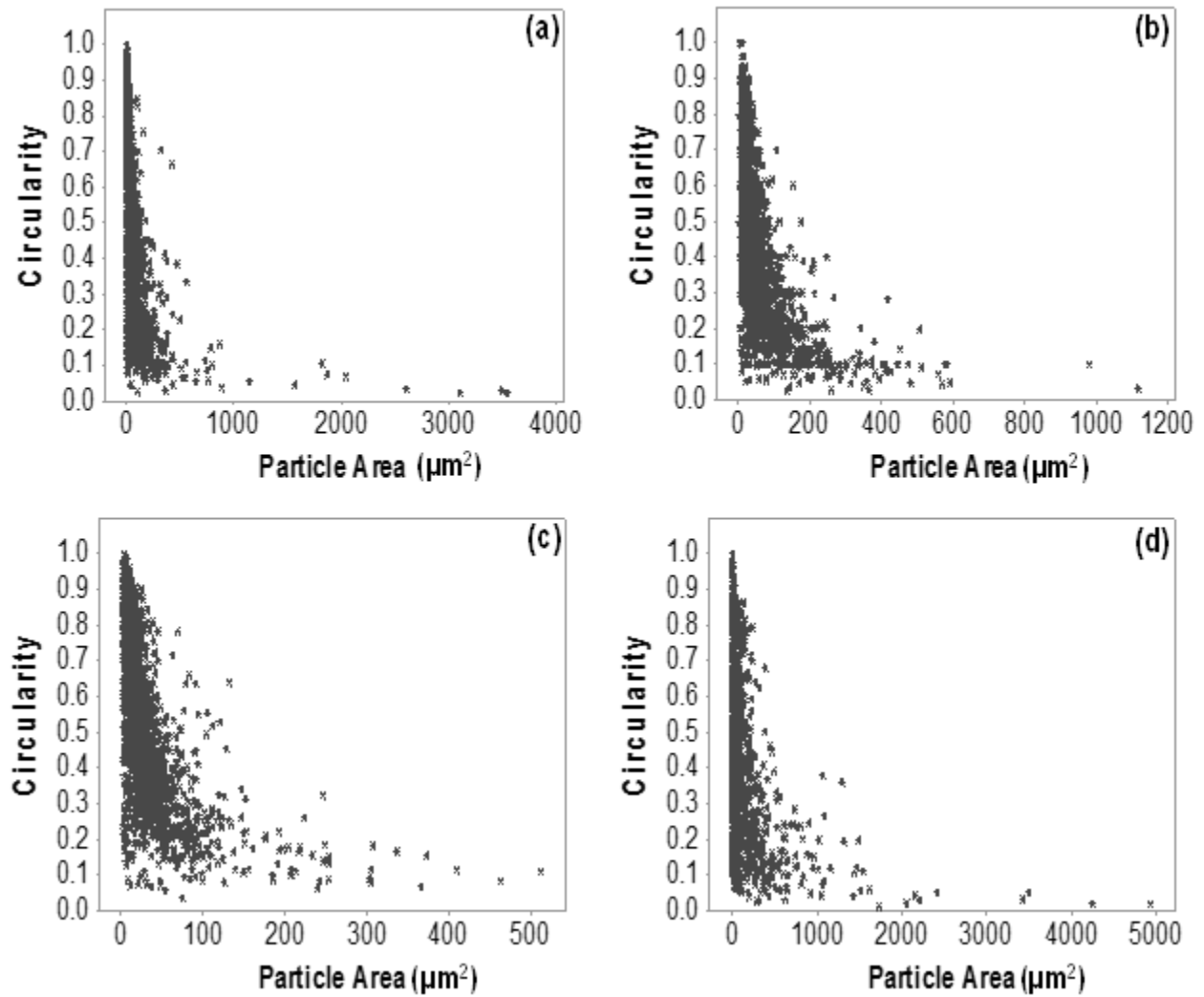


Figure 4.19. Circularity plotted against the corresponding areas in the entire population of particle size data for alloys 356, 356+TiSr, 356+0.5Cu+X, and 356+3.5Cu+X shown by images (a), (b), (c), and (d) respectively).
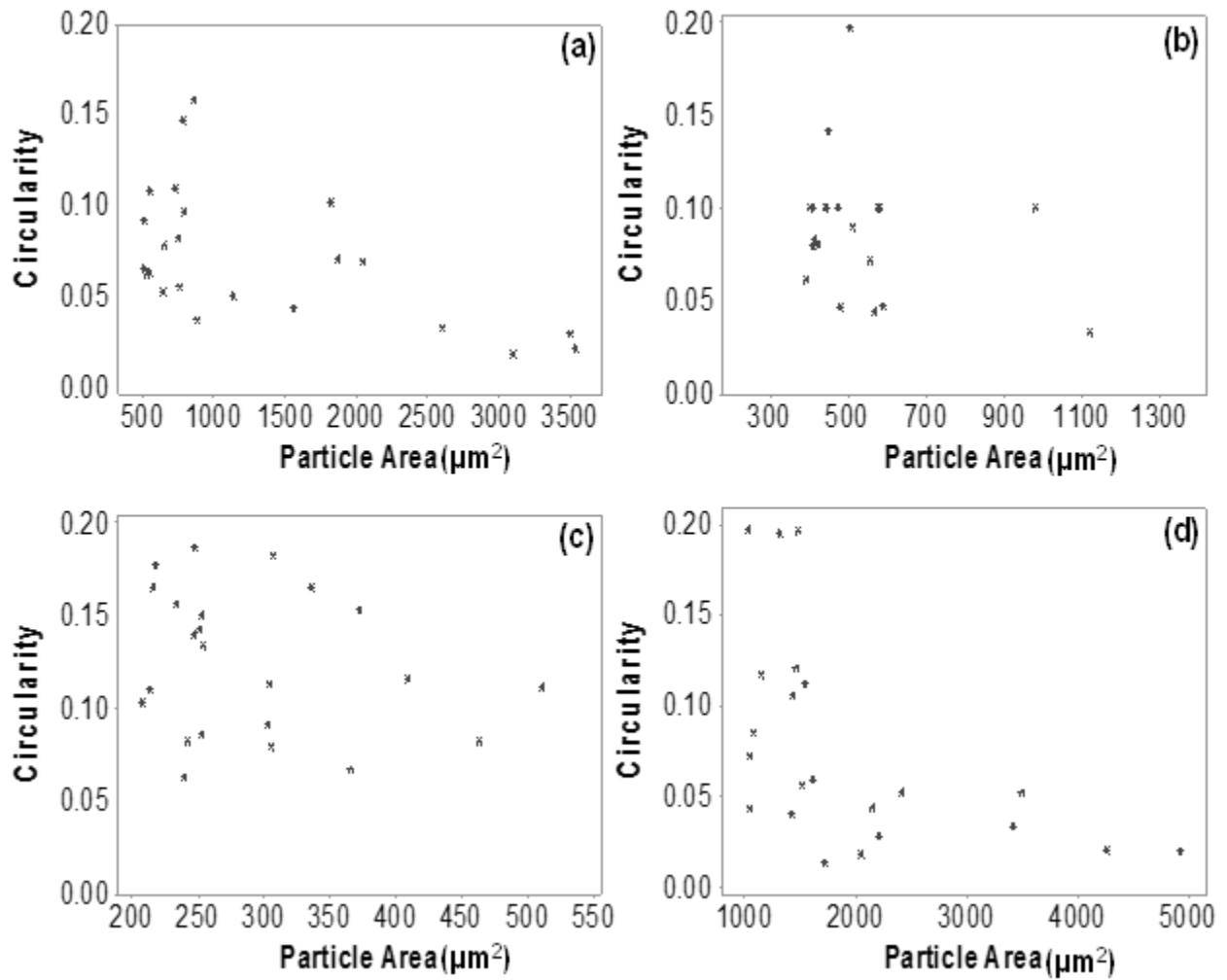
Figure 4.20. The circularity plotted against the corresponding areas in the upper tail of the distribution of particle size data (largest 0.1% particles) for alloys 356, 356+TiSr, 356+0.5Cu+X, and 356+3.5Cu+X shown by images (a), (b), (c), and (d) respectively).

Aspect ratio is another indicator of size and shape and it is a ratio of the major axis to the minor axis of an ellipse that a particle can fit into. Aspect ratio does not take into consideration features like empty holes in a particle which would make a particle with a complex morphology seem to have a larger aspect ratio while on the contrary since circularity consideres these features one would get conflicting data on the same particle and so these two parameters should be used complementarily instead of in place of each other. The aspect ratio ranges between ~1 to 20 for the overall particle population (figure 4.21) but from ~1 to 6 for larger particles as depicted in figure 4.22.
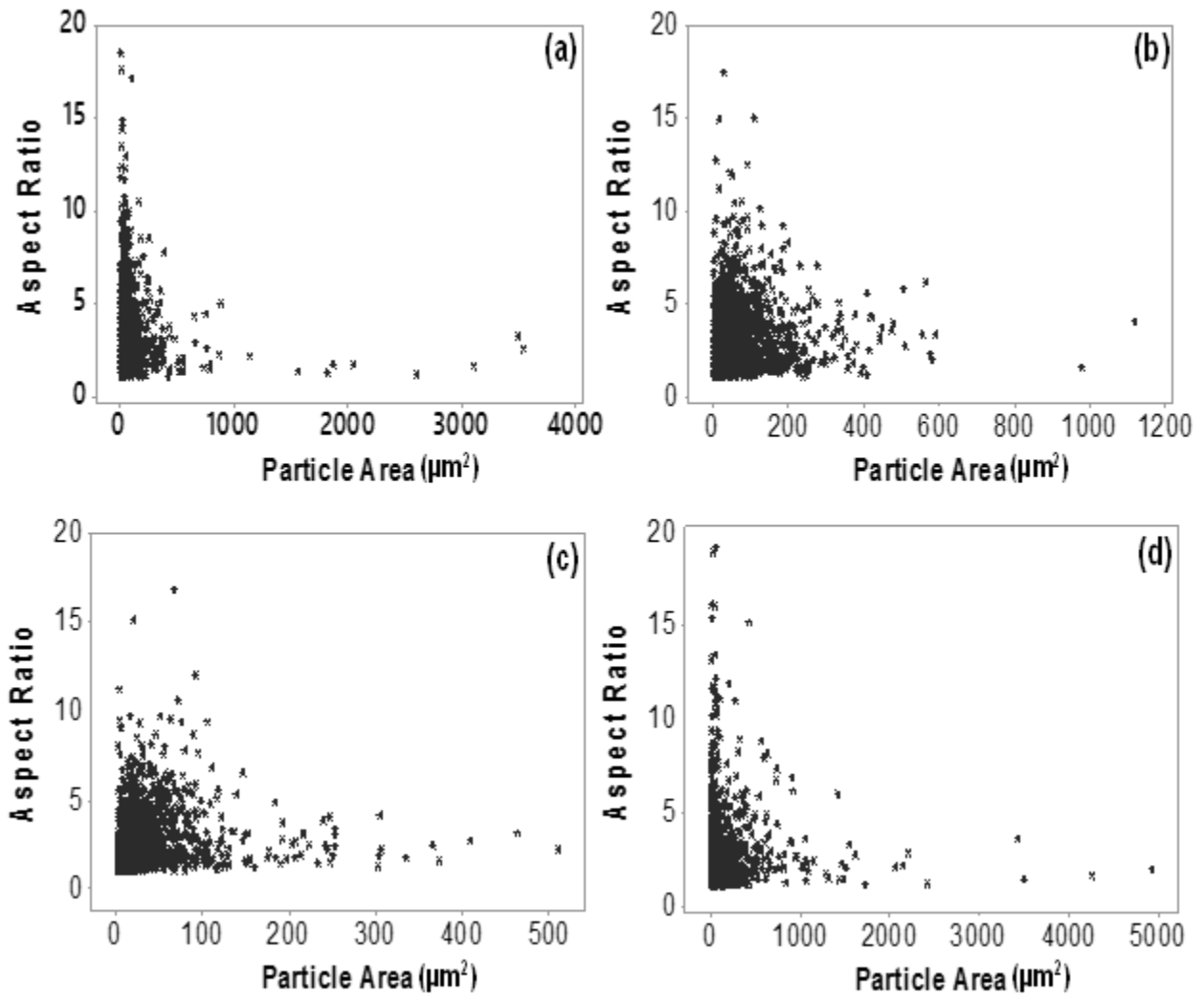
Figure 4.21. The aspect ratio plotted against the corresponding areas in the entire population of particle size data for alloys 356, 356+TiSr, 356+0.5Cu+X, and 356+3.5Cu+X shown by images (a), (b), (c), and (d) respectively).
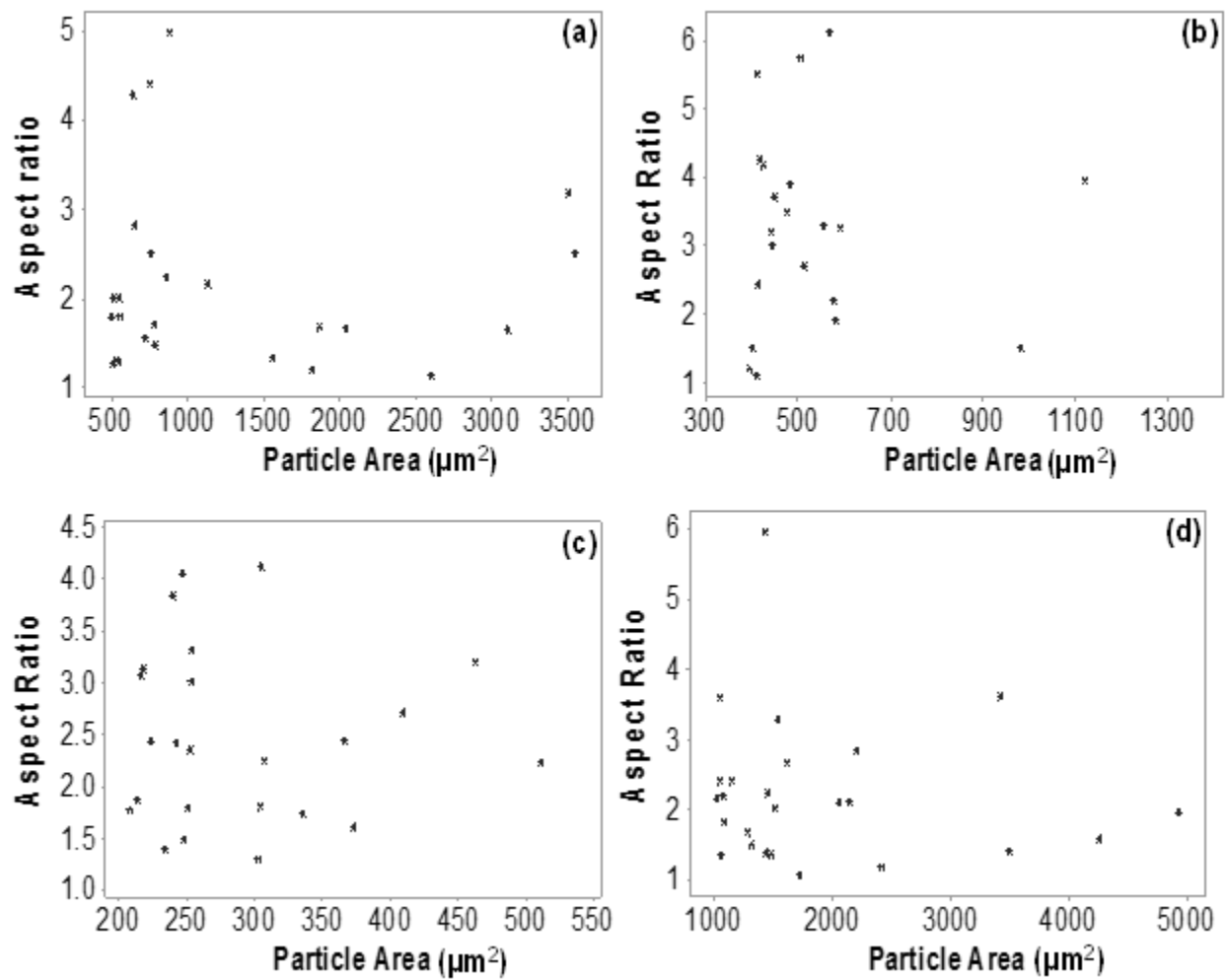
Figure 4. 22. The aspect ratio plotted against the corresponding areas in the upper tail of the particle size distribution for alloys 356, 356+TiSr, 356+0.5Cu+X, and 356+3.5Cu+X shown by images (a), (b), (c), and (d) respectively).

## 4.3 Tensile Results

The results of the tensile tests at room and high temperature are tabulated in appendices 1 and 2 respectively. Figure 4.23 shows the stress-strain characteristics of the alloys at room and high temperatures plotted from the values in appendices 1 and 2. Moreover, Figure 4.24 shows the UTS, Y.S and percentage elongation extracted from the strain–stress curves for each alloy for both room and high temperatures. The bars indicate the average values of three tests and the standard deviation.
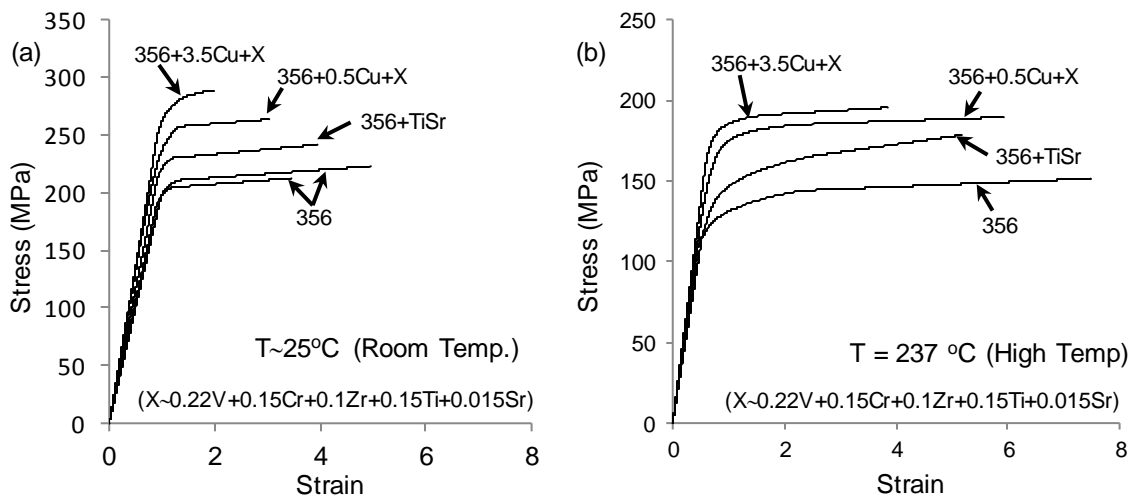


Figure 4.23. (a) Room temperature and (b) high-temperature tensile stress-strain curves obtained for the four alloys.
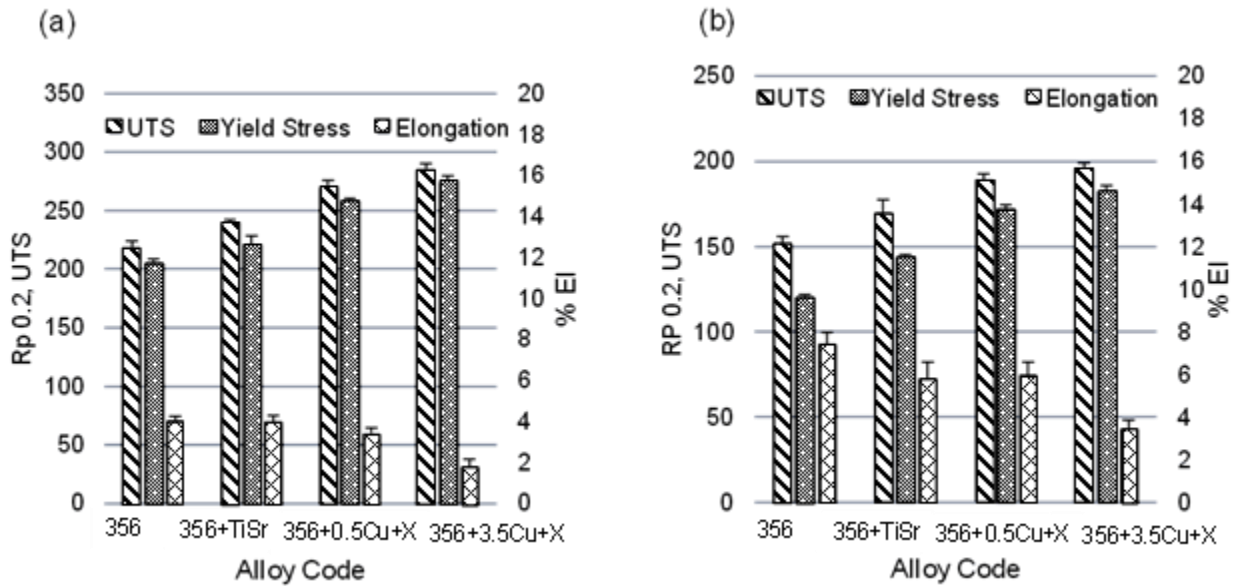
Figure 4.24.Tensile properties at (a) room temperatures and (b) at high temperatures for the alloys.

As noted from Figures 4.23a and 4.24a, the 356 alloy has a UTS of 218 MPa and a YS of 205 MPa. The addition of Ti and Sr has a slight increase on the room temperature strength of the 356 alloy as the UTS and YS of the alloy respectively increase to 240 MPa and 222 MPa. The addition of 0.5 wt. % copper together with 0.015 wt. % Sr, 0.15 wt. % Ti, 0.15 wt. % Zr , 0.25 wt. % V and 0.15 wt. % Cr also increases the properties of the alloy further to a UTS of 272 MPa and a YS of 258 MPa. The greatest increase in UTS to 285 MPa and YS to 274 MPa is observed in the alloy after increasing the Cu content to 3.5 wt. % along with the addition of Sr, Ti, Zr, V, and Cr.

The high temperature (237°C) UTS results are much lower than the room temperature values while the elongation is to some extent higher than that at room temperatures. This is in agreement with

the literature [17, 84] and it is usually due to three probable causes, firstly is the coarsening of the strengthening precipitates, secondly thermal activation of dislocations can occur and finally, possibly, the slidding of the grain boundary. The 356 base alloy has the lowest ultimate tensile strength and yield strength at 152 MPa and 120 MPa respectively. The Ti and Sr additions to 356 gives a notable improvement of UTS to 170 MPa and YS of 143 MPa. The addition of 0.5 wt. % copper together with Sr, Ti, Zr , V and Cr also increases the high temperature UTS to 189 MPa and the YS to 172 MPa. The greatest high temperature UTS and YS were again obtained in the 3.5 % Cu alloy as 194 MPa and 182 MPa respectively.

The 356 alloy has the greatest ductility with a percentage elongation of 7.5%. Addition of Ti and Sr seem to lower the % elongation values of the 356 slightly to 5.4%. However, the percentage elongation of the alloy reduces to 6% with addition of 0.5wt. % Cu together with Sr, Cr, Ti, Zr. This reduction is unexpectedly less than that obtained when Ti and Sr are added. The 3.5% Cu addition has the greatest reduction in the ductility of the 356 alloy to 3.5%. appendix 3 summarizes the percentage improvement in tensile properties of the alloys at 237°C. These values were calculated with respect to the 356 alloy.

The fracture surface after tensile loading showed a mixed type fracture; i.e., brittle failure in the intermetallic particles and a ductile failure in the aluminium matrix. The fractographic studies depicted that the failure mechanisms were comparable in all the alloys analysed. Mostly, inter-granular features that were developed along the grain boundaries were observed along with some flat areas, especially cleavage-type fracture in the plate-shaped intermetallics. As shown in figure

4.25, some eutectic silicon particles and intermetallics were also de-bonded from the matrix suggesting that a strong interaction occurred between the dislocations and the particles.
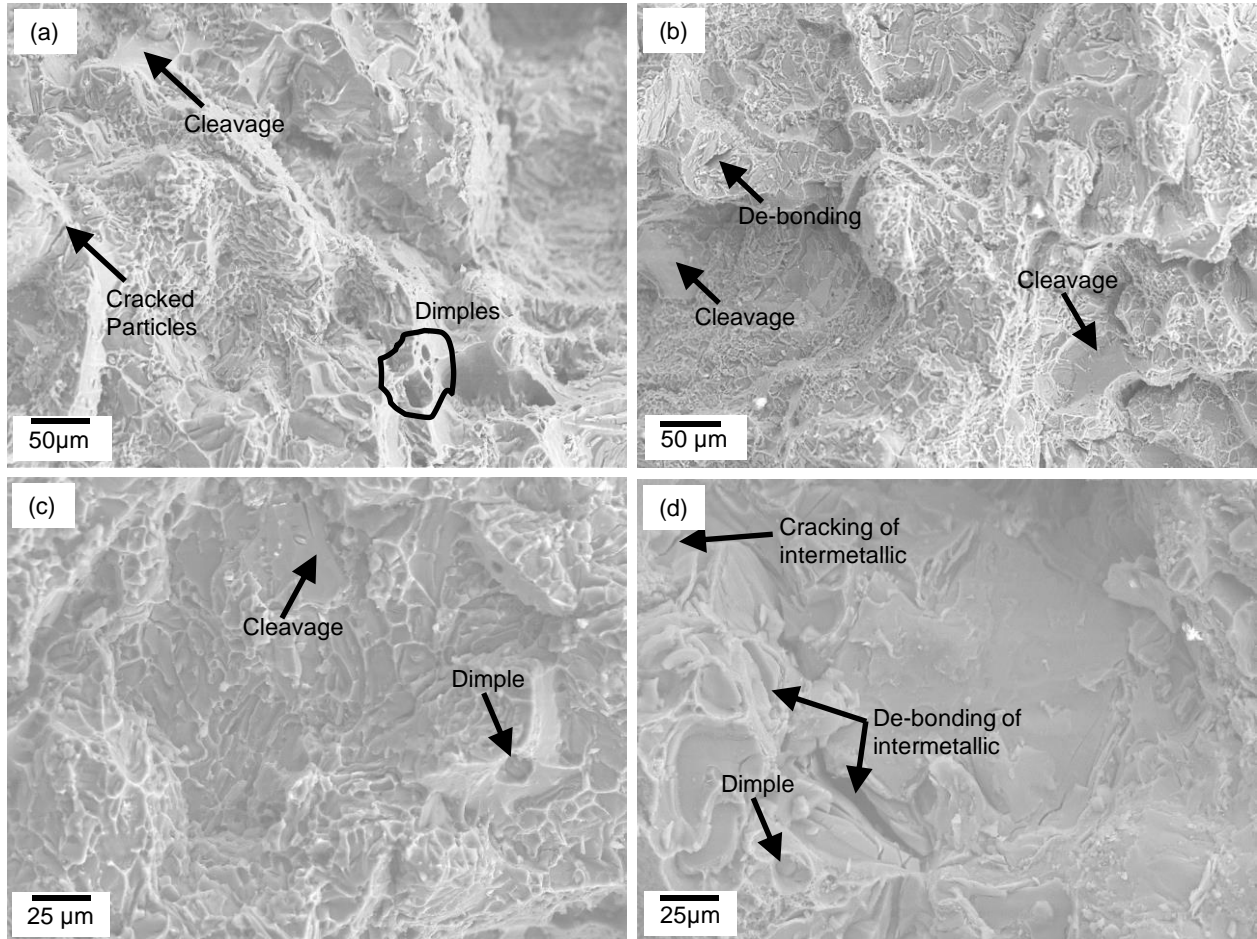


Figure 4.25. Secondary electron fracture surface SEM micrographs of 356, 356+TiSr, 356+0.5Cu+X, and 356+3.5Cu+X (denoted by a, b, c, and d respectively). Note the presence of dimples, cleavages, de-bonding and cracking of intermetallics.

The spherical dimples shown in figure 4.25 is a characteristic of ductile failure, with each dimple being a microvoid that developed and later split into two during fracture process. Other researchers

also discovered similar fracture behaviours for the A356 alloy with additions of Ti, V and Zr during tensile testing [18, 96].

Fracture profiles were analyzed using an optical microscopy so as to comprehend the growth of the crack and the impact of intermetallics. Figure 4.26, shows the crack crossing the inter-dendritic region in which a substantial number of intermetalics and silicon particles are observed. Micro-cracks originating primarily from these constituents can easily link one another propagating through the eutectic regions and finally forming the principal crack.

The microstructure near the fracture profile is shown in Figure 4.26 and it indicates numerous silicon particles which are cracked and other secondary cracks in the parallel orientation to the primary crack and perpendicular to the direction of tensile loading. Cracking also occurred in the intermetallics which are known to be hard and brittle and sometimes needle-like.
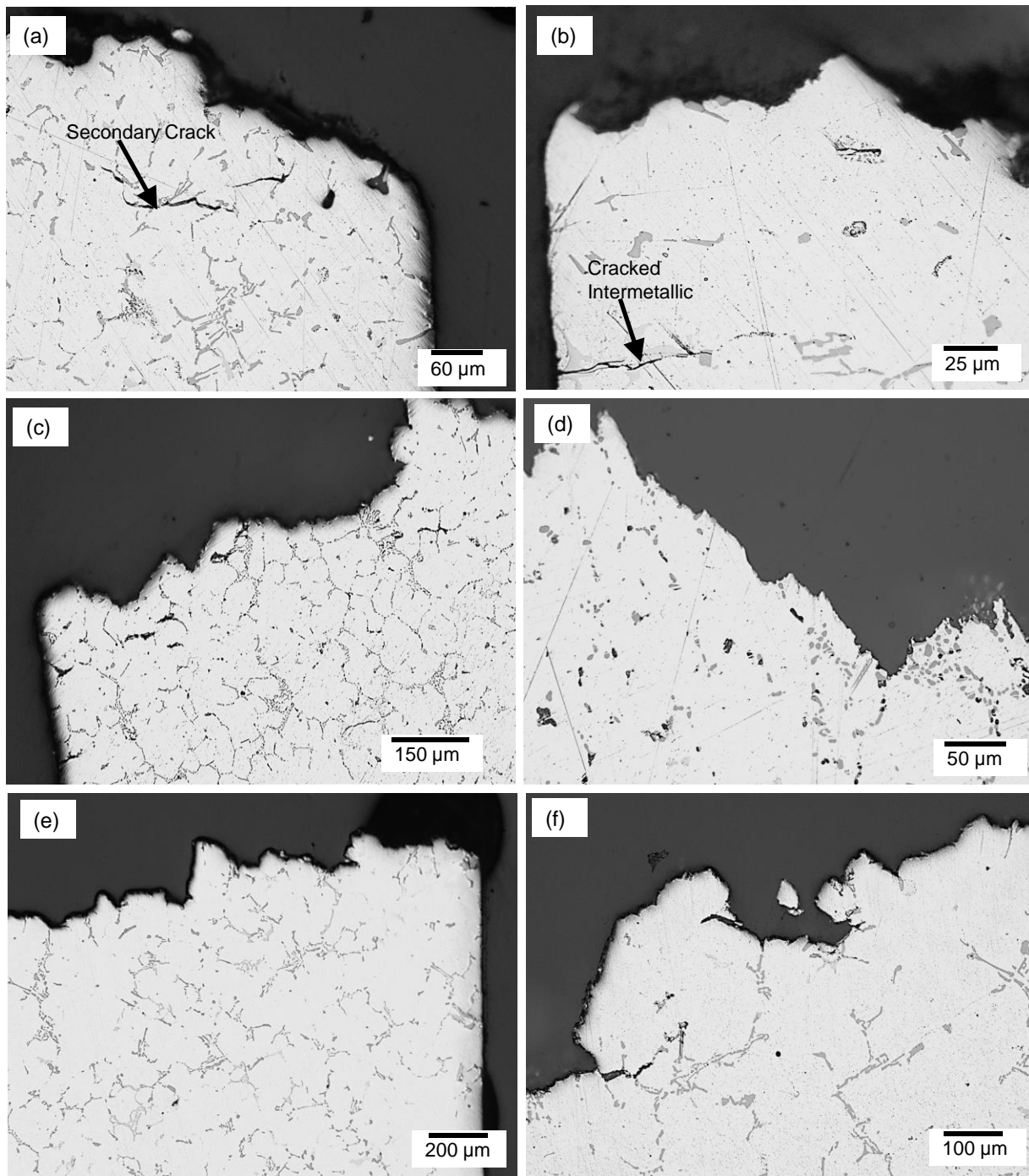
Figure 4.26. Tensile fracture surface optical micrographs of 356 in (a) and (b), 356+0.5Cu+X in (c) and (d), and 356+3.5Cu+X in (e) and (f).

## 4.4 Fatigue Results

The staircase method of determining the fatigue strength at room temperature for all the four alloys yielded the results tabulated in appendix 4. Figure 4.27 is a graphical representation of the same data with the applied stresses plotted against the specimen number.
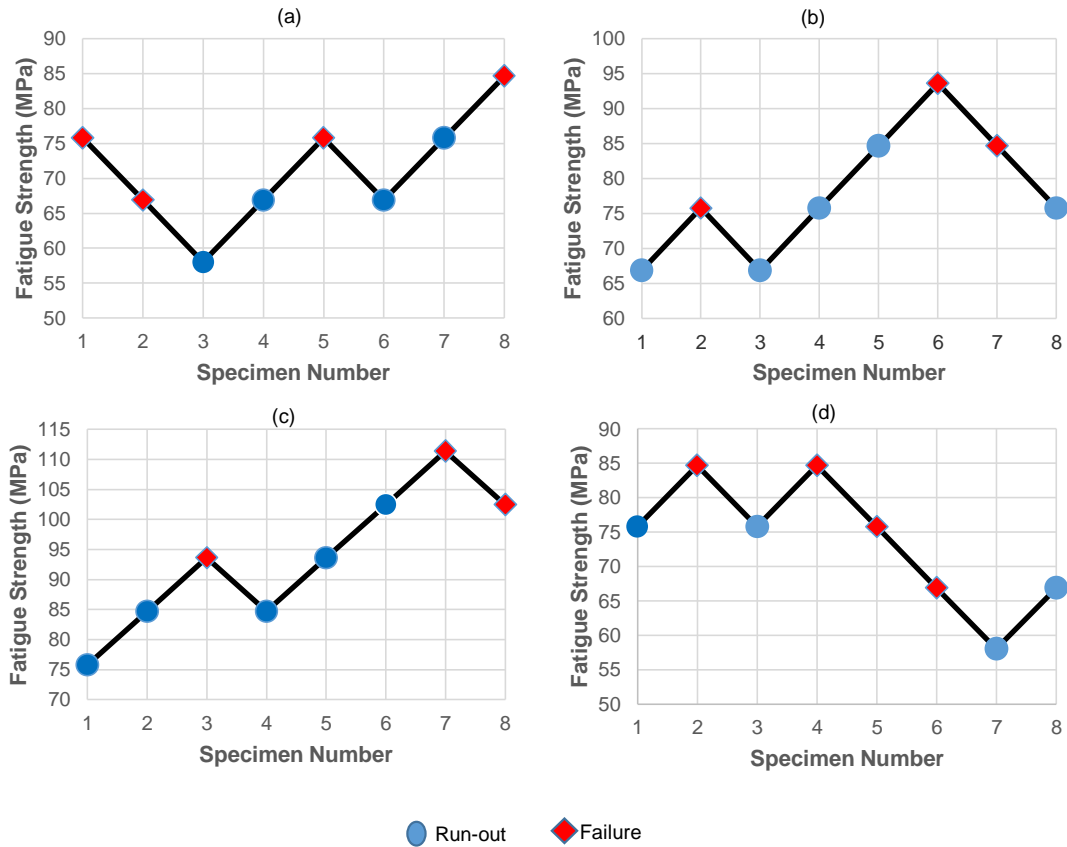


Figure 4.27. Plot of data for staircase fatigue test of 356, 356+TiSr, 356+0.5Cu+X and 356+3.5Cu+X denoted by (a), (b), (c), and (d) respectively.

The results show how many cycles a specimen achieved before fracture. Also shown are the number of cycles a specimen was loaded for run-outs.

Table 4.1. Calculated fatigue strength and standard deviation for the four alloys.

| Alloy | Fatigue strength (MPa) | Standard Deviation |
|---|---|---|
| 356 | 71 | 8 |
| 356 +TiSr | 80 | 10 |
| 356 + 0.5Cu +X | 98 | 10 |
| 356 + 3.5Cu +X | 74 | 10 |

The S-N data is presented in Figure 4.28 as a function of maximum stress versus total fatigue cycles at failure or at run-out. It is noted that the data does not exhibit significant scatter, which could be attributed to HIPping. A comparison among the alloys in Table 4.1 and Figure 4.28 shows that the 356 and 356+3.5Cu+X alloys have the lowest fatigue performance while 356+0.5Cu+X has the highest. It can be seen that the maximum stress of ~111 MPa was reached by 356+0.5Cu+X while the lowest stress a specimen failed was 58 MPa in both 356 and 356+3.5Cu+X.
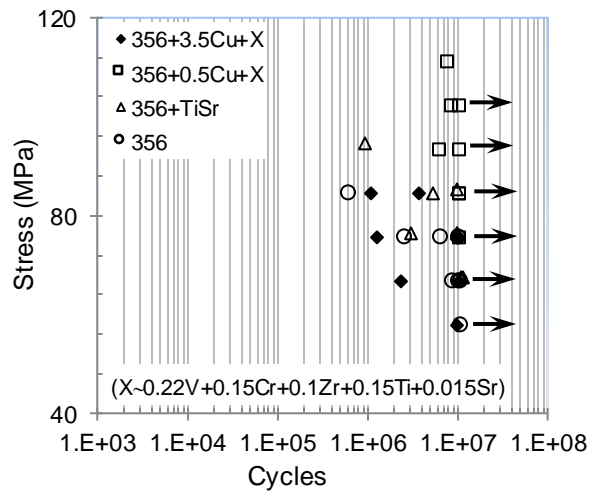


Figure 4.28. Stress amplitude versus cycles to failure (R = -1). The arrows indicate specimens that did not fail after loading for $1x10^7$ cycles (run-outs).

The optical micrographs of 356 after fatigue testing at room temperature are shown in Figure 4.29 while the SEM fracture surfaces are shown in Figure 4.30. Figure 2.29 shows coarse eutectic Si plates and large cracked intermetallics which contributed to failure by cracking due to their brittle nature.
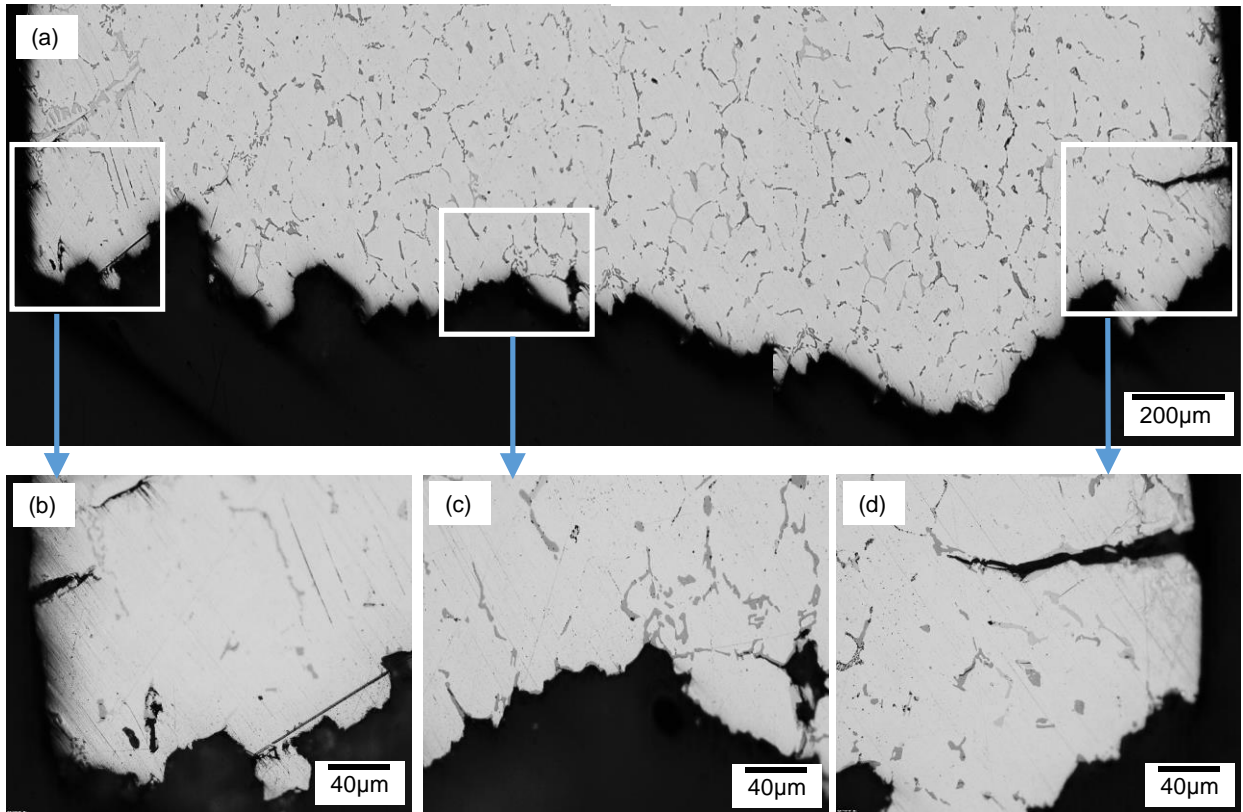


Figure 4.29 Optical micrographs of fatigue fracture profiles of 356 alloy. (b), (c), and (d) are high magnification images taken from the sections shown by the arrows.

The microstructure of 356 is unmodified and thus the eutectic silicon particles are large and irregular. The large eutectic particle size results in more particle fracture and thus lower fatigue

83

strength. On the other hand, Sr-modified alloys 356+TiSr and 356+0.5Cu+X which have small and round eutectic silicon particles give better fatigue strength.



Figure 4.30. Fatigue fracture surface SEM micrographs of 356 alloy (b) and (c) are high magnification images taken from the sections shown by the arrows.

Figure 4.31 are near fracture optical micrographs of 356+0.5Cu+X, while Figure 4.32 shows SEM micrographs of the same. The microstructure of alloy 356+0.5Cu+X is modified and the eutectic silicon particles are small and spherical. They are less susceptible to cracking and therefore expected to result in improved fatigue strength.
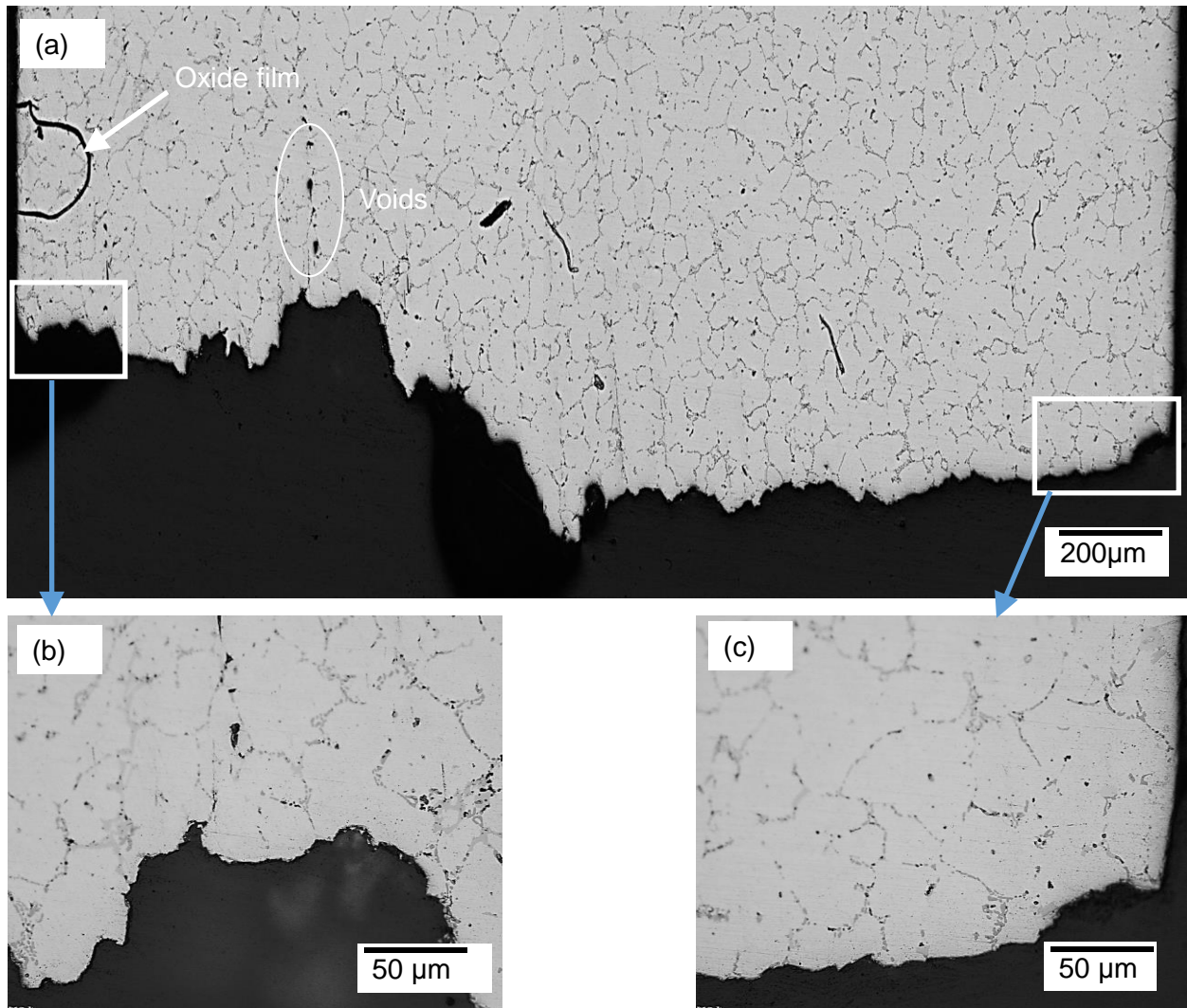
Figure 4.31. Optical micrographs of the fatigue crack profile of 356+0.5Cu+X. (b) and (c) are high magnification images taken from the sections shown by the arrows.

In Figure 4.31, voids and inclusions can be seen. Ductile fracture progresses generally by the process of nucleation-growth-coalescence of the voids.The nucleus of the void is inclusion,

dispersoid or precipitate particle. Which is nucleated by the mechanism of interference of grain boundary and slip band or debonding/cracking of particles starting at a strain $E_N$ [98].

Inclusions, on the other hand, are impurities such as slag from the molten metal, dirt or oxygen that become trapped in the metal as it solidifies. Inclusions are typically the result of poor metal handling or mould cleanliness. Changes to metal pouring or moulding can alleviate their occurrence, though it is hard to completely eliminate it because, for example, even very high purity inert gas used for degassing during casting includes oxygen as an impurity [99].
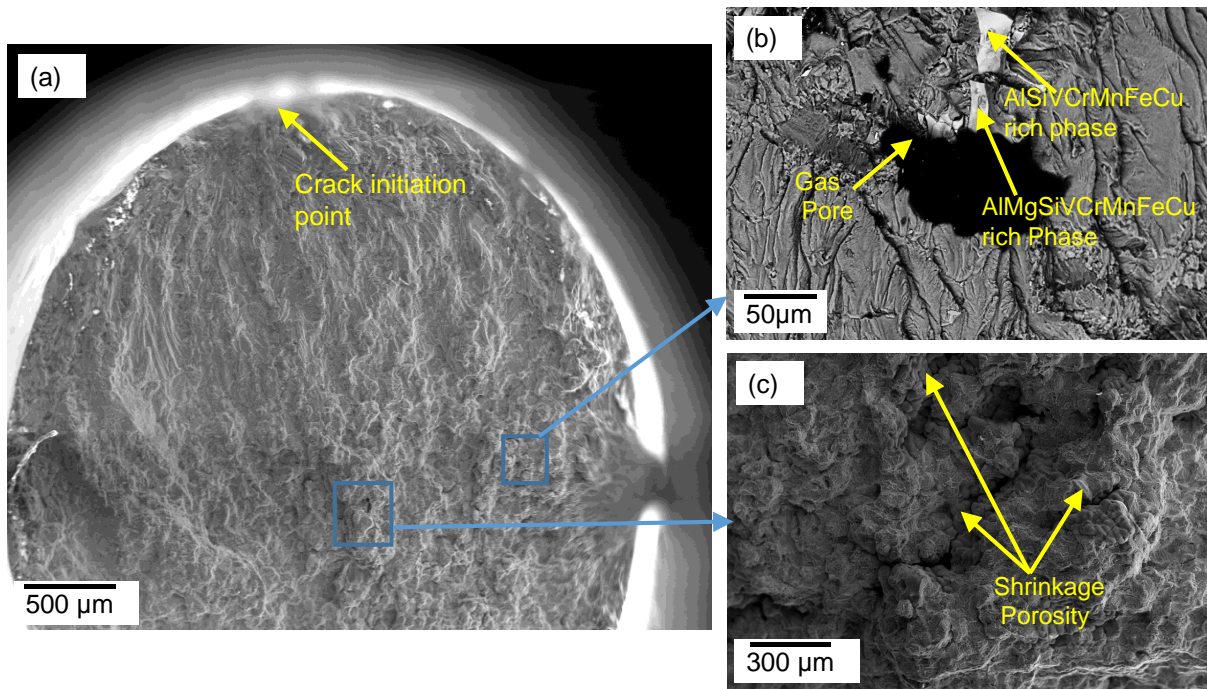


Figure 4.32. SEM fatigue fracture micrographs of 356+0.5Cu+X. (b) and (c) are high magnification images taken from the sections shown by the arrows. Shrinkage and gas porosity and intermetallics are shown in (b) and (c).

SEM micrographs in Figure 4.32 reveal the presence of gas and shrinkage porosities in the rapid fracture sections of the specimen. Also, various phases in the microstructure were identified but it was not determined if these and similar phases and pores were present in the crack initiation point because high magnification SEM images were not taken at the crack initiation site.

Optical and SEM micrographs of 356+3.5Cu+X after fatigue testing at room temperature are shown in Figure 4.33 and in Figure 4.34 respectively. It can be seen from Figure 4.33 that coarse acicular eutectic Si particles and intermetallics are present. The same argument of low fatigue strength due to lack of modification used for 356 also applies here. Although in addition to that, the alloy has a lot of copper, which is also associated increased porosity [39]. Although HIPping may reduce porosity, it is possible that porosity be not be completely be eliminated. Moreover, porosity is often associated with oxides that are not eliminated during HIPping [100].
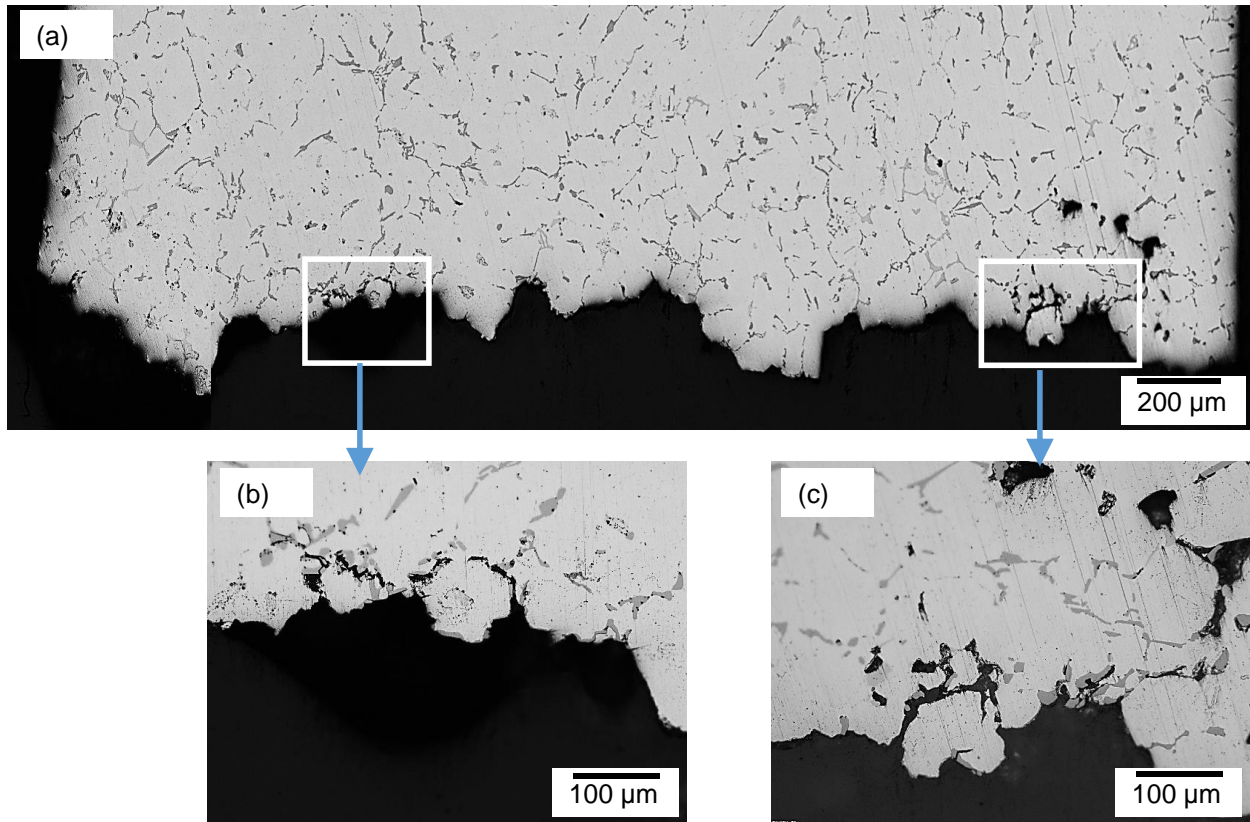
Figure 4.33. Optical fatigue fracture micrographs of 356+3.5Cu+X. (b) and (c) are high magnification images taken from the sections shown by the arrows.

SEM micrographs are shown in Figure 4.34 and confirm the presence of porosity and various phases. Similarly, high magnification SEM images were not taken at the crack initiation site and it cannot be authoritatively stated what initiated fatigue in this alloy.
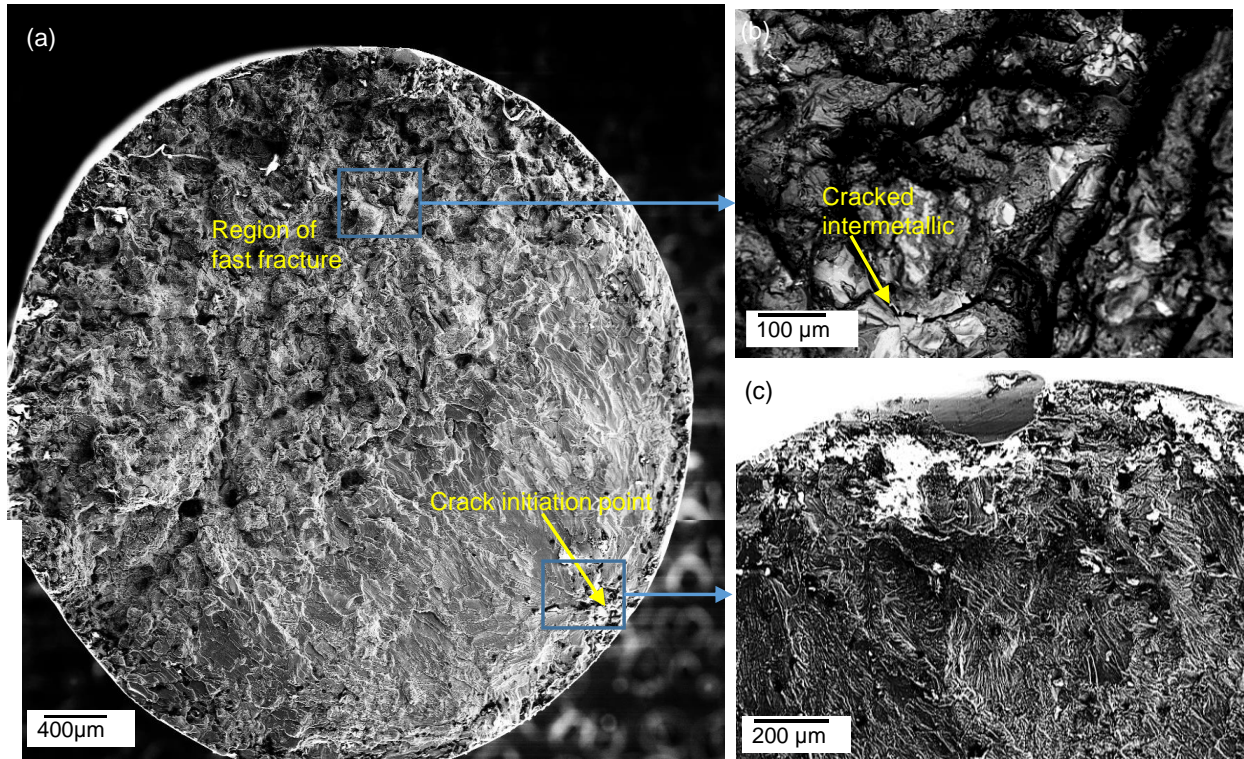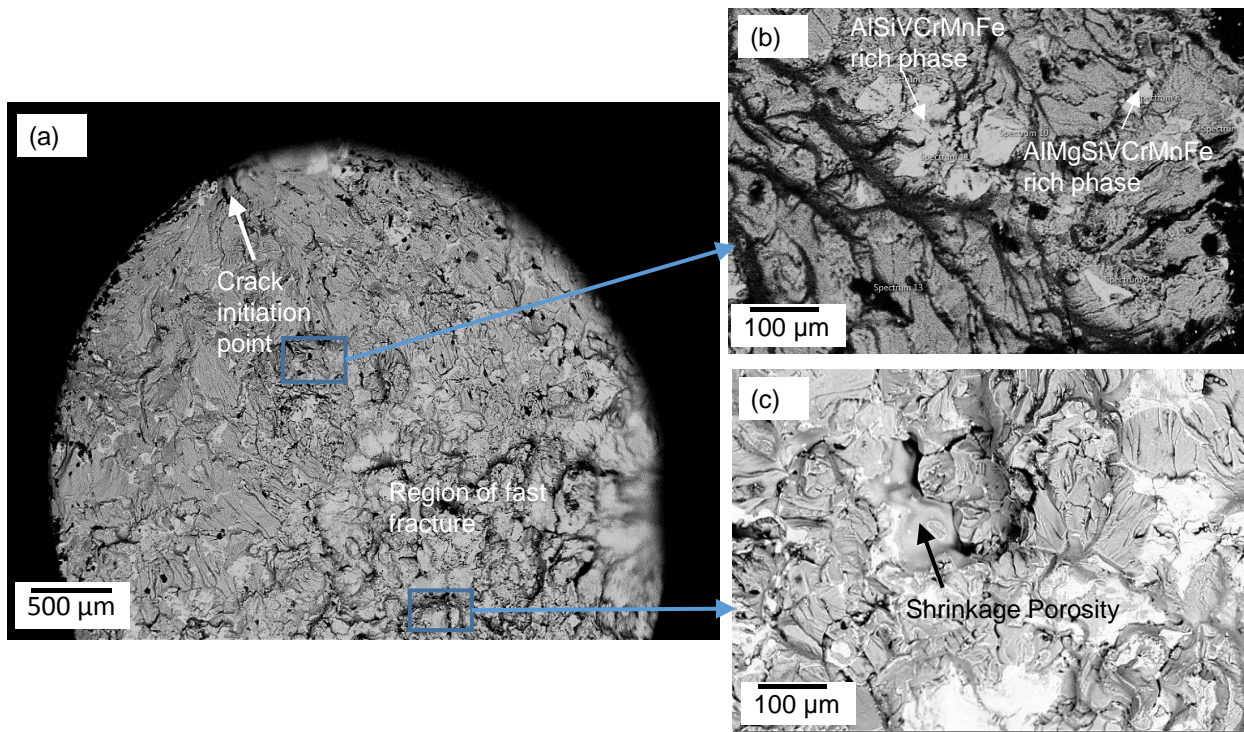
Figure 4.34. SEM Fatigue Fracture Micrographs of 356+3.5Cu+X. (b) and (c) are high magnification images taken from the sections shown by the arrows.

# CHAPTER 5: DISCUSSION

The 356 alloy has an unmodified microstructure with irregular and large eutectic silicon particles and intermetallics, particularly AlSiCrVFeMn and AlSiMgFeMn rich phases. The AlSiMgFeMn phase is believed to be the $\delta$- $Al_4(Fe,Mn)Si_2$. Since the phase is long and needle-like with a small aspect ratio while the spot size of the electron beam is wide, Mg may have been picked up as traces from the matrix. The $\delta$ phases were also observed by other researchers [101,102] and are mostly attributed to low values of ductility and strength due to its stress concentration ability arising from its sharp needle-like morphology. The AlSiCrVFeMn phase formed due to the presence of Cr, V, and Mn present as traces in the microstructure. Usually, the separate addition of Cr and Mn in A356 alloy forms different phases such as $(Fe, Si)_2MnAl_{14}$ [103] and $(Fe, Cr)_3Si_4Al_{25}$ [104] but when a combined addition of Cr and Mn is made, none of these phases exists. The complex phase was observed by many authors [16, 21] and named as $\alpha$-(Al-Cr-Mn-Fe-Si), (hereafter called the $\alpha$ phase, not to be confused with $\alpha$-Al). However, a specific chemical formula was not derived for this phase and it is likely that it has a varying composition range based on the ratios of the elements present in the alloy.

The 356+TiSr alloy on the other hand has a modified Si structure due to the addition of 150 ppm strontium. This resulted in eutectic silicon particles with a fine fibrous morphology. Similarly, as was observed in 356, the AlMgSiFeMn rich phase and its variant, the AlMgSiFe rich phase, is present. A close look at the EDS spectra shows that Mn is in very low quantities and may have

been picked up as traces from the matrix due to the small size of the phase and comparing it to the big spot size of the electron beam. Therefore this could be the $\pi$ phase that was seen in alloy 356.

The microstructure of 356+0.5Cu+X has a modified structure with very fine eutectic silicon particles. The microstructure also has intermetallics particularly AlSiMgTiVCrZr, AlSiMgTiVCrCuZr, AlSiMgTiVCrZrCu and AlSiMgVCrMnFeCu rich phases. Specific chemical formulas were not derived since area scans were done on the alloy instead of specific spot scans, however, the phases are very similar to those observed by other researchers [17], [28].

AlTiVZrCu, AlMgTiVCu and AlVCrMnFeCu phases were identified in 356+3.5Cu+X. These phases are blocky and easily cracked, it was shown that the particles were cracked even before they were loaded, possibly originating from HIPping. It is believed that this cracking, together with the possibility of increased porosity from the addition of copper [20, 38, 85] explains the low ductlity in this alloy.

The composition of 356+3.5Cu+X is similar to 356+0.5Cu+X in that other than the difference in Cu content. However, there are glaring differences in the two microstructures. One of them is the fact that 356+0.5Cu+X is modified while 356+3.5Cu+X is not modified though 150 ppm of strontium was added in both. This lack of modification was not expected. Modification may result with the addition of modifiers like strontium or sodium and/or the cooling rate. For all alloys except 356 alloy, 150 ppm strontium was added to the alloy before casting so as to modify the microstructures. Therefore, all except 356 were expected to be modified. The reason for lack of modification cannot be fully understood. The chemical analysis indicates presence of 150 ppm of

stontium in the alloy, therefore the strontium did not perform its role. Further research should be carried out to investigate the cause of this phenomenon.

Contrary to 356, 356+TiSr, and 356+0.5Cu+X alloys, numerous and coarser precipitates (AlSiTiVCu precipitates) are seen in the interdendritic region in the 356+3.5Cu+X microstructure. These precipitates were found both inside the dendrites and at the interdendritic regions and it is believed that these precipitates are responsible for improved tensile strength especially at high temperatures.

The tensile properties of the alloys at room temperatures exhibit a trend with increasing UTS and yield strength and reduction of ductility with addition of the transition elements Ti, V, Cr and Zr and a much higher increase of UTS and YS on one hand and lower values of elongation with addition of Cu on the other hand. This is similar to what was discovered by other researchers working on addition of transition elements in A356 alloys [9, 17, 65]. The improved UTS and yield can be attributed to the formation of precipitates which acted as barriers to dislocation - movement while low ductility values could be due to defects such as oxides films and intermetallics.

UTS and yield strength of the alloys at high-temperature properties are much lower than the room temperatures ones and this is attributed to coarsening of precipitates as has been pointed out by various researchers [9, 51, 72] but the values, especially for UTS and YS, have greatly improved with addition of transition elements Ti, V, Zr and Cr. A greater increase is observed with addition of Cu together with the transition elements due to formation of precipitates. Fine precipitates of

92

both the transition elements and Cu were observed both at the dendritic and interdendritic regions and these are very effective for resisting propagation of dislocation. However, the exact relationship between Cu and the transition elements was not determined, further work on precipitate formation sequence and identification of the same using TEM is therefore recommended so as to better determine this relationship.

The fatigue strength of the alloys at $10^7$ cycles was 71 MPa, 80 MPa, 98 MPa and 74 MPa for alloys 356, 356+TiSr, 356+0.5Cu+X, and 356+3.5Cu+X respectively. Interestingly, the observation that the microstructures of 356 and 356+3.5Cu+X were unmodified coincides with their poorer fatigue strengths. On the other hand, the modified alloys 356+TiSr and 356+0.5Cu+X had relatively higher fatigue strength.

# CHAPTER 6: CONCLUSIONS AND FUTURE WORK

## 6.1 Conclusion

The Al-Mg-Si base alloy (356) was modified with additions of transition metals at different levels of addition to produce three alloys: 356+TiSr, 356+0.5Cu+X, and 356+3.5Cu+X so as to improve the alloy performance at elevated temperatures. The results of this analysis are summarised as follows.

- Phase analysis of the alloys showed that alloy 356 and 356+TiSr contained needle-like AlSiMgFeMn (believed to be the δ-Al$_4$(Fe,Mn)Si$_2$ phase) together with Al-Si eutectic clusters inside a α-Al dendritic matrix. 356+0.5Cu+X and 356+3.5Cu+X contained massive and numerous (AlSi)$_x$TiVZr, with rod/blocky morphology which precipitated into very fine precipitates after heat treatment.

- The tensile tests of the alloys showed that increasing the testing temperatures from 25°C to 237 °C, the yield strength (YS) and ultimate tensile strength (UTS) decreased while the ductility increased. However, it was seen that the addition of Ti, V, Cr, and Zr increased the YS and the UTS. The greatest increase in YS and UTS came with the highest addition of Cu (3.5 wt. %) together with Ti, V, Zr, and Cr, although Cu alloyed with the aforenamed elements also gave good results.

- The fatigue life of alloy 356+0.5Cu+X with Ti, V, Zr, Cr and 0.5 wt. % Cu was the highest at 98.05 MPa, while the fatigue strength of the base alloy was the least at 71.35 Mpa. Similar to the base alloy, the fatigue strength of alloy 356+3.5Cu+X with Ti, V, Zr, Cr and 3.5 wt% Cu was low at 73.575 MPa, alloy 356+TiSr with the addition of 0.15 wt% Ti had

94

intermediate values of fatigue strength at 80.25 MPa. It can be deduced that the addition of Cu, Ti, V, Zr, and Cr seem to be advantageous in improving the fatigue resistance of the base 356 alloy although too much copper waters down the effects gained by the addition of these elements due to either increased porosity that accompanies the addition of much copper or formation of brittle intermetallics.

- Fractographic studies revealed that the alloys failed under mixed mode of failure with ductile fracture in the matrix and brittle fracture in the silicon particles and the intermetallics. Gas and shrinkage porosity, intermetallics with high aspect ratio and low circularity and unmodified silicon particles acted as points of stress concentration which aided in crack initiation, propagation and failure.

## 6.2 Future Work

From the above experimental results, it was found that the newly modified developed alloys could be a promising material in power train applications as high temperature materials. However, to be placed in service further analysis is important.

1. Fatigue fracture of the materials is a crucial factor in the design of the product. In this study, low cycle fatigue testing was performed at room temperature. However, a detailed investigation of the influence of transition metals Ti-V-Zr in Al-Si-Cu-Mg alloy on high temperature fatigue performance is necessary.

2. The A356 alloys' tensile strength drops drastically with temperature increased above 200 °C. In the present study, thermally stable precipitates were formed in the A356 alloy and its variants by addition of Ti, V, Zr which have limited solid solubility and low diffusivity in Al. Thus, creep behaviour of the alloy should be evaluated and contrasted with the base A356 alloy.

3. The precipitation behaviour of Al-Si alloys, particularly those with additions of the transition elements added is not well understood. A detailed TEM investigation should be carried out so as to demystify how alloying elements affect the precipitation sequence and on the nature of the precipitates in the alloys studied. This could also be supported with Differential Scanning Calorimetric tests.

4. Friction and wear of the materials are important properties of the Al-Si-Cu-Mg alloys in power train applications. Thus, the evaluation of friction and wear behaviour of the

modified alloys at room temperature and elevated temperature will be helpful to use this alloy.

5. Heat treatment is a very important strengthening mechanisms in Al-Si alloys. Therefore heat treatment studies should be performed on the alloys so as to determine the optimum parameters for solutionising, quenching, natural and artificial aging.

# REFERENCES

[1]  J. Dwight, *Aluminium Design and Construction*. Chichester, U.K.: E and FN Spon, 1999.

[2]  R. Lumley, *Fundamentals of Aluminium Metallurgy: Production, Processes and Applications*. Cambridge, U.K.: Woodhead Publishing Limited, 2011.

[3]  S. K. Shaha, F. Czerwinski, W. Kasprzak, J. Friedman, and D. L. Chen, "Low-Cycle Fatigue of Aluminium-Silicon Alloys for Power-Train Applications," in *The Minerals, Metals and Materials Society*, Orlando, FL, USA, 2015, vol. 2015.

[4]  M. Schlesinger, *Aluminium Recycling*. Boca Raton, U.S.A: Taylor and Francis Group, 2007.

[5]  K. H. Zengen, "Aluminium in Future-A Challenge for Materials Science," *Materials Science Forum*, vol. 1201–1208, pp. 519–521, 2006.

[6]  S. Das, "Designing Aluminium Alloys for A Recycling Friendly World," *Material Science Forum*, vol. 1239–1244, pp. 519–521, 2006.

[7]  M. F. Ashby, *Materials Selection in Mechanical Design*, Second Edition. New York, U.S.A: Butterworth-Heinemann, 1999.

[8]  R. Modaresi, A. N. Lvik, and D. B. Muller, "Component and Alloy Specific Modelling for Evaluating Recycling Strategies for Vehicles.," *Minerals, Metals and Materials Society*.

[9]  S. K. Das, J. A. S. Green, and J. G. Kaufman, "The Development of Recycle-Friendly Automotive Aluminium Alloys.," *Journal of Material*, pp. 48–51, 2007.

[10] H. A. Elhadari, H. A. Patel, D. L. Chen, and W. Kasprzak, "Tensile and Fatigue Properties of a Cast Aluminium Alloy with Ti, Zr and V Additions.," *Materials Science and Engineering A*, vol. 528, no. 81, pp. 28–38, 2011.

[11] W. Kasprzak, D. Emadi, M. Sahoo, and M. Aniolek, "Development of Aluminium Alloys for High Temperature Applications in Diesel Engines.," *Materials Science Forum*, vol. 595, pp. 618–619, 2009.

[12] F. Stadler, H. Antrekowitsch, W. Fragner, H. Kaufmann, and P. J. Uggowitzer, "Effect of Main Alloying Elements on Strength of Al–Si Foundry Alloys at Elevated Temperatures.," *International Journal of Cast Metals Research*, vol. 25, no. 4, 2012.

[13] W. Kasprzak, B. Amirkhiz, and M. Niewczas, "Evaluation of Structure and Properties of Cast Al–Si Based Alloy with Zr–V–Ti Additions for High Temperature Applications," *Journal of Alloys and Compounds*, vol. 595, pp. 67–79, 2014.

117

[14] M. Garat and G. Laslaz, "Improved Aluminium Alloys for Common Rail Diesel Cylinder Heads," Transactions of the American Foundrymen's Society," *Transactions of the American Foundrymen's Society*, vol. 7, no. 2, pp. 1–8, 2007.

[15] T. O. Mbuya, B. O. Odera, S. P. Ng'ang'a, and F. M. Oduori, "Effective Recycling of Cast Aluminium for Small Foundries," *Journal of Agriculture, Science and Technology (JAGST)*, vol. 12, no. 2, pp. 162–181, 2010.

[16] F. King, *Aluminium and its Alloys*. Chichester, U.K.: Ellis Horwood Limited, 1987.

[17] W. Kasprzak, B. Amirkhiz, and M. Niewczas, "Structure and Properties of Cast Al–Si Based Alloy with Zr–V–Ti Additions and its Evaluation of High Temperature Performance," *Journal of Alloys and Compounds*, vol. 595, pp. 67–79, 2014.

[18] W. Kasprzak, D. L. Chen, and S. K. Shaha, "Heat Treatment Development for a Rapidly Solidified Heat Resistant Cast Al–Si Alloy," *Journal of Materials Engineering and Performance*, vol. 22, no. 18, pp. 39–47, 2013.

[19] W. S. Miller, L. Zhuang, J. Botemma, A. J. Witterbrood, and P. De Smet, "Recent Development in Aluminium Alloys for the Automotive Indurstry," Materials Science and Engineering A, Vol. 280, pp. 37-49, 2000.," *Materials Science and Engineering A*, vol. 280, pp. 37–49, 2000.

[20] J. G. Kaufman and E. L. Rooy, *Aluminium Alloy Casting: Properties, Processes, and Applications*. ASTM International, 2014.

[21] L. Mondolfo, *Aluminium Alloys: Structure and Properties*. London, U.K.: Butterworths, 1976.

[22] V. S. Zolotorevsky, N. A. Belov, and M. V. Glazoff, *Casting Aluminium Alloys*. Pittsburg, Russia: Elsevier, 2007.

[23] W. M. Edwards, R. C. Thomson, S. J. Barnes, and S. I. Barnes, "Development of Near-Eutectic Al-Si Casting Alloys for Piston Applications," Materials Science Forum," *Materials Science Forum*, vol. 625, pp. 396–402, 2002.

[24] N. Saheb, T. Laoui, A. R. Daud, M. Harun, S. Radiman, and R. Yahaya, "Influence of Ti Addition on Wear Properties of Al–Si Eutectic," *Wear*, vol. 249, no. 8, pp. 656–662, 2001.

[25] R. Stone and J. K. Ball, *Automotive Engineering Fundamentals*. Michigan, U.S.A: SAE International, 2004.

[26] D. Crolla, *Encyclopedia of Automotive Engineering*. New York, U.S.A: John Wiley and Sons Inc., 2015.

[27] M. Javidani and D. Larouche, "Application of Cast Al–Si Alloys in Internal Combustion Engine Components," *International Materials Reviews*, vol. 000, no. 000, pp. 1–27, 2014.

[28] E. Ozbakir, "Development of Aluminium Alloys for Diesel-Engine Applications," Masters, McGill University, Montreal, Quebec, Canada, 2008.

[29] R. Mahmudi, P. Sepehrband, and H. M. Ghasemi, "Improved Properties of A319 Casting Alloy Modified with Zr," *Materials Letters*, vol. 2606, no. 10, pp. 60–71, 2006.

[30] Z. Li, A. M. Samuel, F. H. Samuel, C. Ravindran, S. Valtierra, and H. W. Doty, "Parameters Controlling the Performance of AA319-type Alloys Part I. Tensile Properties," Materials Science and Engineering A, Vol. 367, no. 110, pp. 96, 2004.," *Materials Science and Engineering A*, vol. 367, no. 110, pp. 96–103, 2004.

[31] X. Zhu, A. Shyam, J. W. Jones, H. Mayer, J. V. Lasecki, and J. E. Allison, "Effects of Microstructure and Temperature on Fatigue Behavior of E319-T7 Cast Aluminium Alloy in Very Long Life Cycles," International Journal of Fatigue.," *International Journal of Fatigue*, vol. 28, no. 11, pp. 1566–1571, 2006.

[32] G. N. Mrówka and J. Sieniawski, "Microstructure and Mechanical Properties of C355.0 Cast Aluminium Alloy," *Archives of Materials Science*, vol. 47, no. 2, pp. 85–94, 2011.

[33] *Midland.-Atlantic Casting Services*, 2015. [Online]. Available: www.Mid-Atlantic Casting.Com. [Accessed: 30-Jun-2015].

[34] D. Casari, T. H. Ludwig, M. Merlin, L. Anberg, and G. L. Garagnani, "Impact Behavior of A356 Foundry Alloys in the Presence of Trace Elements Ni and V," *Journal of Materials Engineering and Performance*, no. 24, pp. 894–908, 2015.

[35] J. Feikus, "Optimization of Al-Si Cast Alloys for Cylinder Head Applications," *Transactions of the American Foundrymen's Society*, vol. 106, pp. 225–231, 1998.

[36] "ASM Metals Handbook Alloy Phase Diagrams," *ASM International*, vol. 3, pp. 279–337, 1992.

[37] S. S. Shin, E. S. Kim, G. Y. Yeom, and J. C. Lee, "Modification Effect of Sr. on the Microstructures and Mechanical Properties of Al-10.5Si-2.0Cu Recycled Alloy for Die Casting," *Materials Science and Engineering A*, vol. 535, pp. 151–157, 2012.

[38] I. Alfonso, C. Maldonado, G. Gonzalez, and A. Bedolla, "Effect of Mg Content and Solution Treatment on the Microstructure of Al-Si-Cu-Mg Alloys," *Journal of Materials Science*, vol. 41, pp. 1945–1952, 2006.

[39] S. G. Shabestari and H. Moemeni, "Effect Of Copper And Solidification Conditions On the Microstructure and Mechanical Properties of Al-Si-Mg Alloys," *Journal of Materials Processing*, vol. 153, pp. 193–198, 2004.

[40] H. Y. Kim, S. W. Han, and H. M. Lee, "The Influence of Mn and Cr on the Tensile Properties of A356-0.20Fe Alloy," *Materials Letters*, vol. 60, no. 15, pp. 1880–1883, 2006.

[41] Q. G. Wang, P. E. Jones, and M. Osborne, "Effect of Iron on the Microstructure and Mechanical Properties of an Al-7%Si-0.4%Mg Casting Alloy," *SAE-Technical Publication*, vol. 823, no. 1, 2003.

[42] Y. Zheng, W. Xiao, S. Ge, W. Zhao, S. Hanada, and C. Ma, "Effects of Cu content and Cu/Mg ratio on the microstructure and mechanical properties of Al-Si-Cu-Mg alloys.," *Journal of Alloys and Compounds*, vol. 649, pp. 291–296, 2015.

[43] R. Jahn, W. T. Donlon, and J. E. Allison, in *TMS conference proceedings*, San Diego, 1999.

[44] S. G. Shabestari and H. Moemeni, "Effect of Copper and Solidification Conditions on the Microstructure and Mechanical Properties of Al–Si–Mg Alloys Journal of Materials Processing Technology 153–154 (2004) 193–198," *Journal of Materials Processing*, vol. 153–154, pp. 193–198, 2004.

[45] M. Murayama, K. Hono, W. F. Miao, and D. E. Laughlin, "The Effect of Cu Additions on the Precipitation Kinetics in an Al-Mg-Si Alloy with Excess Si," *Metallurgical and Materials Transactions A*, vol. 32A, pp. 239–246, Feb. 2001.

[46] H. Yang, S. Ji, W. Yang, Y. Wang, and Z. Fan, "Effect of Mg level on the microstructure and mechanical properties of die-cast Al–Si–Cu alloys.," *Materials Science&Engineering A*, vol. 642, pp. 340–350, 2015.

[47] C. H. Caceres, C. J. Davidson, J. R. Griffiths, and Q. G. Wang, "The Effect of Mg on the Microstructure and Mechanical Behavior of Al-Si-Mg Casting Alloys," *Metallurgical and Materials Transactions A*, vol. 30A, pp. 2611–2618, 1999.

[48] J. Y. Hwang, H. W. Doty, and M. J. Kaufman, "The Effects of Mn Additions on the Microstructure and Mechanical Properties of Al–Si–Cu Casting Alloys," *Materials Science and Engineering A*, vol. 488, pp. 496–504, 2008.

[49] D. H. Lee, J. H. Park, and S. W. Nam, "Enhancement of mechanical properties of Al-Mg-Si alloys by means of manganese dispersoids.," *Materials Science and Technology*, vol. 15, no. 4, pp. 450–455, 1999.

[50] Y.-H. Cho, D.-H. Joo, C.-H. Kim, and H.-C. Lee, "The Effect of Alloy Addition on the High Temperature Properties of Over-aged Al-Si(CuNiMg) Cast Alloys," *Materials Science Forum*, vol. 519–521, pp. 461–466, 2006.

[51] A. Couture, "Iron in Aluminium Casting Alloys - A Literature Survey," *International Cast Metals Journal*, vol. 6, no. 4, pp. 9–17, 1981.

[52] P. N. Crepeau, "Effect of Iron in Al-Si Alloys: A Critical Review.," *Transactions of the American Foundryman's Society*, vol. 103, pp. 361–366, 1995.

[53] J. A. Taylor, "Iron-containing intermetallic phases in Al-Si based casting alloys," in *11th International Congress on Metallurgy & Materials*, Rosario, Argentina., 2012, vol. 1, pp. 19–33.

[54] P. Sepehrband, R. Mahmudi, and F. Khomaimizadeh, "Effect of Zr Addition on the Aging Behavior of A319 Aluminium Cast Alloy," *Scripta Materialia*, vol. 52, pp. 253–272, 2005.

[55] W. Yuan and Z. Liang, "Effect of Zr Additions on Properties of Al–Mg–Si Aluminium Alloy Used for All Aluminium Alloy Conductor," *Materials and Design*, vol. 32, no. 8–9, pp. 4195–4200, 2011.

[56] B. Badarani and R. Raiszadeh, "Precipitation Hardening of Cast Zr-Containing A356 Aluminium Alloy," *Materials and Design*, pp. 935–940, 2011.

[57] F. A. Fasoyinu, D. Cousineau, P. Newcombe, T. Castles, and M. Sahoo, "Grain Refinement of Aluminium Alloy 356.0 with Scandium, Zirconium, and a Combination of Titanium and Boron," *Transactions of the American Foundrymen's Society*, vol. 109, no. 44, pp. 1–21, 2001.

[58] T. H. Ludwig, P. L. Schaffer, and L. Anberg, "Influence of Vanadium on the Microstructure of a 356 Foundry Alloy," in *Light metals*, New Jersey, U.S.A: John Wiley and Sons Inc., 2013.

[59] D. Casari, T. H. Ludwig, M. Merlin, L. Anberg, and G. L. Garagnani, "The Effect of Ni and V Trace Elements on the Mechanical Properties of A356 Aluminium Foundry Alloy in As-Cast and T6 Heat Treated Conditions," *Materials Science and Engineering A*, vol. 610, pp. 414–426, 2014.

[60] A. H. Maitland and D. Rodriguez, "Vanadium in Aluminium," in *8th International Light Metals Congress*, 1987, pp. 423–425.

[61] J. Majed and C. Torbjörn, "Effect of Titanium Additions on the Microstructure of DC-Cast Aluminium Alloys," *Materials Science and Engineering A*, vol. 413, pp. 277–282, 2005.

[62] M. Zeren and E. Karakulak, "Microstructural Chracterisation of Al–Si–xTi Cast Alloys," *Materials Science and Technology*, vol. 25, no. 10, pp. 1211–1214, 2009.

[63] K. E. Knipling, D. C. Dunand, and D. N. Seidman, "Criteria for Developing Castable, Creep-Resistant Aluminum-Based Alloys, A Review," *Zeitschrift fur Metallkunde*, vol. 97, no. 3, p. 246, 2006.

[64] Z. Jia *et al.*, "Precipitation behaviour of Al3Zr precipitate in Al-Cu-Zr and Al-Cu-Zr- Ti-V alloys," *Transactions of the Nonferrous Metal Society of China*, vol. 22, pp. 1860–1865, 2012.

[65] E. M. Elgallad and A. M. Samuel, ""Effects of Additives on the Microstructures and Tensile Properties of a New Al-Cu Based Alloy Intended for Automotive Castings," *Transactions of the American Foundrymen's Society*, vol. 42, no. 10, pp. 1–8, 2010.

[66] F. Czwerwinski *et al.*, "High Temperature Aluminium Alloys for Automotive Powertrains," *Advanced Materials and Processes*, pp. 16–20, Mar. 2016.

[67] M. N. E. Efzan, H. J. Kong, and C. K. Kok, "Review: Effect of Alloying Element on Al-Si Alloys," *Advanced Material Research*, vol. 845, pp. 355–359, 2014.

[68] M. Abdulwahab, "The effect of Chromium and Manganese on the mechanical properties and corrosion resistance of Al-Si-Fe alloy in 0.5M HCl solution," Masters Thesis, Ahmadu Bello University, Zaria, Nigeria, 2007.

[69] B. R. Mose, T. O. Mbuya, and S. M. Maranga, "Effect of Minor Elements on Castability, Microstructure and Mechanical Properties of Recycled Aluminium Casting Alloys," Masters, JKUAT, Nairobi, Kenya, 2009.

[70] S. Boontein, W. Prukkanon, K. Puparatanapong, C. Limmaneevichitr, and J. Kajornchaiyakul, "Effect of Minor Sb Additions on Sdas, Age Hardening and Mechanical Properties of a356 Aluminum Alloy Casting," *Materials Science Forum*, vol. 519–521, pp. 537–542, 2006.

[71] A. M. A. Mohamed, F. H. Samuel, A. M. Samuel, and H. W. Doty, "Effects of Individual and Combined Additions of Pb, Bi, and Sn on the Microstructure and Mechanical Properties of Al- 10.8Si-2.25Cu-0.3Mg Alloy.," *Metallurgical and Materials Transactions A*, vol. 40A, pp. 240–254, 2009.

[72] C. R. Loper and J. I. Cho, "Influence of Trace Amounts of Phosphorus in Aluminum Castings," *AFS Transactions*, vol. 108, pp. 667–672, 2000.

[73] I. F. Major and I. W. Rutter, "Effect of Strontium and Phosphorus on Solid/Liquid Interface of Al-Si Eutectic.," *Materials Science and Technology*, vol. 5, no. 7, pp. 645–656, 1989.

[74]  N. Tenekedjiev, D. Argo, and J. E. Gruzleski, "Sodium, Strontium and Phosphorus Effects in Hypereutectic Al-Si Alloys.," *AFS Transactions*, vol. 97, pp. 127–136, 1989.

[75]  C. R. Loper, H. G. Seong, and J. I. Cho, "Interaction of Phosphorus and Bismuth (with Sr) in A356.2 Alloy.," *AFS Transactions*, vol. 109, pp. 1–13, 2001.

[76]  A. M. Samuel, H. W. Doty, S. Valtierra, and F. H. Samuel, "Effect of Sr-P Interaction on the Microstructure and Tensile Properties of A413.0 Type Alloys.," *Advances in Materials Science and Engineering*, vol. 2016, p. 11, 2016.

[77]  M. Zuo, D. Zhao, X. Teng, H. Geng, and Z. Zhang, "Effect of P and Sr complex modification on Si phase in hypereutectic Al–30Si alloys," *Materials and Design*, vol. 47, pp. 857–863, 2013.

[78]  G. K. Sigworth, "The Modification of Al-Si Casting Alloys: Important Practical and Theoretical Aspects.," *International Journal of Metalcasting*, vol. 91, pp. 7–16, 2008.

[79]  J. Gobrecht, "The Influence of Alloying Elements on the Duration of Modification of Na and Sr in Al-Si Cast Alloys.," *Giesserei*, vol. 65, pp. 158–164, 1978.

[80]  T. J. Hurley and R. G. Atkinson, "Effects of Modification Practice on Aluminum A356 Alloys," *AFS Transactions*, vol. 93, pp. 191–196, 1985.

[81]  M. Garat, G. Laslay, S. Jacob, P. Meyer, P. R. Gaerin, and R. Adam, "State of the Art Use of Sb-, Na- and Sr-modified Al-Si Casting Alloys.," *AFS Transactions*, vol. 100, pp. 821–832, 1992.

[82]  A. M. A. Mohamed and F. H. Samuel, "A Review on the Heat of Al-Si-Cu/Mg Casting Alloys.," *Heat Treatment – Conventional and Novel Applications*, pp. 55–72, 2012.

[83]  A. Lombardi, C. Ravindran, and R. MacKay, "Optimization of the Solution Heat Treatment Process to Improve Mechanical Properties of 319 Al Alloy Engine Blocks using the Billet Casting Method," *Materials Science and Engineering A*, vol. 633, pp. 125–135, 2015.

[84]  G. Wang, X. Bian, W. Wang, and J. Zhang, "Influence of Cu and minor elements on solution treatment of Al–Si–Cu–Mg cast alloys," *Materials Letters*, vol. 57, pp. 4083–4087, 2003.

[85]  Y. M. Han, A. M. Samuel, F. H. Samuel, S. Valtierra, and H. W. Doty, "Effect of Solution Heat Treatment type on the Dissolution of Copper Phases in Al-Si-Cu-Mg type Alloys," *AFS Transactions*, vol. 116, pp. 79–90, 2008.

[86]  ASM International, *ASM Handbook: Heat Treatment*, vol. Volume 4. ASM International.

[87] S. K. Shaha, F. Czwerwinski, W. Kasprzak, J. Friedman, and D. L. Chen, "Ageing characteristics and high-temperature tensile properties of Al–Si Cu–Mg alloys with micro-additions of Cr, Ti, V and Zr," *Materials Science and Engineering A*, 2015.

[88] P. A. Rometsch and G. B. Schaffer, "An Age Hardening Model for Al–7Si–Mg Casting Alloys," *Materials Science and Engineering A*, vol. 325, pp. 424–434, 2002.

[89] N. D. Alexopoulos and S. G. Pantelakis, "Quality Evaluation of A357 Cast Aluminum Alloy Specimens Subjected to Different Artificial Aging Treatment," *Materials and Design*, vol. 25, pp. 419–430, 2004.

[90] E. Sjölander and S. Seifeddine, "Artificial Ageing of Al–Si–Cu–Mg Casting Alloys," *Materials Science and Engineering A*, vol. 528, pp. 7402–7409, 2011.

[91] J. L. Colley, "Microstructure-Property Models For Heat Treatment of A356 Aluminum Alloy.," PhD Dissertation, University of British Columbia, Vancouver, Canada, 2011.

[92] ASTM, "Standard Practice for Sampling Non-Ferrous Metals and Alloys in Cast Form for Chemical Composition E88-91," 2001.

[93] ASTM, "Standard Practices for Sampling Aluminium and Aluminium alloys for Spectrochemical Analysis E716-94," 2002.

[94] T. O. Mbuya, "Analysis of Microstructure and Fatigue Micromechanisms in Cast Aluminium Piston Alloys," PhD Thesis, University of Southampton, Southampton, U.K, 2011.

[95] M. Tiryakioglu, "Statistical distributions for the size of fatigue-initiating defects in Al-7% Si-0.3% Mg alloy castings: A comparative study.," *Materials Science and Engineering: A*, vol. 497, no. (1-2), pp. 119–125, 2008.

[96] M. Zhu, Z. Jian, G. Yang, and Y. Zhou, "Effects of T6 heat treatment on the microstructure, tensile properties, and fracture behavior of the modified A356 alloys," *Materials and Design*, vol. 36, pp. 243–249, 2012.

[97] T. O. Mbuya, I. Sinclair, A. J. Moffat, and P. A. S. Reed, "Analysis of fatigue crack initiation and S-N response of model cast aluminium piston alloys," *Materials Science and Engineering A*, vol. 528, pp. 7331–7340.

[98] N. A. Fleck, J. W. Hutchinson, and V. Tvergaard, "Softening by void and growth in tension and shear," *Journal of the Mechanics and Physics of Solids*, vol. 37, no. 4, pp. 515–540, 1989.

[99] J. Campbell, *Casting Practice - The Ten Rules of Casting*, First. Oxford, U.K: Elsevier Butterworth-Heinemann, 2004.

[100] H. V. Atkinson and S. Davies, "Fundamental aspects of Hot Isostatic Pressing: An overview," *Fundamental aspects of Hot Isostatic Pressing*, vol. 31A, pp. 2981–3000, Dec. 2000.

[101] C. Bidmeski, V. Abouei, H. Saghafian, S. G. Shabestari, and M. T. Noghani, "Effect of Fe-rich intermetallics morphology and dry slidding wear investigation of hypereutectic Al-17.5%Si alloys," *Journal of Materials Research and Technology*, vol. 5, no. 3, pp. 250–258, 2016.

[102] H. J. Huang, Y. H. Cai, H. Cui, J. F. Huang, J. P. He, and J. S. Zhang, "Influence of Mn addition on microstructure and phase formation of spray deposited Al-25Si-xFe-yMn alloy.," *Materials Science and Engineering A*, vol. 502, no. 1–2, pp. 118–125, 2009.

[103] S. Murali, K. S. Raman, and K. S. S. Murthy, "Morphological Studies on [β]-FeSiAl5 Phase in Al-7-Si-0.3Mg Alloy with Trace Additions of Be, Mn, Cr, and Co," *Materials Characterization*, vol. 33, no. 2, pp. 99–112, 1994.

[104] G. Gustafsson, T. Thorvaldsson, and G. L. Dunlop, "The Influence of Fe and Cr on the Microstructure of Cast Al-Si-Mg Alloys," *Metallurgical Transactions A-Physical Metallurgy and Materials Science*, vol. 17, no. 1, pp. 45–52.

[105] R. S. Rana, R. Purohit, and S. Das, "Reviews on the influences of alloying elements on the microstructure and mechanical properties of aluminium alloys and alluminium alloy composites," *International Journal of Scientific and Research Publications*, vol. 2, no. 6, pp. 1–7, Jun. 2012.

# APPENDICES

Appendix 1. Room Temperature Properties of the alloys.

| | | Room Temperature | | | |
|---|---|---|---|---|---|
| | | 356 | 356+TiSr | 356+0.5Cu+X | 356+3.5Cu+X |
| | a | 214 | 233 | 272 | 288 |
| | b | 223 | 242 | 279 | 28 |
| | c | 217 | 244 | 264 | 286 |
| | Avg. | 218 | 240 | 272 | 285 |
| | a | 3.4 | 3.6 | 3.7 | 2.0 |
| | b | 5.0 | 4.0 | 4.4 | 1.7 |
| | c | 3.7 | 4.0 | 4.3 | 1.7 |
| | Avg. | 4.0 | 3.9 | 4.2 | 1.8 |
| | a | 202 | 219 | 258 | 277 |
| | b | 210 | 221 | 264 | 270 |
| | c | 204 | 225 | 253 | 275 |
| | Avg. | 205 | 222 | 258 | 274 |

Appendix 2. High-Temperature Properties of the alloys.

| | | High Temperature | | | |
|---|---|---|---|---|---|
| | | 356 | 356+TiSr | 356+0.5Cu+X | 356+3.5Cu+X |
| | a | 149 | 167 | 190 | 195 |
| | b | 156 | 173 | 186 | 189 |
| | c | 151 | 170 | 193 | 199 |
| | Avg. | 152 | 170 | 189 | 194 |
| | a | 8.0 | 4.8 | 5.9 | 3.9 |
| | b | 6.9 | 6.3 | 6.6 | 3.1 |
| | c | 7.5 | 5.0 | 5.5 | 3.5 |
| | Avg. | 7.5 | 5.4 | 6.0 | 3.5 |
| | a | 122 | 141 | 172 | 183 |
| | b | 116 | 146 | 169 | 177 |
| | c | 120 | 143 | 175 | 186 |
| | Avg. | 120 | 143 | 172 | 182 |

Appendix 3. Percentage improvement in tensile properties of the developed alloys at 237 °C.

| Alloy Code | % UTS increase | % YS increase | % Elongation |
|---|---|---|---|
| 356+TiSr | 11.71 | 19.40 | -28.32 |
| 356+0.5Cu+X | 24.51 | 43.33 | -19.64 |
| 356+3.5Cu+X | 27.72 | 51.67 | -53.77 |

Appendix 4: Fatigue data for the four alloys.

| Specimen No. | Alloy 356 | | Alloy 356+TiSr[a] | | Alloy 356+0.5Cu+X[b] | | Alloy 356+3.5Cu+X | |
|---|---|---|---|---|---|---|---|---|
| | Stress (MPa) | Results (Cycles $x\ 10^6$) | Stress (MPa | Results (Cycles $x\ 10^6$) | Stress (MPa | Results (Cycles $x\ 10^6$) | Stress (MPa | Results (Cycles $x\ 10^6$) |
| 1 | 75.8 | Failure at 2.6159 | 66.9 | Run-out at 10.725 | 75.8 | Run-out at 10.150 | 75.8 | Run-out at 10.102 |
| 2 | 66.9 | Failure at 8.6859 | 75.8 | Failure at 3.0440 | 84.7 | Run-Out at 10.200 | 84.7 | Failure at 3.8185 |
| 3 | 58 | Run-out at 11.154 | 66.9 | Run-out at 11.540 | 93.6 | Failure at 6.0707 | 75.8 | Run-out at 10.571 |
| 4 | 66.9 | Run-out at 10.185 | 75.8 | Run-out at 10.010 | 84.7 | Run-out at 10.191 | 84.7 | Failure at 1.0935 |
| 5 | 75.8 | Failure at 6.6038 | 84.7 | Run-out at 10.030 | 93.6 | Run-out at 10.161 | 75.8 | Failure at 1.2951 |
| 6 | 66.9 | Run-out at 11.007 | 93.6 | Failure at 0.9421 | 102.5 | Run-out at 10.176 | 66.9 | Failure at 2.3545 |
| 7 | 75.8 | Run-out at 10.349 | 84.7 | Failure at 5.2371 | 111.4 | Failure at 7.4858 | 58 | Run-out at 10.106 |
| 8 | 84.7 | Failure at 0.6356 | 75.8 | Run-out at 10.003 | 102.5 | Failure at 8.3106 | 66.9 | Run-out at 10.242 |